

MELANOPSIN SENSITIVITY IN THE HUMAN VISUAL SYSTEM

Manuel Spitschan

A DISSERTATION

in

Psychology

Presented to the Faculties of the University of Pennsylvania

in

Partial Fulfillment of the Requirements for the

Degree of Doctor of Philosophy

2016

Supervisor of Dissertation

Co-Supervisor of Dissertation

David H. Brainard

Geoffrey K. Aguirre

Professor of Psychology

Associate Professor of Neurology

Graduate Group Chairperson

Sara Jaffee, Professor

Department of Psychology

Dissertation Committee

David F. Dinges, Professor of Psychology in Psychiatry

Johannes Burge, Assistant Professor of Psychology

Christopher M. Fang-Yen, Assistant Professor of Bioengineering and Neuroscience

MELANOPSIN SENSITIVITY IN THE HUMAN VISUAL SYSTEM

COPYRIGHT

2016

Manuel Spitschan

Dedicated to my parents.

ACKNOWLEDGMENTS

My first and foremost thanks go to my advisors David H. Brainard and Geoffrey K. Aguirre.

I wish to express my gratitude to my partner Ekaterina Kel; my parents Martina Kanzer-Spitschan and Bernd Spitschan whom this dissertation is dedicated to; my brothers Benjamin and Dominik and their families for their continued brotherhood and friendship; the following people at or previously associated with the University of Pennsylvania (in last-name alphabetical order): Mayank Agrawal, Sakibul Alam, Andrew Bock, Chris Broussard, Nicolas Cottaris, Giulia Fazzetta, Grace Han, Aleksandra Igdalova, Sandeep Jain, Tanya Kurtz, Freddie Letterio, Long Luu, Jessica Marcus, Marcelo Mattar, Jacqueline Meeks, Patricia O'Donnell, Jack Ryan, Andrew Stern, Alison Sweeney, Laurel Sweeney, Yuni Thornton, Alice Zhou; and many more.

ABSTRACT

MELANOPSIN SENSITIVITY IN THE HUMAN VISUAL SYSTEM

Manuel Spitschan

David H. Brainard

Geoffrey K. Aguirre

The human retina contains long [L]-wavelength, medium [M]-wavelength, and short [S]-wavelength cones, rods, and intrinsically photosensitive retinal ganglion cells expressing the blue-sensitive ($\lambda_{\text{max}} = \sim 480$ nm) photopigment melanopsin. Previous animal studies have pointed to a role of melanopsin in advancing circadian phase, melatonin suppression, the pupillary light reflex (PLR), light avoidance, and brightness discrimination, often relying on genetic tools to study melanopsin in isolation in animal models. This work addresses the question of human melanopsin sensitivity and function *in vivo* using a spectrally tunable light source and the method of silent substitution, allowing for the selective stimulation of melanopsin in the human retina, in combination of pupillometry, psychophysics, and BOLD functional neuroimaging (fMRI). In three studies, we find (1) that the temporal transfer function of melanopsin in controlling the pupil in humans is low-pass, peaking at slow temporal frequencies (0.01 Hz), with a sharp drop off at higher frequencies (1-2 Hz); (2) that signals originating from S cones get combined in an antagonistic fashion with melanopsin signals and signals from L and M cones cones, demonstrating spectral opponency in the control of the human PLR; (3) that nominally cone-silent melanopsin-directed spectral modulations stimulate cones in the partial shadow of the retinal blood vessels (termed penumbral cones), leading to the entoptic percept of the subjective retinal vasculature; and (4) that there is no measurable signal due to melanopsin stimulation in human visual cortical areas (V1, V2/V3, MT, LOC; measured with BOLD fMRI) at temporal frequencies most relevant to spatial vision (0.5–64 Hz) while modulations directed at L+M, L–M and S photoreceptor combinations yield characteristic temporal transfer functions in these areas. This

work advances to our understanding of the functional significance of melanopsin function in the human visual system, contributing to the study of human health in relation to light and color.

TABLE OF CONTENTS

ACKNOWLEDGMENTS	iv
ABSTRACT	v
TABLE OF CONTENTS	vii
LIST OF TABLES	ix
LIST OF ILLUSTRATIONS.....	x
INTRODUCTION	1
OPPONENT MELANOPSIN AND S-CONE SIGNALS IN THE HUMAN PUPILLARY LIGHT RESPONSE (Spitschan <i>et al.</i> , 2014)	15
Abstract	15
Significance Statement.....	15
Background	16
Results.....	18
Discussion	21
Methods Summary	24
Supplementary Information: Methods.....	25
Acknowledgements	36
Figures.....	37
SELECTIVE STIMULATION OF PENUMBRAL CONES REVEALS PERCEPTION IN THE SHADOW OF RETINAL BLOOD VESSELS (Spitschan <i>et al.</i> , 2015)	63
Abstract	63
Introduction.....	64
Results.....	65

Discussion	69
Detailed Methods and Supplemental Experiment	72
Acknowledgements	83
Figures.....	84
HUMAN VISUAL CORTEX RESPONSES TO RAPID CONE AND MELANOPSIN DIRECTED FLICKER (Spitschan <i>et al.</i> , 2016)	
Abstract	93
Significance Statement.....	94
Introduction.....	94
Materials & Methods.....	96
Results.....	106
Discussion	112
Acknowledgements	117
Figures.....	118
GENERAL DISCUSSION	127

LIST OF TABLES

Table 1.1: Uncertainty in photoreceptor isolation.	59
Table 1.2: Two-filter linear model.	62
Table 2.1: Modulations and contrast values.	92
Table 3.1: Predicted contrasts of the modulations.	126

LIST OF ILLUSTRATIONS

Figure 1.1: Experimental design.....	37
Figure 1.2: S input to the PLR is opponent to L+M and melanopsin.....	38
Figure 1.3: PLR phase reveals synergy and opponency.....	39
Figure 1.4: A two-component linear filter model accounts for the photoreceptor-specific temporal transfer functions of the PLR via S-cone opponency.....	40
Figure 1.5: Group PLR data are well fit by the two component linear filter model.....	41
Figure 1.6: Pupil response to L+M-, melanopsin-, and S-directed modulation scales with background light level.	43
Figure 1.7: Observed S opponency is not due to artifactual stimulation of melanopsin.....	44
Figure 1.8: Similar results obtained with standard and alternative S-directed modulations.	46
Figure 1.9: Similar results obtained when silencing penumbral cones.....	47
Figure 1.10: L+M contrast response function.....	50
Figure 1.11: Pupil responses at the second harmonic.	52
Figure 1.12: Mean pupil diameter does not depend on modulation direction or frequency.....	53
Figure 1.13: Isochromatic responses are approximated by the sum of photoreceptor specific responses.....	54
Figure 1.14: Observed isochromatic and cone-driven temporal transfer functions compared with prior reports.....	55

Figure 1.15: Noise properties of the measures	57
Figure 2.1: Spectral sensitivities and apparatus.....	84
Figure 2.2: Purkinje-tree percepts.....	85
Figure 2.3: Psychophysical rating results.....	86
Figure 2.4: Contrast splatter.....	88
Figure 2.5: Raw fundus photographs.....	90
Figure 2.6: Rating data from the supplemental experiment.	91
Figure 3.1: Overview and experimental design.....	118
Figure 3.2: Temporal transfer functions for the postreceptoral cone pathways.	120
Figure 3.3: Psychophysical nulling.....	121
Figure 3.4: Temporal transfer functions for melanopsin-directed (a) and cone control flicker (b).	122
Figure 3.5: V1 response to melanopsin and control modulations.	123
Figure 3.6: Pupil response to 0.1 Hz modulations.....	124
Figure 3.7: Temporal transfer functions for penumbral cone ($L^* + M^*$)-directed flicker.....	125

INTRODUCTION

"Psychophysicists lose interest in anything as soon as you can see it."

—Donald MacLeod quoting Fergus Campbell

(Vision Sciences Society 2016)

The following introduction was written as an in-depth background to the melanopsin photopigment and its functional significance, with special emphasis on the topics most relevant for this dissertation, including its functional significance and its spectral sensitivity. It is recognized that this introduction is neither exhaustive nor definitive and represents merely a snapshot of the state of knowledge when this dissertation was written (2016). The three chapters of this dissertation each also have an introduction, serving as background information to the questions they address individually.

Chapters 1, 2, and 3 in this dissertation were published as peer-reviewed articles [1-3]. To ensure consistency within this dissertation, the reference style was homogenized. Therefore, there will be differences between the published papers and the reproductions of these within this document. Parts of this work have been presented at conferences with published abstracts [4-7]. In Chapter 1, Supplemental Figures S1-S10 from the original paper have been relabeled Figures 1.6-1.15.

The human retina contains three classes of cones (L, M and S cones), rods, and the recently discovered *intrinsically photosensitive retinal ganglion cells* (ipRGCs) expressing the photopigment melanopsin. These ipRGCs receive synaptic inputs from rods and cones, which

has the effect that response of ipRGCs is a mixture of drive from synaptic inputs (extrinsic photosensitivity) as well as their intrinsic photosensitivity.

The intrinsic photoresponse of ipRGCs is sluggish, while the extrinsic photosensitivity has similar kinetics to other non-melanopsin-expressing RGC types [8]. ipRGCs have been found to spike continuously in response to 10 hour steps of increases in light intensity [9], suggesting that these cells could track gradual irradiance changes through spiking over long time scales. However, this sustained firing can also be induced in the absence of melanopsin in knock-out mice, and in response to light steps below the melanopsin threshold [9]. It is therefore possible that the sluggishness of ipRGCs is not simply mediated by the presence of the melanopsin as ipRGCs appear to preserve their sluggishness in the absence of melanopsin.

Melanopsin is encoded by the OPN4 gene [10]. This gene produces multiple variants of the melanopsin protein called *isoforms* due to a process called alternative splicing. Two melanopsin isoforms OPN4L and OPN4S have been found in mice [11] and humans [12]. The previously identified M1 ipRGC subtype contains both OPN4L and OPN4S, while the M2 ipRGC subtype contains exclusively OPN4L [13]. Since M1 and M2 cells and the expression of these isoforms appear at different developmental stages, it has been suggested that the different isoforms also fulfill different developmental roles [13]. While both isoforms regulate sleep and circadian control, OPN4S is differentially involved in the regulation of pupil size, while OPN4L mediates negative masking to light in mice [12]. The role of these two isoforms in humans has so far not been established.

While different *isoforms* refer to different forms of a protein encoded by the same gene, a different source of genetic variability exists by virtue of *single nucleotide polymorphisms* (SNPs). SNPs are variations in a single base pair in a DNA sequence. In humans, OPN4 has two known functional single nucleotide polymorphisms (SNPs) in humans: The I394T or Ile394Thr (*rs1079610*) polymorphism [14, 15], and the P10L (*rs2675703*) polymorphism [16, 17]. In the I394T

polymorphism, carriers of the C allele have found to have smaller steady-state pupil sizes under high illumination and larger pupil sizes under low illumination than TT carriers [15]. There were also differences in the dynamic pupillary light reflex, with more constriction in C allele carriers for broadband white light [15], and for blue and green light relative to red light [14]. There is also evidence for a modulation of post-illumination of blue responses to blue light [18] by I394T, and evidence that CC carriers have later sleep onset [19]. The P10L variant appears to be implicated in seasonal affective disorder (SAD), with the TT genotype being associated with SAD [17], and later sleep onset [16]. Large-population studies assessing phenotypic differences due to these polymorphisms are still outstanding.

ipRGC projections and subtypes

Rodents. In mice, melanopsin-containing retinal ganglion cells have been found to project to a variety of structures in the hypothalamus (suprachiasmatic nucleus (SCN) [20-25], ventral subparaventricular zone (*vSPZ*) [22], habenula [23]), the thalamus (dorsal and ventral lateral geniculate nucleus (*dLGN/vLGN*) [25]; intergeniculate leaflet (*IGL*) [21, 23]; lateral posterior thalamic nuclei (LP; pulvinar) [26]; dorsal posterior thalamus (Po) [26], midbrain structures (olivary pretectal nuclei (*OPN*) [21, 24, 25], superior colliculus (SC) [23, 25]), and the amygdala [23, 25]. ipRGCs densely innervate a large variety of brain structures, underlining the importance of melanopsin on behavioural light responses.

The rodent retina has at least five ipRGC subtypes which differ in their size, dendritic field, stratification and projections [27]. The M1 cell stratifies in the OFF layer, while M2, M4 and M5 stratify in the ON layer; M3 cells bistratify in both ON and OFF sublamina [27]. The M1 cell type can be further subdivided into two classes defined by the presence of the Brn3b transcription factor. Brn3b-negative M1 cells innervate the SCN, while Brn3b-positive M1 cells innervate other brain regions including the OPN shell [28]. M2, M4 and M5 cells project to the dLGN, SC and OPN core [27]; the projections of M3 cells are not known. The M4 subtype is considered to be the

same as the previously identified ON alpha cell [29, 30], displaying long and persistent irradiance responses. Across the five known subtypes, there is also a large diversity of photoresponses, center-surround structure and kinetics [31].

Future work disentangling the heterogeneous population of RGCs in the mouse retina using morphological, genetic or multi-electrode assays [e.g. 32] will further clarify the mapping between traditional RGC classifications and melanopsin expression and subtypes, and disentangle the diversity of ipRGCs.

Primates. An early study of melanopsin expression in the human retina proposed that the melanopsin-containing retinal ganglion cells project to the SCN in hypothalamus [10]. This was confirmed by the finding that melanopsin and pituitary adenylate cyclase-activating polypeptide (*PACAP*), a protein expressed in neurons in the retinohypothalamic tract (RHT), are co-localized within ipRGCs [33]. Later work in macaque monkeys found that ipRGCs project to LGN and the pretectum [34], the SCN, and superior colliculus (SC) [35]. There are two known morphologically distinct ipRGC populations [36-38], separated by the primary location of their stratification (inner vs. outer retina). Inner stratifying cells furthermore had larger somas and a higher degree of dendritic branching than outer stratifying cells. It has been suggested that these represent the primate homologue to the M1 and M2 cells in rodents, respectively. Both subtypes stratifying cells project to LGN [38], but it is not known if they differ in their projections to other brain areas.

In the retina, melanopsin is thought to be exclusively expressed in RGCs, with two notable exceptions. One immunohistological study found cones in the human peripheral retina (estimated to be ~0.1-0.5% of the total cone population) expressing melanopsin in the outer segments in the absence of other opsins [39]. Whether these ‘melanopsin cones’ provide functional output, and contribute to vision is not known. Another study found melanopsin expressed in the retinal pigment epithelium in mice [40]. Outside of the retina, melanopsin has also been found to be expressed in the mouse iris [41, 42], mediating retina-independent pupillary responses (found

previously in other animal species [43-45]), and in murine blood vessels where melanopsin is thought to mediate photorelaxation [46].

Spectral sensitivity of melanopsin

Spectral sensitivity determined from direct measurements of isolated melanopsin. Because of its low natural abundance, direct characterization of melanopsin spectral absorbance has been technically challenging. Only one direct measurement aggregating ipRGCs from multiple mouse retinae found a peak spectral absorbance at 500 nm [47]. Key data on the spectral sensitivity of the melanopsin photopigment comes from studies in which the melanopsin gene is expressed in a host organism which does not naturally carry it called the heterologous host or heterologous expression system [48]. Most of these studies, reviewed by Shirzad-Wasei and DeGrip [48], find peak absorbance between in the 460-490 nm range for murine [49-52], amphioxus [53], chicken [54], teleost [55] and human [56, 57] melanopsin. It is to be noted that these studies were largely performed in the HEK293 (human embryonic kidney cells) heterologous expression system (except for Panda, et al. [49], performed in oocytes of *Xenopus*; and Shirzad-Wasei, et al. [52] using the Sf9 insect cell line). Studies using a different heterologous host have previously found maximum absorbance shifted towards shorter wavelengths for murine [58] melanopsin expressed in COS-1 cells and murine [11] and human [59] melanopsin in Neuro-2a cells, with a higher sensitivity at 420 nm than at the purported peak at 480 nm. These data are not easy to reconcile at present [48].

Spectral sensitivity determined from electrophysiological recordings of ipRGCs. Electrophysiological recordings under synaptic blockade have found that ipRGCs have a peak spectral sensitivity around 480 nm in mice [60, 61] and macaque monkeys [34]. A full characterization of the spectral properties of the melanopsin-mediated photosensitivity in all ipRGC subtypes (at least five in mice; at least two in primates; see above) is presently not available.

Spectral sensitivity determined from PLR. In mice lacking cones and rods (*rd/rd cl*), the spectral sensitivity of the steady-state pupil constriction has a peak spectral sensitivity at ~480 nm [62], consistent with the melanopsin photopigment. This was also found for macaque monkeys with pharmacological blockade of the synaptic input from rods and cones [63], and for the persistent pupillary constriction after stimulus offset in humans [63]. This persistent pupillary constriction was termed the post-illumination pupil reflex (PIPR), and its spectral sensitivity was corroborated to be consistent with a 480 nm photopigment [64, 65], which is robust to metrics addressing early and late components of the post-illumination persistent pupil constriction [66].

The steady-state pupil diameter in humans is dominated mostly by the melanopsin response, though for light levels below the melanopsin threshold rods also contribute the steady-state pupil diameter [67]. Studies on the steady-state spectral sensitivity of the pupil predating the discovery to melanopsin are largely in agreement with this finding [68-70], with the notable exception of Alpern and Campbell [71]. In determining the spectral sensitivity of the steady-state pupil response, there are choices of field size of the stimulus, exposure duration, criterion response, and presence or absence of an adapting light which may contribute to different empirical spectral sensitivities [67]. Of note is that the *transient* pupillary constriction as measured with the exchange of monochromatic lights [71, 72], incremental light stimuli on an adapting background [73], or by only considering the transient pupillary response to a light onset [70, 74] follows a three-lobed spectral sensitivity typically found for the psychophysical determination of increment thresholds [75, 76].

Spectral sensitivity determined from circadian entrainment. The spectral sensitivity of circadian phase shifting in transgenic mice lacking cones and rods (*rd/rd cl*) as assayed by wheel-running [77] has been found to peak at 481 nm. This is consistent with the spectral sensitivity of ipRGCs *in vivo*, and provides evidence that melanopsin indeed mediates circadian phase shifting in the absence of cone and rod photoreception. A study on circadian phase shifting in hamsters

predating the discovery of melanopsin had similarly found that phase shifting is mediated by a photopigment with a maximum spectral sensitivity around 500 nm, but with threshold and temporal properties inconsistent with rod phototransduction [78], foreshadowing the discovery of melanopsin.

Spectral sensitivity determined from melatonin suppression. Two studies published in 2001 found that suppression of melatonin is driven by a non-rod, non-cone photopigment with a peak sensitivity at 459 nm [79] and 464 nm [80] which is accepted to be melanopsin. The inconsistency of melatonin suppression with cone spectral sensitivity had been noted previously, and it had been suggested that rods mediated melatonin suppression [81, 82]. It is notable that the peak spectral sensitivity found in by Brainard, et al. [80] and Thapan, et al. [79] is shifted by ~20 nm relative to the ‘standard’ 480 nm peak spectral sensitivity of melanopsin (which is further shifted due to pre-receptoral filtering, see below). This may be due to signals from cones contributing to melatonin suppression [83-85], or combinations of cone signals [86]. A more recent study [87] found that the peak spectral sensitivity of melatonin suppression is ~484 nm in a young population and ~494 nm in an older population. This spectral shift is consistent with the “yellowing” of the lens of the eye as a function of age. The difference of peak spectral sensitivity by ~20 nm between this recent study and the earlier two studies [79, 80] may be related to differences in the methods used to assess melatonin suppression. While the two earlier studies [79, 80] measured the dose-response relationship of melatonin suppression as a function of irradiance, and then extracting a criterion response (constant response), the study by Najjar, et al. [87] measured the melatonin suppression response to a stimuli of various wavelengths at a the same intensity (constant energy), which could induce biases in the determination of the spectral sensitivity.

Spectral sensitivity determined from ERG modulation. In an early study, Hankins and Lucas [88] investigated how prior light exposure can modulate the implicit time of the *b* wave in the human

electroretinogram (ERG). The *b* wave timing becomes shorter upon light exposure, the spectral sensitivity of which peaks at 483 nm. This peak is in close agreement with the spectral sensitivity of melanopsin measured electrophysiologically *in vivo*, under heterologous expression, or inferred from circadian photoentrainment in mice, and the certain features of the PLR. Later work (see below) has elucidated a role of melanopsin in modulating the sensitivity of cone and rod sensitivity in mice [89, 90].

Melanopsin multistability. The melanopsin photopigment has been found to have multiple photoresponsive states, making it a bistable [53, 59] or even multistable [91] photopigment. Recent work has found that the spectral sensitivity of deactivation of heterologously expressed melanopsin is around 560 nm for both murine and human melanopsin [57]. Using the human PLR as a behavioral assay, Mure, et al. [92] found that pre-exposure to long-wavelength light enhanced pupil constriction amplitude, while pre-exposure to short-wavelength light had the reverse effect. This finding was interpreted as a direct functional consequence of melanopsin bistability, with melanopsin existing in two conformations with different peak spectral sensitivities (481 nm and 587 nm). Whether or not melanopsin bistability has important functional consequences is not known. An alternative explanation for the enhancement of short-wavelength responses after long-wavelength exposure compared to after short-wavelength exposure might simply be that after short-wavelength exposure, the melanopsin system is more adapted., leading to a smaller evoked response to a subsequent stimulus.

Standardization of melanopsin sensitivity curves. Spectral sensitivity measurements are typically summarized by fitting a standard photopigment template — a *nomogram* — to the empirically determined data points. The use of a common template is motivated by the observation that frequency scaling of spectral sensitivities derived from electrophysiological and psychophysical measurements provide a common shape [93, 94]. Investigators have previously used the Dartnall [95] nomogram [e.g. 62, 79], the Lamb [94] nomogram [e.g. 60, 61], the Partridge & De Grip [96]

nomogram [e.g. 80, 88] as well as the Govardovskii [97] nomogram [e.g. 56, 57]. Efforts to derive a standardized action spectrum for circadian light applicable to humans [e.g. 98, 99] have employed a combination of the empirical melatonin suppression curves [79, 80]. More recently, ‘melanopic’ spectral sensitivity curves [100, 101] have been proposed, the latest of which provides a spectrum to calculate ‘melanopic’ illuminance [102, 103]. At present, there is no melanopsin standard similar to the photopic luminosity function $V(\lambda)$ [104], the scotopic luminosity function $V'(\lambda)$ [105], or other functions to calculate photometric and colorimetric quantities.

The significance of the 480 nm peak. Direct spectral measurements of the melanopsin photopigment, and spectral sensitivities inferred from physiological and behavioral measurements place the peak sensitivity of melanopsin at 480 nm. It has been suggested that this spectral peak serves to encode the blue shifted twilight illumination [106, 107], representing a key point in the diurnal cycle relevant for circadian rhythm control. A theoretical analysis of which photopigments could optimally encode spectral shifts during twilight is still outstanding. A computational analysis of photoreceptor excitations based on hyperspectral natural images has found that including melanopsin provides at best a modest advantage over a model including just L, M, and S cones and rods for optimally encoding image content [108].

Spectral sensitivity shifts due to lens aging. The human crystalline lens increases in optical density as a function of age [e.g. 109, 110], with an increase in the filtering of short-wavelength light. Using empirical data, it has been found that at 480 nm, the peak spectral sensitivity of melanopsin, up to 72% less light is transmitted for an 80-year old observer compared to a 10-year old observer [111]. However, not only does the absolute sensitivity change with increasing lens optical density, but also the relative spectral sensitivity, displacing the peak spectral sensitivity to longer wavelengths for older observers: The peak spectral sensitivity of melanopsin after pre-receptoral filtering (including lens) is ~488 nm for a 20-year old observer, and ~496 nm for an 80-year old observer. Empirical data on melatonin suppression in young and old observers are

consistent with this prediction [87], showing a shift in the spectral sensitivity of melatonin suppression towards longer wavelengths for older people. However, the overall melatonin suppression was not affected, suggesting that there are compensatory and adaptive mechanisms in place to discount the light loss due to the reduction in lens transmittance.

It is to be noted that many studies assessing the spectral sensitivity of melanopsin-mediated functions assayed in the living animal or human or in the dish do not consider that the expected peak spectral sensitivity of melanopsin function should be displaced to longer wavelengths due to pre-receptoral filtering. Due to large differences in the transmittance spectra of the ocular media across species [112], these shifts will differ between different animal models. Furthermore, the pigment optical density might also be different in the dish compared to in the eye, adding yet another uncertainty in the spectral sensitivity.

Melanopsin contributions to visual function

Regulation of pupil size. Melanopsin has been found to control pupil size (see above for discussion of the spectral sensitivity of pupil size). In humans, direct measurements of melanopsin function have been performed with the *method of silent substitution* [113]. In brief, in the method of silent substitution, two pairs of lights are shown to an observer which have an equal amount of action on one class of photoreceptors and a differential amount of excitation of a different class of photoreceptors. For example, using four independent light sources under photopic conditions, it is possible to find so-called metamers which are matched in cone excitation and only differ in melanopsin excitation [114, 115]. Due to the technical challenges that are involved in finding these metamers, the method of silent substitution has only recently become practical to study melanopsin responses *in vivo* in humans, and few studies have been performed [116-120].

As an alternative and indirect pupillometric assay of ipRGC function, the post-illumination pupil response (PIPR), has seen rapid adoption for measurement of clinical indices of retinal and ocular disease. In brief, red and blue light are flashed from dark, and the pupil response is measured. The PIPR corresponds to the difference in recovery from constriction due to the flash, with the response to blue light being delayed [121]. Previous investigators have investigated the PIPR in glaucoma [122-126], retinitis pigmentosa [127-129], diabetic retinopathy [130], Leber's congenital amaurosis (LCA) [128, 131], Leber's hereditary optic neuropathy (LHON) [132, 133], *RPE65* mutations [134], hereditary optic neuropathy [124], outer retinal disease [135], unilateral anterior ischemic optic neuropathy [136-138], age-related macular degeneration [139], autosomal dominant optic atrophy [140], rod dysfunction [136], achromatopsia [136], enhanced S cone syndrome [141], and after cataract surgery and implantation of interocular lenses [142]. ipRGC has also been assessed with the PIPR in non-ocular clinical conditions such as seasonal affective disorder [18], Gaucher disease [143], and idiopathic intracranial hypertension [144]. Basic studies investigating the PIPR have focused on its relationship with circadian rhythms [145, 146], age [147, 148], refractive status [148], iris thickness and other ocular parameters [149], its temporal [66, 128, 150, 151] and spatial [152] properties, its test-retest reliability [128, 152-155], in response to pharmacological agents [156], differences between the direct and consensual PIPR measure [157], as a function of season [158], as a function of viewing conditions [159].

The PIPR continues to be an attractive tool for researchers wishing to investigate melanopsin-mediated pupillary function. It is a convenient method to preferentially target certain photoreceptor classes with relative robustness towards uncertainty in the photoreceptor spectral sensitivities. However, the method is not without limitations: From first principles it follows that preferential photoreceptor activation is not the same as selective isolation of a photoreceptors. Furthermore, the precise contributions of rods, cones and ipRGCs to the PIPR and their spatial, temporal and adaptive components are not fully understood.

ERG. As discussed earlier, an early study found that the timing of the *b* wave in the human ERG [88] can be shifted by light exposure, with the likely encoding mechanism being melanopsin. Direct influences of melanopsin on the ERG have also been reported in humans [160, 161]. More work needs to be done to establish measurable melanopsin-mediated responses in the human ERG and their mechanisms. Due to the relatively low number of melanopsin-containing ipRGCs, the possibility of a melanopsin contribution to ERG responses not attributable to stimulus uncertainty seems unlikely.

Psychophysical detection and discrimination. Evidence for melanopsin signals contributing to visual perception in humans comes from a case report [162] in which a subject with total cone and rod loss due to autosomal cone-rod dystrophy was able to identify flashes of 481 nm light significantly above a chance, and at chance at other wavelengths. Due to the wavelength specificity of this residual visual function, it was inferred that melanopsin may provide signals to aid light detection in the absence of cones and rods in humans. Later work utilizing the silent substitution methodology identified a role for melanopsin in brightness discrimination [163] with higher melanopsin contrast leading to brighter percepts. Psychophysical measurements of peripheral sensitivity to high frequency flicker in the cone-silent direction at rod-saturating conditions revealed sensitivity not accounted for by cones and rods [120, 164].

Light adaptation. Work in mice has identified a role of melanopsin in mediating cone- and rod-driven responses [89, 90], implicating that melanopsin can provide a parallel pathway for light adaptation that is relatively robust to moment-to-moment changes in illumination. Whether melanopsin also modulates cone- and rod-driven responses in the human retina is not at present known.

Photophobia. Painful responses to light stimuli are common in migraine sufferers [165, 166], even in the absence of functional light sensitivity [167, 168], with a bias towards short-wavelength lights [169]. In mice, a neural mechanism for photophobia has been found in the form of ipRGCs

projecting to trigeminal dura-sensitive neurons in the thalamus projecting to somatosensory cortices [168]. Whether abnormal or heightened melanopsin sensitivity is also the mechanism for photophobia in migraineurs is at present not known. Recent work has also pointed to a role of cones in mediating photophobia [170], so it is likely that melanopsin may not be the only photopigment mediating photophobia.

Retinal feedback. Melanopsin knock-out mice ($\text{Opn}4^{-/-}$) have been found to lack diurnal modulation of cone ERG signals [171], pointing to a role for ipRGCs in providing retinal feedback. Indeed, ipRGCs provide feedback to dopamergetic amacrine neurons in mice [172], likely via an AMPA-mediated pathway [173], and to displaced non-dopaminergic amacrine cells in rats [174]. However, the regulation of retinal dopamine can also take place independent of melanopsin [175], pointing to a complicated relationship between the regulation of dopamine release in the retina and ipRGC function. In macaques and humans, the axons of ipRGCs appear to have axon collaterals, i.e. nerve fibers branching off from the main axon [176], suggesting that these collaterals may be the conduit for intraretinal regulation through ipRGCs.

Other NIF functions. In humans, short-wavelength light has been found to affect other non-image-forming visual function apart from the pupil and melatonin suppression, namely circadian phase shifting [177-179], modulation of alertness [180-185], sleep architecture [186], waking EEG [182], and cortisol levels [187-189]. Whether this bias towards shorter wavelength is solely due to melanopsin is not at present clarified.

Roles of melanopsin in development. The expression of melanopsin in murine and human retina occurs before birth [190], and melanopsin is photosensitive well before rods and cones in mice [191]. Melanopsin also contributes to developmental programs controlling the number of retinal neurons and retinal vasculature growth [192], and alters the structure of the visual system in development through retinal waves [192]. It has been suggested that ipRGCs may be involved in

the development of refractive error or myopia [193], but at present no empirical data support this claim.

The preceding discussion only served as a snapshot of the research relevant for the following chapters. It should already be clear from this introduction, however, that research on melanopsin remains a fascinating and fruitful ground for discovery.

OPPONENT MELANOPSIN AND S-CONE SIGNALS IN THE HUMAN PUPILLARY
LIGHT RESPONSE (Spitschan *et al.*, 2014)

Note: This chapter was published as Spitschan, et al. [1].

Abstract

In the human, cone photoreceptors (L, M, and S) and the melanopsin-containing, intrinsically-photosensitive retinal ganglion cells (ipRGCs) are active at daytime light intensities. Signals from cones are combined both additively and in opposition to create the perception of overall light and color. Similar mechanisms appear to be at work in the control of the pupil response to light. Uncharacterized however, is the relative contribution of melanopsin and S-cones, with their overlapping, short-wavelength spectral sensitivities. We measured the response of the human pupil to the separate stimulation of the cones and melanopsin at a range of temporal frequencies under photopic conditions. The S-cone and melanopsin photoreceptor channels were found to be low-pass, in contrast to a band-pass response of the pupil to L+M cone signals. An examination of the phase relationships of the evoked responses revealed that melanopsin signals add with signals from L and M cones but are opposed by signals from S-cones in control of the pupil. The opposition of the S-cones is revealed in a seemingly paradoxical dilation of the pupil to greater S-cone photon capture. This surprising result is explained by the neurophysiological properties of ipRGCs found in animal studies.

Significance Statement

Our eyes sense bright light using cones (L, M, and S) and recently discovered melanopsin-containing ganglion cells. Both S-cones and melanopsin respond to blueish (short-wavelength) light. How does melanopsin interact with the cones in visual function? We measured the response of the human pupil to isolated stimulation of the different photoreceptors. Our work reveals a curious, opponent response to blue light in the otherwise familiar pupillary light

response. Increased stimulation of S-cones can cause the pupil to dilate, but this effect is usually masked by a stronger and opposite response from melanopsin-containing cells. Our results have clinical importance because the sensing of blue light is known to be related to seasonal depression, sleep, and pain from bright light.

Background

Under daylight conditions, human visual perception originates with signals generated by three classes of cone photoreceptors (the L, M, and S-cones; Fig. 1.1a, left) with peak sensitivities at long, middle, and short wavelengths of visible light (Fig. 1.1a, center).

Distinct neural pathways process signals originating in cone photoreceptors for visual perception. Luminance pathways combine signals from separate classes of cones synergistically, providing a spectrally-broadband indication of the overall light intensity at each location in the retinal image. Red-green and blue-yellow chromatic channels combine signals from separate classes of cones in an opponent (subtractive) fashion, providing sensitivity to the relative spectral content of light and supporting the perception of color independent of luminance [194].

A parallel set of pathways contribute to the response of the pupil of the eye to light. Most familiar is a synergistic cone effect that causes the pupil to constrict in response to increased luminance. Illustrating a commonality of principles that characterize neural mechanisms for perception and pupil response, rectified signals from red-green and blue-yellow opponent channels also contribute to the pupil light response [72-74, 195-197].

Recently, it has been discovered that mammalian retinas contain an additional photoreceptor class that also operates under daylight conditions. Intrinsically-photosensitive retinal ganglion cells (ipRGCs) express the photopigment melanopsin, which has a peak spectral sensitivity (480 nm) between that of S and M cones [10, 60]. Among other, “non-image-forming” functions of the eye, melanopsin containing ipRGCs contribute to a delayed and sustained constriction of the

pupil [63]. Studies in patients with loss of photoreceptor function [162] suggest that melanopsin may also contribute to conscious visual perception.

The discovery of an additional photoreceptor class raises the fundamental question of how melanopsin signals are combined with those from the cones. Do melanopsin signals add to cones to measure overall light intensity? Or do they interact in an opponent fashion, enhancing the ability to detect changes in the relative spectrum of incident light?

Single-unit studies of the primate retina find that L and M cone signals add with those of melanopsin to produce the responses of ipRGCs, but suggest that signals from S-cones are inhibitory [34] (Fig. 1.1a, right). Prior studies of short-wavelength light upon the human pupil response preceded the discovery of melanopsin and have offered complicated results. A transient constriction of the pupil was found to follow the offset of a short-wavelength stimulus on a long-wavelength background [74], and the results were interpreted in terms of an S-cone opponent input to the control of the pupil. On the other hand, alternation between short and long wavelength tritanopic metamers which yielded equivalent excitation of L and M cones was found to modulate the pupil in a manner suggesting in-phase S and L/M cone contributions to the pupillary light response [198]. Critically, the interpretation of these earlier results—and particularly the relative contribution of the S-cones and melanopsin to the pupil response—must be revisited given the overlapping spectral sensitivities of these two photoreceptor classes and the unknown role of melanopsin in mediating the earlier results.

Here we study how melanopsin and the three classes of cones contribute to the human pupillary light response (PLR). Despite the intuition that pupil size should be responsive to the overall intensity of the incident light, our results reveal that a spectrally-opponent system involving melanopsin contributes to pupil control at photopic light levels. The nature of this response reflects, qualitatively, the spectral opponency seen in ipRGCs: signals from melanopsin combine additively with those from L and M cones, and are opposed by signals from S-cones.

Results

Using an infrared camera, we measured the consensual pupillary light response (PLR) of human participants while they observed sinusoidal modulations in the spectrum of a light (Fig. 1.1b). The stimulus modulations were designed to target specific photoreceptors. The cones and melanopsin have different but overlapping spectral sensitivities. Despite the overlap, it is possible to create sets of light spectra such that the absorption of photons is constant for all of the photoreceptor classes except one [113, 116, 199] (Fig. 1.1c). Modulation between a pair of these “silent substitution” spectra increases and decreases the response of (for example) melanopsin containing ipRGCs, while maintaining nominally constant stimulation of the cones. Separate modulations were designed for melanopsin, S-cones, and L+M cones together (a modulation that varied luminance as well as chromaticity). An isochromatic modulation (melanopsin+S+M+L) was also used. All modulations were designed to produce 50% contrast on their targeted photoreceptor(s). Rods were silenced by modulating the spectra about a photopic background ($\sim 800 \text{ cd/m}^2$). The stimulus was wide-field (27°), spatially uniform, and had the central 5° obscured to avoid variation in photoreceptor spectral sensitivity across the visual field caused by the presence of the foveal macular pigment [200]. Simulations and control experiments support the specificity of the photoreceptor isolation (see Figs. S1-5, Table 1.1).

We measured pupil responses from sixteen subjects while they observed the different photoreceptor directed modulations at two flicker rates (0.05 and 0.5 Hz). The effect of the stimulation is apparent as a sinusoidal oscillation at the stimulation frequency in the raw traces of pupil response from one subject (Fig. 1.2a). Measurable pupil responses at the second harmonic of the stimulation frequency were also observed (Fig. 1.11). As the mean pupil diameter was equivalent across photoreceptor stimulation directions and frequencies (Fig. 1.12), the pupil response can be expressed as a percent change.

The average response across cycles of the modulation at the stimulus frequency (Fig. 1.2b) reveals in both individuals and the group data that the L+M and melanopsin directed modulations produce pupil responses of similar phase. The S-cone modulation, however, produced responses with markedly different phase.

The relations between the different photoreceptor-driven responses are more easily apprehended on a polar plot (Fig. 1.3). Retinal ganglion cell electrophysiology suggests that melanopsin and L+M signals combine additively [34]. We examined the relative amplitude and phase response for each subject to L+M and melanopsin modulations at the two frequencies (Fig. 1.3a). For each subject and temporal frequency these responses are expressed relative to the complex sum of responses across the L+M, melanopsin, and S photoreceptor directions for that subject (which approximates the pupil response to an isochromatic modulation; Fig. 1.13). This normalization removes from the data individual differences in an overall delay between stimulus onset and pupil response common to all photoreceptors.

At high temporal frequency (0.5 Hz), the melanopsin and L+M evoked pupillary responses are in phase (Fig. 1.3a, upper panel). At the lower frequency (0.05 Hz), L+M and melanopsin evoked responses become desynchronized in quadrature phase (Fig. 1.3b, lower panel); this phase effect is examined further below.

Electrophysiology studies suggests that the S-cone inputs to ipRGCs are opponent to the melanopsin and luminance signals [34 Allen, 2011 #17642]. We examined the relationship between S-cone driven pupil responses and a putative “pupil brightness” channel, constructed as the complex sum of the melanopsin and L+M cone driven responses. Across subjects, the S-cones produced an anti-phase, steady-state pupil response at 0.5 and 0.05 Hz relative to the pupil brightness driven response (Fig. 1.3b).

Despite the generally anti-phase relationship of S-cone responses across subjects, there were individual differences in the phase effects greater than individual measurement error (see on-line dataset, SI Text S2). Additionally, we wished to understand the origin of the quadrature phase desynchronization between melanopsin and L+M driven pupil responses at lower frequencies. We studied two subjects in greater depth, measuring pupil responses to the photoreceptor directed modulations at six temporal frequencies between 0.01 and 2 Hz. Fig. 1.4a presents the amplitude responses across temporal frequencies for both subjects. These transfer functions characterize the temporal filtering properties of each photoreceptor channel. The pupil response mediated by the L+M cone pathway was band-pass, with a maximum response at 0.1 Hz, rolling off for higher frequencies. The responses to melanopsin and S-cone stimulation were low-pass, maximal at the lowest measured modulation frequency (0.01 Hz), and markedly reduced by 0.5 Hz.

Fig. 1.4b presents the phase of the response across frequencies of stimulation. We modeled simultaneously the amplitude and phase data with a time-invariant, linear model composed of a “fast” and “slow” temporal filter [201]. The amplitude and phase data were well fit by the model, including a fixed temporal delay in both observers across photoreceptor channels of approximately 250 msec and a negative amplitude response to S-cone modulation for the fast filter (see on-line dataset, SI Text S2). The separate filter properties for L+M and melanopsin account for the quadrature phase desynchronization of these responses at lower temporal frequencies. Further, differences in model parameters account for the finding in subject 02 of an S-cone response that appears in-phase with L+M and melanopsin responses at low frequencies, despite having an S-cone opponent input to the fast filter of the model PLR. This individual difference arises, at least in part, because the slow filter S-cone component is of the same sign as the melanopsin component of the response for this subject.

We then applied this model to the group data. We obtained the average amplitude and phase of response across the 16 subjects for each combination of photoreceptor target and modulation frequency. The two filter model fits the average amplitude and phase data (Fig. 1.5a) with parameters similar to those found for subject 01 (see on-line dataset, SI Text S2). When expressed as a polar plot (Fig. 1.5b), the agreement between the group data and model fits are apparent. Interestingly, there is systematic “rotation” of the phase of both the pupil brightness and S-cone responses at the lower temporal frequency that is not captured by the model. This may result from individual differences in the phase of S-cone responses at low temporal frequencies, as is seen between subject 01 and subject 02 (Fig. 1.4), as the average data do not fully constrain the model and the fits shown are based on parameters obtained for subject 01.

Discussion

We examine how signals originating in the melanopsin ipRGCs combine with signals from cones to regulate the size of the human pupil under daylight conditions. Although it is intuitive that the pupil should contract when more light stimulates any of these photoreceptors, we find instead that signals from L+M cones and melanopsin are opposed by signals from S-cones in the PLR.

This result, although counterintuitive for the pupil, is consistent with the cellular properties of the ipRGCs. Giant ipRGCs receive inhibitory input from S-cones [34] but it is not immediately clear which synaptic inputs mediate this S-OFF sensitivity [202]. As there is presently no evidence for an S-OFF bipolar cell in the primate retina [202], the opponent pupil response we observe to S-cone stimulation seems likely explained by the negative S-cone input to ipRGCs.

Our finding of antagonistic effects of short-wavelength light upon the human pupil response helps clarify prior results. In a previous study, weak short-wavelength contributions relative to L and M cones were observed variably across observers [198]. The weak nature of the responses they found may result from opposed S and melanopsin stimulation. Another study examined the transient, miotic pupil OFF response to cessation of a temporally extended light pulse [74]. This

constrictive OFF response was observed under all wavelength conditions, but the size of the constriction was found to decrease with increasing peak wavelength of the monochromatic light used in the study. The authors observed that the shape of the short-wavelength lobe of the transient OFF response changed with stimulus amplitude, which they interpreted as a ‘failure of univariance’ and consistent with the existence of an additional, then unknown, photopigment [74]. The opposed S-cone and melanopsin driven pupillary responses we find helps explain this result.

Despite the opponent S-cone effect, a paradoxical dilation of the pupil in response to a narrow-band blue light stimulus is not seen under physiologic conditions. It appears this is because the constrictive effect of melanopsin stimulation overwhelms the smaller S-cone driven responses. Interestingly, a transient, paradoxical constriction of the pupil when switching to darkness from bright light is a feature of several human retinal disorders [203] raising the possibility that relative disruption of photoreceptor classes can reveal the opponency inherent in the PLR.

In agreement with prior work [204] we find that melanopsin provides an ever greater input to pupil control at ever longer time scales, reaching a plateau at our lowest studied frequency of 0.01 Hz. This is consistent with a long time scale of integration of melanopsin signals [34, 60, 205]. At higher frequencies the melanopsin contribution to the pupil is markedly attenuated, falling to a fractional component above 0.5 Hz. The small response that remains at higher temporal frequencies could derive from imperfections in our stimulus precision. We calculate that our nominally melanopsin isolating stimulus might produce approximately 4% of residual stimulation of L and M cones, respectively (Fig. 1.7; this residual stimulation was approximately 2% in control experiments with further stimulus refinements, Fig. 1.10). While this small degree of stimulus “splatter” cannot account for the robust melanopsin driven response observed at low temporal frequencies (where it matches and exceeds L+M driven responses) it could contribute to the small response that remains above 0.5 Hz.

There have been several prior studies of the pupil temporal transfer function using either broadband spectral modulation [206-213] or monochromatic light [214, 215]. A low-pass pupil response with maximal amplitude at the lowest measured modulation frequency is generally found (Fig. 1.14), as is the case for our isochromatic modulation (Fig. 1.13). This overall response combines the contributions of the individual photoreceptors, shown here to be low-pass for S-cone and melanopsin and band pass (peaking at 0.1 Hz) for L+M driven modulation. A band-pass response to cone (L+M+S), rod and combined cone-rod directed modulations was also recently reported [119] under mesopic conditions ($\leq 1 \text{ cd/m}^2$), and a faster peak response (1 Hz) was found as compared to the current work. This may be related to the marked difference in luminance and contrast regimes between this prior work as compared to our study [212].

We found that the amplitude and phase responses of the pupil to differential photoreceptor stimulation were well fit with a linear model of temporal filters. There were, however, systematic aspects of our data not fit by the model. Second harmonic (frequency doubled) pupil responses were observed to each of the photoreceptor directed stimulations (Figure 1.11). These harmonic responses are indicative of a non-linearity in the pupil response and have been reported previously in response to sinusoidal light flux [207]. Our data cannot locate the stage of the non-linearity between the retina and pupillary muscles (including in sub-cortical or cortical pathways). Also, systematic differences were observed between individuals in the phase of S-cone driven responses relative to [L+M+melanopsin] driven responses at low temporal frequencies. We regard the model as a useful tool for capturing the systematic properties of the data, relating individual results to average group effects, and demonstrating the extent of the integrated pupil response that may be explained by linear summation of its photoreceptor components. We do not, however, have a strong stance regarding its plausible implementation in biological systems. Clearly, there is additional information in the photoreceptor specific temporal responses at both the group and individual level to be characterized and related to the neurophysiology of the visual pathway.

Could the synergistic and opponent pupil responses we find also be reflected in perception? Similar to our findings in the pupil response, there is evidence of S-cone opponency in the perception of the luminance of stimuli [216, 217]. In the pupil response, we find that S-cone signals oppose the sum of melanopsin and L+M signals, which we term here pupil “brightness”. Melanopsin may combine with L+M signals in perception as well to provide an overall sense of image brightness. Evidence for this synergy has been reported in mice and people [163]. Our results suggest that the intimate relationship between visual perception and pupil control may continue to hold even as novel photopigments and opponency expand our understanding of the retina.

Methods Summary

Cone spectral sensitivities for construction of photoreceptor directed modulations were taken from tabular values [200], and in the case of melanopsin by shifting the Stockman-Sharpe nomogram to have peak spectral sensitivity at $\lambda_{\text{max}} = 480$ nm. Pre-receptoral filtering of melanopsin was assumed to match that of cones, and we assumed a peak optical density for melanopsin of 0.3.

Observers viewed the sinusoidal spectral modulations in peripheral stimulation with a field diameter of 27.5°. The central 5° diameter of visual angle was obscured and a hair-line vertical, horizontal and annular grid was visible. Pupillary responses were recorded using an infrared eye tracker (Cambridge Research Systems) sampling at 50 Hz.

Two primary observers (sub01 and 02; authors GKA and SJ) viewed the four modulation directions at 0.01, 0.05, 0.1, 0.5, 1 and 2 Hz in trials of 120 seconds each. An additional 14 observers viewed the L+M, melanopsin and S directed stimulation at 0.05 and 0.5 Hz during 45 second trials. Four other observers were recruited for the study but excluded from the protocol because of poor eye tracking due to epicanthal folds or an inability to suppress blinking. All stimuli were presented in counterbalanced sequence. Stimulus onset was windowed by a 3 second half-cosine and stimulus phase was randomized for subs 3-16. A five minute adaptation to the

background preceded each data collection session, and the subject remained exposed to the background between trials.

Responses were averaged across trials. The first 20 or 5 seconds (for the 120 and 45 second duration trials, respectively) of each trial were discarded before fitting to allow measurement of the steady-state pupil response. Response amplitude (in % change units; Fig. 1.12) and phase were obtained by least-squares fitting of a sine and cosine to the average response. Noise measures were obtained by similar fitting to the residuals of the data and analyzing responses at non-stimulated temporal frequencies (Fig. 1.15). We did not correct the data for stimulus-locked noise, but the effect of such corrections would be small (Fig. 1.15).

Detailed methods are described in the SI Methods (SI Text S1).

Supplementary Information: Methods

Overview

To quantify the contributions of different photoreceptors to the pupillary control system and characterize its temporal properties, photoreceptor-directed light stimuli were delivered using the method of silent substitution while the consensual pupillary light response (PLR) was measured. The PLR was probed with spectral modulations directed towards L+M cones, melanopsin, and S cones. An isochromatic modulation that stimulated all photoreceptors with equal contrast and phase was also used.

Observers

A total of 16 observers (age 23 \pm 6; 9 male, 7 female) took part in the experiments. All had corrected visual acuity of 20/30 or better and normal color vision as assessed with Ishihara plates [218]. Two of these observers (subjects 01 and 02; both male; ages 43 and 23; both authors of this paper: GKA and SJ) took part in extensive measurements. Four other observers were recruited for the study but excluded from the protocol because of poor eye tracking due to

epicanthal folds or an inability to suppress blinking. The study was approved by the University of Pennsylvania Institutional Review Board, and all subjects provided written informed consent.

Visual stimuli

Visual stimuli were presented using a custom apparatus that allowed modulation of the spectral content of the light reaching the eye. This was achieved with a digital light integrator (OneLight VISX Spectra Digital Light Engine), which produces arbitrary spectral power distributions within the visible wavelengths. The digital light integrator device works as follows: Light from a xenon arc lamp is collimated and passed through a diffraction grating to spatially separate individual wavelengths. Each wavelength is then imaged on individual columns of a digital light processing (DLP) chip (768 rows by 1024 columns). Each row in a column on the chip can be turned on or off, controlling the emitted power at each wavelength, and thus allowing for the construction of arbitrary spectral power distributions. Rather than individually addressing the 1024 columns of the DLP, chip columns were grouped in bands of 8, yielding a device space with 128 effective monochromatic primaries with a peak spectral power between 414 and 780 nm, spanning the visible spectrum (mean full width at half max of 16 nm \pm 0.6 nm). For the control data presented in Figures S4 and S5, which were collected some months after the main experiments, chip columns were instead grouped in bands of 16 and some of the other parameters provided below (background luminance and chromaticity) also differed slightly from those used in the main experiments.

Stimulus modulations were constructed to selectively stimulate specific classes of photoreceptors (see Dataset S2 for a tabulation of the spectra used), as described below. The contrast of each modulation followed a sinusoidal temporal profile (200 discrete steps), alternating between maximum positive and negative contrast in photoreceptor contrast space around a neutral background (the origin of the photoreceptor contrast space), which was defined as approximately 50% of the maximal intensity of the device primaries (CIE 1931 xy chromaticity, mean \pm 1SD

across experimental sessions: $x = 0.398 \pm 0.01$ $y = 0.433 \pm 0.002$). In a typical experiment, the stimuli were modulated around a background well above rod-saturating levels [219] (background light level varied somewhat as the lamp in the device aged; mean value across sessions 802 cd/m²; range across sessions 382-1033 cd/m²). Stimuli were modulated at 0.01, 0.05, 0.1, 0.5, 1 and 2 Hz for subjects 01 and 02. Subjects 03-16 were studied only at 0.05 and 0.5 Hz.

Four primary directions in photoreceptor contrast were probed: melanopsin-directed, S-cone-directed, L+M (stimulating L and M cones with equal contrast) and isochromatic (equal contrast stimulation of cones and melanopsin). Two variants of the S directed modulation were used, as described below. All modulations produced ~50% predicted contrast on their targeted photoreceptors.

We tested the effect of background luminance on pupil responses by placing neutral density filters with known spectral transmissivity in the optical path (Fig. 1.6). We also examined, in subjects 01 and 02, whether the complex sum of the individual photoreceptor directed modulations (S+M+L+melanopsin) resembled the response to isochromatic modulations (Fig. 1.13). This was the case to good approximation, and the isochromatic response across temporal frequencies resembled previously published data (Figure 1.14). While broad-band, the isochromatic modulation was not simply a scaling of the background spectrum; it was constructed to produce equal predicted contrast on all photoreceptor classes (cones and melanopsin).

Silent substitution

The method of “silent substitution” was used to direct visual stimuli to specific photoreceptors or sets of photoreceptors [113, 116, 199]. Silent substitution stimuli were produced by minimizing an error function over modulation of the device primaries which quantified the quadratic loss between the desired contrast across targeted photoreceptor classes and the photoreceptor contrasts computed from predicted spectra given the device primary modulations [198], subject to

the constraint that the predicted contrast for the to-be-silenced photoreceptors was zero. MATLAB's fmincon routine was used to perform the constrained optimization.

Because the number of device primaries exceeded the number of photoreceptor classes, the optimization was additionally constrained by enforcing smoothness on the predicted modulation spectral power distributions. Modulations were also required to avoid the extrema of the device gamut.

The tabulated 10° Stockman-Sharpe/CIE cone fundamentals were used as estimates of LMS-cone spectral sensitivities [200, 220]. Spectral sensitivity of the melanopsin photopigment was estimated by shifting the Stockman-Sharpe nomogram [220] to have peak spectral sensitivity at $\lambda_{\max} = 480$ nm in accordance with previous reports of melanopsin peak spectral sensitivity [100, 101]. Pre-receptoral filtering was assumed to match that of cones. Melanopsin peak optical density was taken as 0.3, within the range of values (between 0.1 and 0.5) used in other recent pupillometric and psychophysical studies of melanopsin response in human [114, 116, 164] but higher than values suggested by neurophysiology [101, 205]. The spectral sensitivities of the photoreceptors are shown in Fig. 1.1a.

Checks on photoreceptor isolation

The degree to which isolation of specific classes of photoreceptors is achieved by a nominally isolating modulation depends on both certainty regarding the spectral sensitivities of the photoreceptors in question and the quality of the spectral characterization of the digital light integrator.

Uncertainty in photoreceptor sensitivity is produced by individual variation as well as with variation in effective photoreceptor sensitivity across the retina. The CIE standard for cone fundamentals [200] has parameters to account for field size, pupil size, and observer age. These in turn control physiological parameters such as lens and macular pigment density. We explored

how much contrast the ‘standard’ S directed modulation, computed as described above, produced for melanopsin. To do so, we computed the contrast seen by melanopsin photoreceptors as we varied estimates of their spectral sensitivity as illustrated in Fig. 1.7, panels a and b. The lefthand plots in Fig. 1.7c show the results for the modulations predicted by our device characterization. Melanopsin contrast is zero for the targeted melanopsin spectral sensitivity (top left panel of Fig. 1.7c). There is, however, modest contrast ‘splatter’ onto melanopsin when wavelength of peak spectral sensitivity (λ_{\max}) and the CIE standard age parameter (which affects primarily lens density) are varied. Repeating the same explorations but with direct measurements of the modulating spectra at maximal and minimal contrast levels revealed somewhat larger splatter than obtained with respect to the predicted spectra (Fig. 1.7c, top right panel). The differences between predicted and measured spectra presumably reflect drifts in the digital light integrator between calibration and validation measurement, as well as deviations between the performance of the light integrator and that of an ideal device. Similar splatter plots are obtained if instead we use a physiologically-based estimate of melanopsin spectral sensitivity (Fig. 1.7c, bottom two panels).

Although the contrast splatter for the S directed stimulus onto melanopsin was modest compared to the ~50% modulation produced in the S-cones, for some parameter choices it was negative. This raised the possibility that the measured out-of-phase S response arises not from S-cone signals but from out-of-phase contrast splatter from our S directed stimulus onto the melanopsin photoreceptors. To eliminate this possibility, we computed an ‘alternative’ S-cone modulation. This modulation was constructed using the silent substitution procedure as described above, but with an increased number of photoreceptor sensitivities that were silenced. In particular, we silenced not only the L cones, M cones, and standard melanopsin photoreceptors, but also the rods and a variant of melanopsin with its λ_{\max} value shifted to 495 nm. Rod spectral sensitivity was estimated by taking $\lambda_{\max}=500$ nm and peak optical density as 0.333, within the range of previous estimates [221, 222]. The alternative S modulation reduces the contrast splatter

onto melanopsin for the predicted spectra (Fig. 1.7d, left column) but increases it for the measured spectra (right column). Importantly, however, the contrast splatter for the measured spectra was positive for all melanopsin parameters and thus there is little chance of an out-of-phase melanopsin-based response for this modulation. The alternative S splatter onto L and M cones was small and also positive. The ‘standard’ modulation was used for subjects 01 and 02. A direct empirical comparison for these subjects indicates that their response to the standard and alternative S directed modulations was not different (Fig. 1.8). For subjects 03-16, the alternative S-directed modulation was used.

To calculate splatter in a biologically plausible range of age of λ_{\max} parameter values, we estimated the variability in these parameters as follows. For the estimates in λ_{\max} , we assumed standard deviations of 1.5, 0.9 and 0.8 nm about their nominal λ_{\max} for L, M and S cones [223]. For melanopsin, we assumed a standard deviation of 1.5 nm, conservatively corresponding to the largest standard deviation across the cone classes. To estimate variability in lens density, we extracted the standard deviation of the vertical measurement residuals of predicted vs. chronological age from a two-component lens density model [110]. We found that the standard deviation of the predicted age parameter for lens density due to individual variability is 7 years. Using these estimates, we derived 95% and 99% confidence regions (± 2 and ± 3 SDs), assuming independence between λ_{\max} and age and obtained the minimum and maximum splatter values in these ellipses (Fig. 1.7). For the main modulations, we determined these confidence ellipses using a two-dimensional Gaussian with mean age 21 years (mean age of all subjects excluding subject 01), and a standard deviation of 7 years, and the nominal λ_{\max} specific to each cone class and its standard deviation given above. In the same fashion, we furthermore determined the confidence ellipses for subject 01 only using the observer’s age (43 years) and the same age variability as well as λ_{\max} , and calculated splatter within these ellipses for both the main modulations and the supplementary control modulations (Figs. S4 and S5). To obtain an estimate of the expected value for absolute splatter, we used the same two-dimensional Gaussians and

calculated expectation. Table 1.1 provides the resulting values for contrast splatter for each of our main stimulus modulations onto each photoreceptor class, computed in this way. The legend of Fig. 1.10 provides the key values for the supplementary control modulations. In all of these calculations, we assumed that L, M and S cones underwent self-screening according to a percentage of pigment bleached corresponding to the background spectrum with a photopic luminance of 800 cd/m² seen through our 4.7 mm diameter artificial pupil (see below), corresponding approximately to the mean light level across sessions. This corresponded to percentage pigment bleached of 44.37%, 37.03% and 3.25% for L, M and S cones, respectively.

Across observer age and nominal λ_{\max} , both S directed modulations produce very little splatter onto the L and M cones, making it unlikely that our measured S responses are artifactually mediated by L or M cones. The expected absolute value of the contrast splatter of our L+M directed modulation onto S and melanopsin is generally small (3.34% and 1.3%, respectively, for the younger observers and melanopsin-a spectral sensitivity estimate; see Table 1.1 for other variants of the calculations), but for some spectral sensitivity estimates does approach 10%. Note, however, that if our L+M response was mediated primarily by an artifactual S or melanopsin response, we would expect the S or melanopsin responses to be larger than the L+M response at all temporal frequencies. This is not the case (Figs. 3 and 4). Similarly, the expected absolute value of contrast splatter of our melanopsin modulation onto L, M, and S-cones is also small (4.63%, 3.43% and 8.2%, respectively). There can, however, be as much as ~10% splatter onto the M cones ~13% splatter onto the S cones for some spectral sensitivity estimates, with the sign of such splatter being negative in some cases. Again, the possibility that our melanopsin response might be cone mediated is ruled out by the fact that if our melanopsin response were mediated by splatter onto cones, we would expect the L+M or S-cone response to exceed the melanopsin response at all temporal frequencies. This is clearly not the case for subject 02 (Fig. 1.4, and not the case for S-cone responses for subject 02 (Fig. 1.4, low temporal frequencies). With respect to the S-cone case, the average melansopsin response of subjects 01-

16 also clearly exceeds their average S-cone response at 0.05 Hz (Fig 5a). In addition, the shape of the TTF between melanopsin and L+M differs markedly for both subjects 01 and 02, also speaking against the possibility that the melanopsin response is mediated by L+M splatter. Further evidence that the melanopsin response is not mediated by splatter onto L+M cones is provided by the control data for subject 01 presented in Figs. S4 and S5.

Stimulus display

Light from the digital spectral integrator is collected and passed out of the device through a fiber optic cable (FTIIG16860-40, Fiberoptics Technology, Inc.; total length 40') to a custom-made eye piece. Within the eye piece, light first passed through a lens (12 mm diameter, -18 mm focal length), diffusing the light and back-projecting it onto an opal diffusing glass (35 mm diameter). Located on the front surface of the diffusing glass was a plexiglass disk (5.5 mm thickness, 35 mm diameter), which had a reticular etched surface pattern. The central 5° of visual angle (2.18 mm diameter) was blackened and the etched vertical, horizontal and two annular grid markers were visible. The observer was instructed to fixate the center of the blackened central disc.

The observer viewed the diffusing glass through an additional lens (25 mm diameter, 25 mm focal length) which could be adjusted to bring the diffuser into focus. A rubber eye cup was affixed to the viewing end of the eye piece and held in place a black, opaque plastic disc with a 4.7 mm central aperture. The observer viewed the stimulus using their dilated eye through this artificial pupil to equate retinal irradiance across subjects. Dilation was achieved with 0.5% proparacaine hydrochloride as a local anesthetic followed by 1% tropicamide. Throughout the experiment, artificial tears were applied if needed. An adjustable chin and forehead rest was used to position the head of the observer in the rig.

Stimulus calibration

The light exitant from the eyepiece was characterized using a spectroradiometer (PR-670 SpectraScan, Photo Research, Inc.), which imaged the eyepiece diffuser through the eyepiece

lens. The power at each wavelength was measured for each of the 128 primaries individually to allow a forward characterization of the device. To characterize non-linearities between settings of the device primaries and the exitant light, measurements were taken at 16 device primary intensity levels for three of the 128 effective primaries. These ‘gamma functions’ were of similar shape and were averaged and linearly interpolated to produce an overall function for linearization of each primary. The additivity of a subset of effective primaries was verified to hold to good approximation. Finally, measurements were taken of dark response, i.e. when all primaries are turned off. Following the production of device primary settings that produced the specified desired contrasts on the photoreceptors with respect to the background, these modulations were validated with spectroradiometric measurements.

Pupilometry

Pupil diameter at the non-stimulated eye was measured using an infrared red video pupilometry system (Cambridge Research Systems Ltd., Video Eye Tracker). The diameter was polled at a frequency of 50 Hz, with a few dropped measurements. Absolute size was calibrated prior to the experiments using a supplied calibration scale. The pupil detection algorithm supplied by the eye tracker was used; data traces were recorded for offline processing.

Raw data traces were smoothed and resampled using a 7th-order polynomial Savitzky-Golay filter. Missed samples due to polling delay, blinks, or eye movements were identified, as were “spikes” (data point windows in which the signal changed by 20% overall, or in which the signal changed by more than 2 SD of the signal in the entire time series). Trials with more than 20% of samples being thus identified as “bad” were discarded entirely. The first 20 or 5 seconds (for the 120 and 45 second duration trials, respectively) of each trial were discarded prior to fitting to allow measurement of the amplitude and phase response with the pupil in a steady state. Mean pupil diameter was not found to be different across modulation directions and frequencies (see Fig. 1.12). For this reason, the pupillary response was quantified as proportion change from baseline.

To characterize the pupillary control system, amplitude and phase of the pupillary response were obtained by performing least-squares spectral fitting: sine and cosine waves were fit to obtain amplitude and phase of the pupillary response at the stimulus frequency (fundamental) and the second harmonic. The primary analyses in this paper are of the response at the fundamental.

The standard error of the mean of the pupillary response across trials was estimated by a bootstrap procedure. Trials were randomly sampled with replacement up to the total number of trials, and the average response across this sampling obtained. The standard deviation of the bootstrapped averages was taken as the standard error of the mean response.

Procedure

For subjects 01 and 02, data were collected in blocks of 36, 120 second trials. Each block consisted of 6 trials at each of the 6 temporal frequencies, all of a single photoreceptor directed modulation. Both subjects completed two blocks each of the four photoreceptor directions (L+M, Mel, ‘standard’ S, and isochromatic). Subject 02 completed an additional block of 27 trials of each photoreceptor direction that contained only the three lowest frequencies of modulation to address the greater measurement noise present at lower temporal frequencies. All blocks used a different, counter-balanced ordering of stimuli. Each block began with 5 minutes of adaptation to the background, and the static background was presented between each trial. The subject pressed a button to initiate each trial. After confirming the quality of the eye-tracking signal, the modulation was presented, windowed at onset by a 3 second half-cosine. All measurements were obtained in a darkened room.

For subjects 03-16, data were collected in blocks of 27, 45 second trials. Each block consisted of 9 trials of each of the photoreceptor directed modulations (L+M, Mel, and ‘alternative’ S), all at a single temporal frequency. Each subject completed four blocks at 0.05 Hz stimulation and two blocks at 0.5 Hz. All blocks used a different, counter-balanced ordering of the stimuli. Additionally, the phase of stimulus onset was randomized across trials in units of $\pi/8$ to remove possible

anticipatory pupil responses to trial onset. Stimulus phase randomization was accounted for in the data analysis procedures so that data were aggregated with respect to a common stimulus phase.

Model

The amplitude and phase of pupillary response for two subjects (sub01 and sub02) were fit with a two filter model of temporal sensitivity¹⁷. For both the fast and slow filters, the model implements an impulse response of the form:

$$h(t) = u(t)[\tau(n - 1)!]^{(-1)}(t/\tau)^{(n-1)}e^{(-t/\tau)}$$

where $u(t)$ is the unit step function, n the order (number of stages) of the filter, and τ is a time constant. For such a filter, the amplitude and phase as a function of temporal frequency are [201]:

and $|H(w)| = (i2\pi w\tau + 1)^{-n}$

$$\angle H(w) = -n \tan^{-1}(2\pi w\tau) - 2\pi w t_0$$

The pupil response is described by a difference of the fast and slow responses, where the fast and slow filters have independent time constants (τ_1 , τ_2) and amplitudes (k_1 , k_2). The two filters could be synergistic (opposite sign for k_1 and k_2) or opponent (same sign for k_1 and k_2). We used a first-order filter ($n_1=1$) for the fast component and a fourth order for the slow component, with these values chosen via examination of the fit quality obtained with various choices of filter order.

Amplitude and phase of the pupil responses across stimulation frequency were fit jointly for each modulation direction. The error function weighted the amplitude and phase residuals by the

standard error of the mean of each. Best-fitting parameters were found using constrained minimization. A common time delay was fixed for each observer independently (250 ms for sub01; 230 ms sub02) and kept constant across modulation directions. These values are consistent with the pupillary response latencies observed for the ages of our subjects [224]. The linear phase effect corresponding to the delay was incorporated into the model predictions.

The group average data (subjects 01-16) were fit using the same model. Initial fit parameters were derived from those obtained for subject 01. For both the fast and slow components of the filter, time constants were fixed and the time delay was set to 250 ms. The amplitude parameters were then fit to minimize quadratic loss between observed and model amplitude and phase. As the fits to the data are under-constrained due to experimental sampling at only two frequencies (0.05 and 0.5 Hz), allowing changes only in the amplitude parameters provides an adequate compromise between overfitting and preserving the shape of the temporal transfer functions obtained from the extensively studied subjects. The parameters for subject 01 were used because the data from this subject are more representative of the group data than that of subject 02.

Acknowledgements

This work was supported by NIH Grant 1 R01 EY020516 (GKA), RO1 EY10016 (DHB), P30 EY001583 (Core Grant for Vision Research) and Deutscher Akademischer Austauschdienst (MS). We thank Sakibul Alam, Christopher Broussard, Nicolas Cottaris and Fred Letterio for technical assistance. Long Luu assisted with implementation of the linear filter model.

Figures

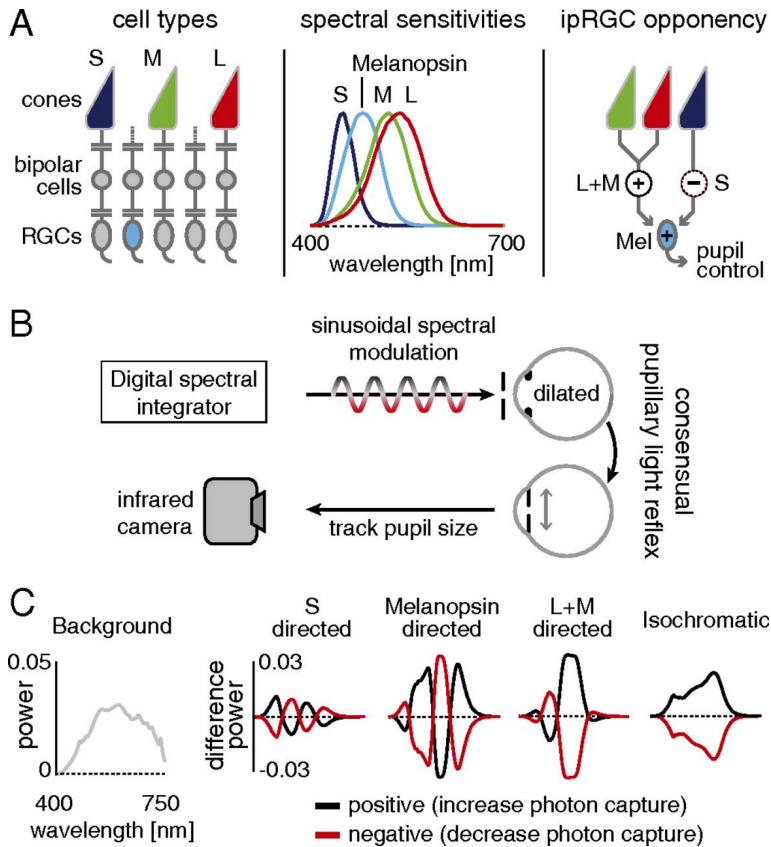


Figure 1.1: Experimental design.

(A, Left) L, M, and S cones and melanopsin-containing ipRGCs mediate vision at daytime light levels. (Center) Photoreceptor spectral sensitivities. (Right) Physiological measurements of ipRGCs find excitatory L and M cone inputs and inhibitory S-cone inputs (12). (B) A digital spectral integrator produces sinusoidal photoreceptor-directed modulations that pass through an artificial pupil into the pharmacologically dilated left eye. The consensual pupil response of the right eye is recorded. (C) Photoreceptor-directed modulations. Balanced changes in the spectrum of light around a background spectrum nominally isolate targeted photoreceptors.

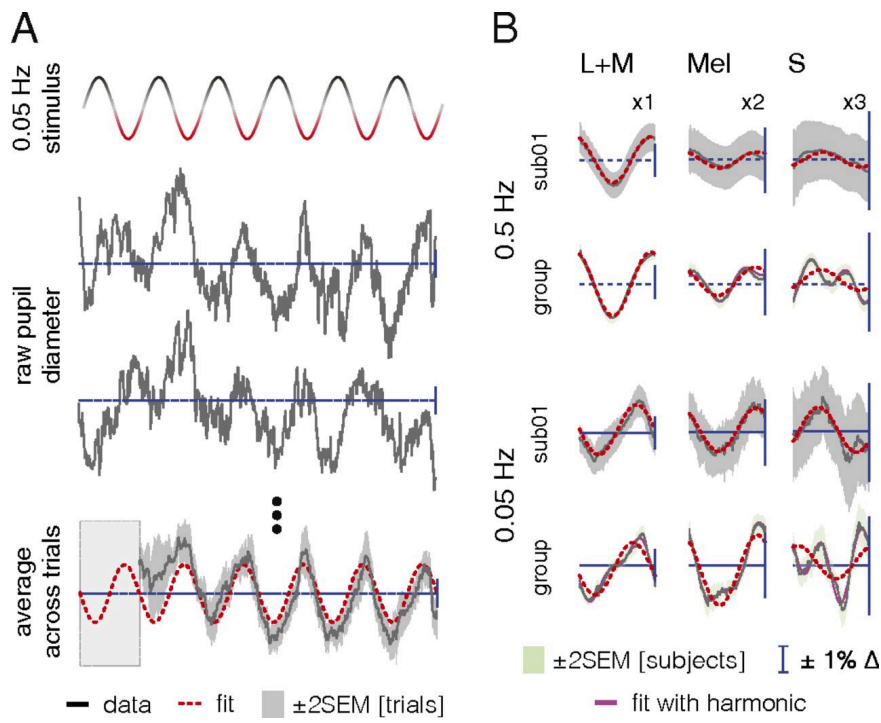


Figure 1.2: S input to the PLR is opponent to L+M and melanopsin.

(A, Top) Stimulus modulation over time between positive and negative spectra. (Middle) Pupil traces for two 120-s trials (sub01, 0.05 Hz, L+M). (Bottom) Average data (12 trials; same subject/condition; first 20 s discarded) fit with a sinusoid at the stimulus fundamental. (B) One cycle of the PLR [sub01 and group average over 16 subjects (black lines); melanopsin responses $\times 2$ scale, S responses $\times 3$]. Red dashed lines show fit with fundamental. Where visible, magenta lines are the fits with fundamental and second harmonic.

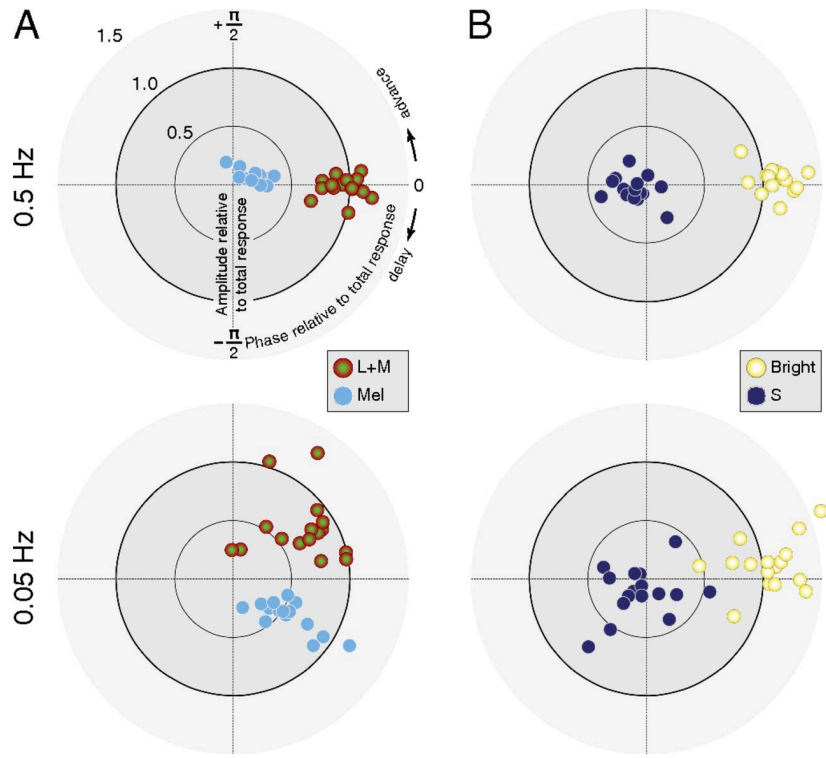


Figure 1.3: PLR phase reveals synergy and opponency.

(*A, Upper*) L+M and melanopsin responses are in phase at 0.5 Hz. Each point shows data for one subject. (*Lower*) L+M and melanopsin responses are in quadrature phase at 0.05 Hz. (*B*) For most subjects, S responses are opponent to the complex sum of L+M and melanopsin (pupil brightness) at both 0.5 Hz and 0.05 Hz. In all plots, amplitude and phase for each subject are shown relative to the complex sum of L+M, melanopsin, and S responses for that subject/temporal frequency.

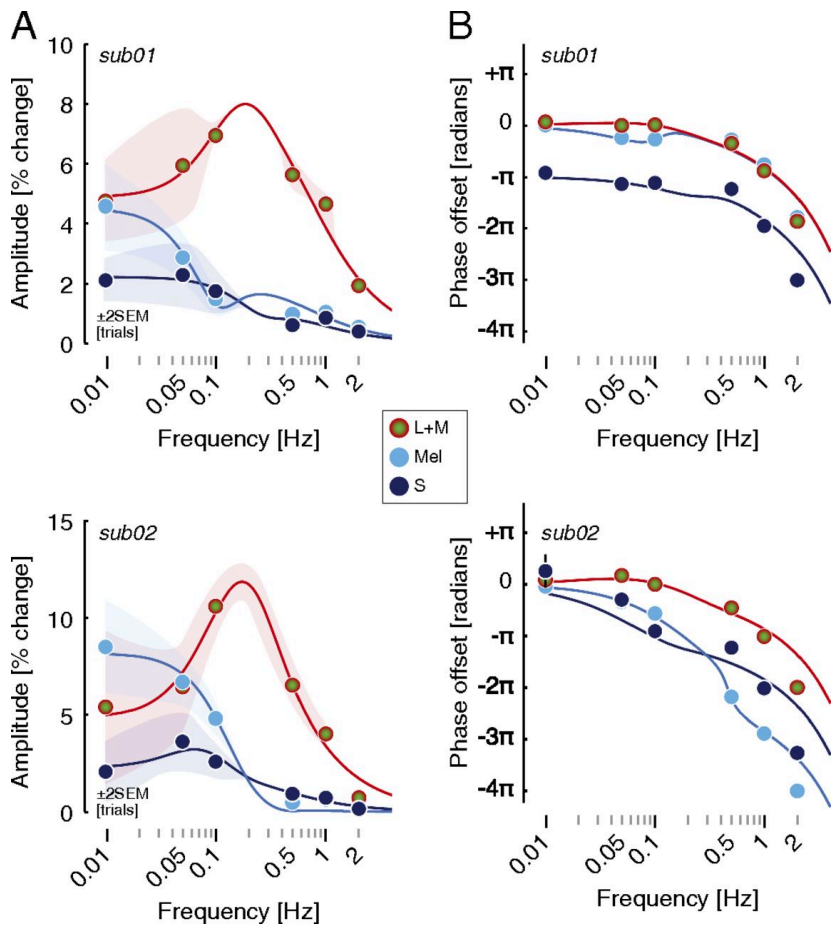


Figure 1.4: A two-component linear filter model accounts for the photoreceptor-specific temporal transfer functions of the PLR via S-cone opponency.

A two-component linear filter model accounts for the photoreceptor-specific temporal transfer functions of the PLR via S-cone opponency. (A) Amplitude of the PLR fundamental for three photoreceptor-directed modulations from two subjects. Points show data and solid lines show the fit of the linear filter model. The sign of the S input to the fast component of the model is negative relative to the sign of the L+M and melanopsin input. (B) Phase of the PLR fundamental of the pupil as a function of stimulus temporal frequency. Error bars are generally smaller than plot symbols.

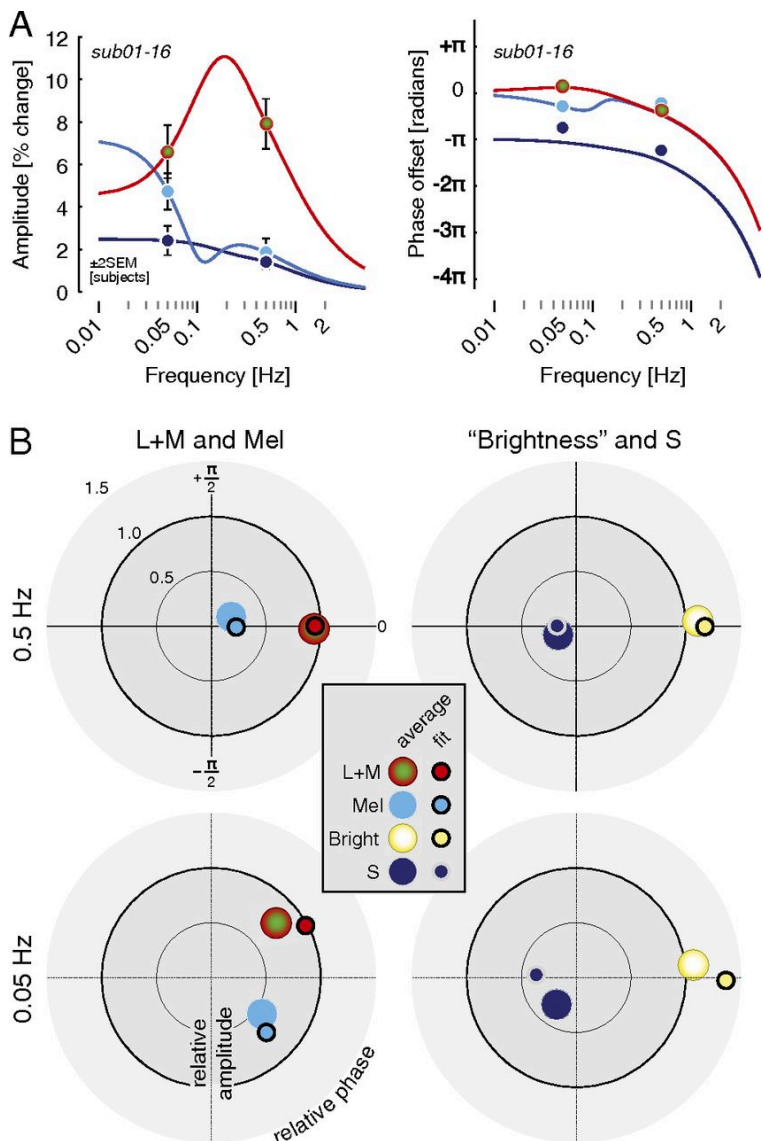


Figure 1.5: Group PLR data are well fit by the two component linear filter model.

Group PLR data are well fit by the two component linear filter model. (A) The mean response across all subjects (01–16) is shown at 0.05 and 0.5 Hz, for L+M-, melanopsin-, and S-cone-directed modulations. Fit values are derived from those found for subject 01, with only amplitude parameters adjusted (Table 1.2). This is because the average data are available at only two temporal frequencies and do not sufficiently constrain all parameters of the model. To obtain the average data plotted, amplitudes and phases were averaged separately (i.e., average amplitude

obtained without consideration of phase, average phase obtained without consideration of amplitude). The model was fit to the data as plotted. (*B*) Polar-plot representations of the group data with model fit points, following conventions as in Fig 1.3. The data are normalized separately for each temporal frequency. Error bars (± 2 SEM across subjects) are smaller than the plot points for the data.

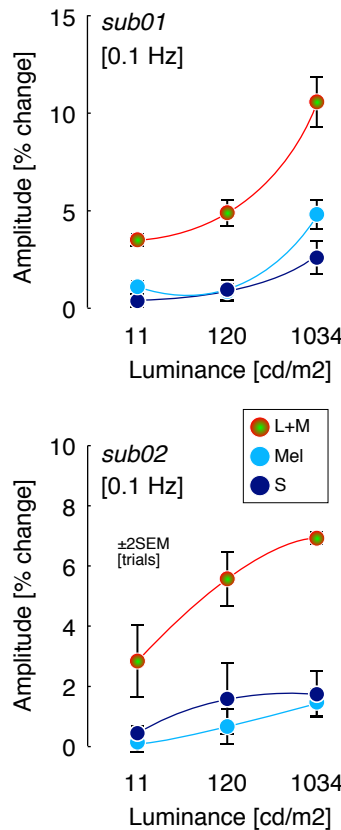


Figure 1.6: Pupil response to L+M-, melanopsin-, and S-directed modulation scales with background light level.

Pupil response to 0.1-Hz modulation as a function of background light level. Each panel shows the results for one subject and three photoreceptor targeted modulations. If rod signals were playing a substantial role in the response at the highest background luminance, that contribution would be expected to increase as the background light level dropped. Although such an increase could be balanced by a concomitant decrease in cone or melanopsin contribution to the responses, these data speak against the possibility that rod signals—which might arise through stimulation by scattered light onto relatively dark adapted rods outside of area of the stimulus—are contributing to the pupil response studied in this paper.

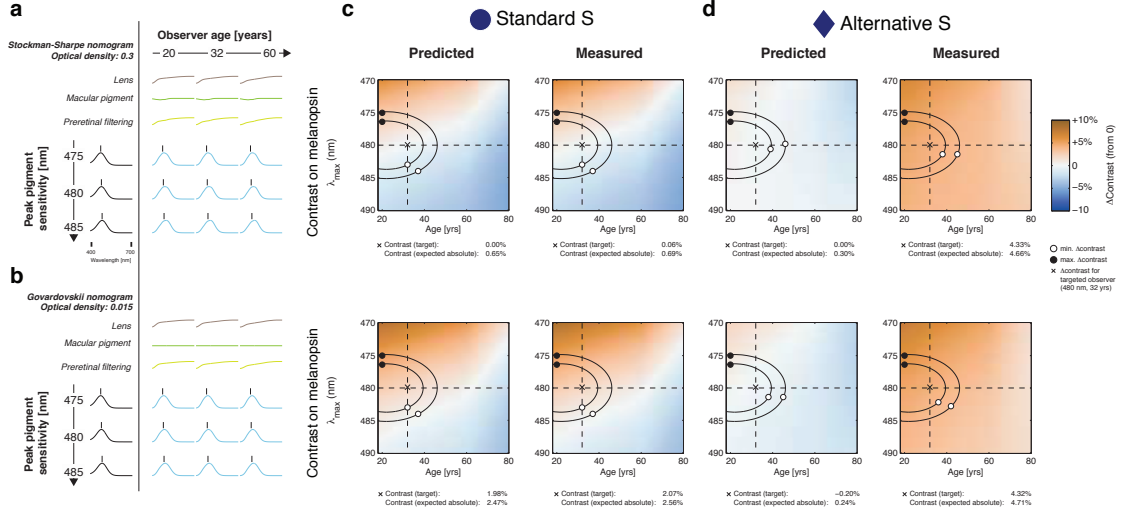


Figure 1.7: Observed S opponency is not due to artifactual stimulation of melanopsin.

The degree to which silent substitution is successful in isolating photoreceptor classes depends on the spectral sensitivity estimates used to calculate modulation spectra and the precision of stimulus control. To rule out negative contrast splatter of the nominally S-silencing modulation on melanopsin, which could produce an artifactual out-of-phase response in our measurements of the S-directed modulation, we explored the effect of variation in melanopsin spectral sensitivity. (A) Spectral sensitivity estimates of melanopsin obtained using the Stockman–Sharpe nomogram [220], a field size of 10° , adjusting for prereceptoral filtering according to the CIE standard for cone fundamentals using the observer age parameter (20–80 y) [200], and assuming a peak optical density of 0.3 (melanopsin-a). Wavelength of peak sensitivity λ_{\max} was varied between 470 and 490 nm. Vertical bars above spectral sensitivity plots indicate nomogram λ_{\max} . Prereceptoral filtering can shift λ_{\max} of the fundamental from that of the nomogram. (B) Physiologically based [101] spectral sensitivity estimate of melanopsin obtained using the Govardovskii nomogram [97], a field size of 27.5° , adjusting for prereceptoral filtering according to the CIE standard for cone fundamentals using the observer age parameter (20–80 y) (2), and assuming a peak optical density of 0.015 (melanopsin-b). Wavelength of peak sensitivity λ_{\max} was varied between 470 and 490 nm. (C) Contrast splatter of the standard S-directed modulation onto melanopsin as a

function of melanopsin λ_{\max} and observer age for both predicted spectra (Left) and spectroradiometrically measured spectra (Right). The upper panels are for the estimate of melanopsin spectral sensitivity in A; the lower panels are for the estimate of the melanopsin spectral sensitivity in B. Crosshairs indicate contrast for the theoretically targeted observer (melanopsin $\lambda_{\max} = 480$ nm, observer age 32 y). Ellipses trace the photoreceptor contrast associated ± 2 and ± 3 SD of the expected population variation in the CIE age parameter (SD estimated as 7 y) and variation in the λ_{\max} of melanopsin. Subjects 2–16 in the study had a mean (\pm SD) age of 21 ± 6 y, which centers the ellipse to the left of the nominal targeted age of 32 y of the observer. No measure of the variability of λ_{\max} of melanopsin exists for human observers; an SD of 1.5 nm was assumed [which is the maximum of the variability estimated for the human L, M, and S cone classes [223]]. The points of maximum and minimum contrast observed within the biological variability ellipses are indicated and reported in Table 1.1, as is the mean absolute expectation of contrast. (D) Contrast splatter of the alternative S-cone modulation onto melanopsin. Same format as in C.

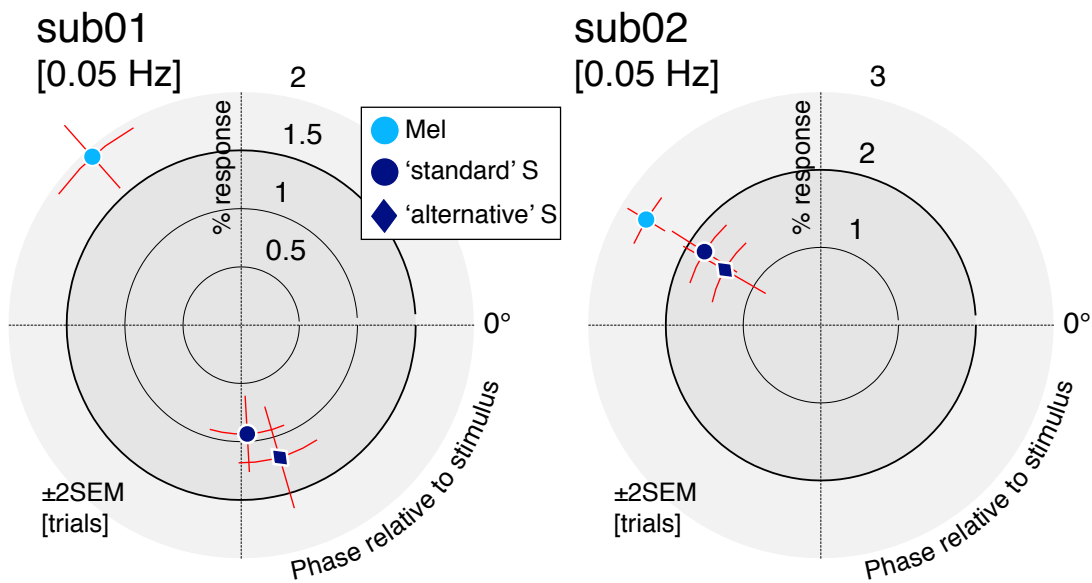


Figure 1.8: Similar results obtained with standard and alternative S-directed modulations.

For subjects 01 and 02, we measured responses at 0.05 Hz for both standard S-directed modulation (120-s trials) and the alternative S-directed modulation (45-s trials). Results for the two modulations are similar. Each panel shows response amplitude and phase for one subject, for the melanopsin-directed modulation and the two S-directed modulations. In this polar plot amplitude is in units of percentage of pupil diameter change, whereas phase is relative to stimulus onset.

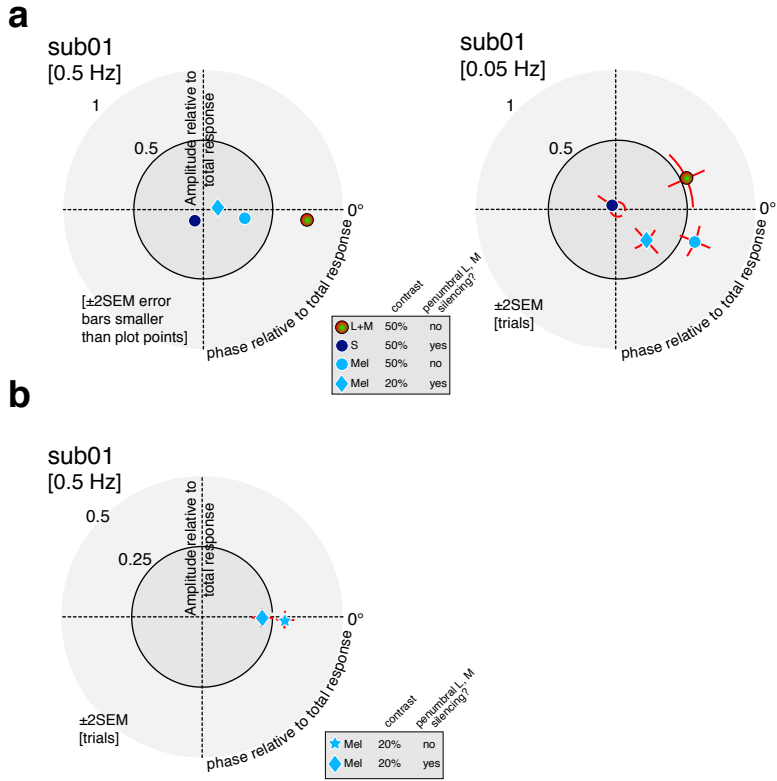


Figure 1.9: Similar results obtained when silencing penumbral cones.

A recent study [164] reported that four photopigment classes were required to fit human psychophysical data of detection of four primary stimuli, raising the possibility of melanopsin-mediated visual perception. This was observed to persist even when the spectral change was presented as 40-Hz flicker. The authors considered (but did not experimentally address) the possibility that this fourth photopigment class was actually L and M cones positioned in the shadow (penumbra) of retinal blood vessels, and thus subject to a hemoglobin spectral filter. Because of the minimal retinal surface subtended by penumbral cones, we consider it unlikely that the stimulation of penumbral cones would contribute substantially to the pupil response. Nonetheless, we created an S-cone-directed and melanopsin-directed modulation that also silences the predicted spectral sensitivities of penumbral cones. The maximum melanopsin contrast available for the penumbral cone silent, melanopsin-directed modulation was 20%,

compared with the 50% melanopsin contrast available in the primary experiments that did not attempt to silence penumbral cones. For these control experiments, we implemented modulations tailored to the age of the subject and the field size of our experiment (27.5°) and that incorporated an estimate of fraction of pigment bleached. By the time we conducted these experiments, we had also made refinements to our stimulus control procedures (primarily better fitting of the gamma functions of our device) that led to better agreement between predicted and measured modulations. Information on estimated splatter for these experiments is provided in the legend to Fig. 1.10. The mean background light level used in these control experiments had a luminance of $1,566 \text{ cd/m}^2$, and the estimates of pigment bleaching were with respect to this value. (A) For subject 01, we measured the pupil response to 0.5- and 0.05-Hz stimulation with L+M- (50% contrast), S-cone-, and melanopsin-directed (50% contrast) and melanopsin-directed/penumbral cone silent (20% contrast) modulations using 45-s trials. Points are plotted relative to the complex sum of the responses to the three 50% contrast modulations (Mel, S, and L+M). The penumbral cone silent modulations produce the same form of responses recorded earlier for this subject. Appropriately, the response to the penumbral cone silent melanopsin modulation is reduced, corresponding to the decrease in available melanopsin contrast. The amplitude of pupil response to the 50% melanopsin contrast modulation at 0.5 Hz was ~1.9% and ~4.3% at 0.05 Hz, similar to the values obtained in the main experiments and with similar phase relations (Figs. 3 and 4). The S-cone response is similar to that obtained in the main experiments at 0.5 Hz and smaller at 0.05 Hz (but with a large SE because fewer trials were used in this control experiment). The opponent nature of the S-cone response continues to be observed in these control data. (B) In a second set of measurements for subject 01, we measured the pupil response to 0.5-Hz melanopsin-directed stimulation that did or did not silence the penumbral cones, with the modulations matched at 20% contrast. There was minimal difference in the amplitude or phase of the pupil response evoked by these stimuli. These results establish that penumbral cone stimulation cannot fully account either for the measured response to melanopsin-directed stimulation or for the opponent S-cone

response. We note that these results do not speak generally to the role that incidental penumbral cone stimulation might play in measurement of perceptual responses to putative melanopsin-directed stimuli, where sensitivity to stimulus spatial structure might be enhanced relative to what is observed for the pupillary response.

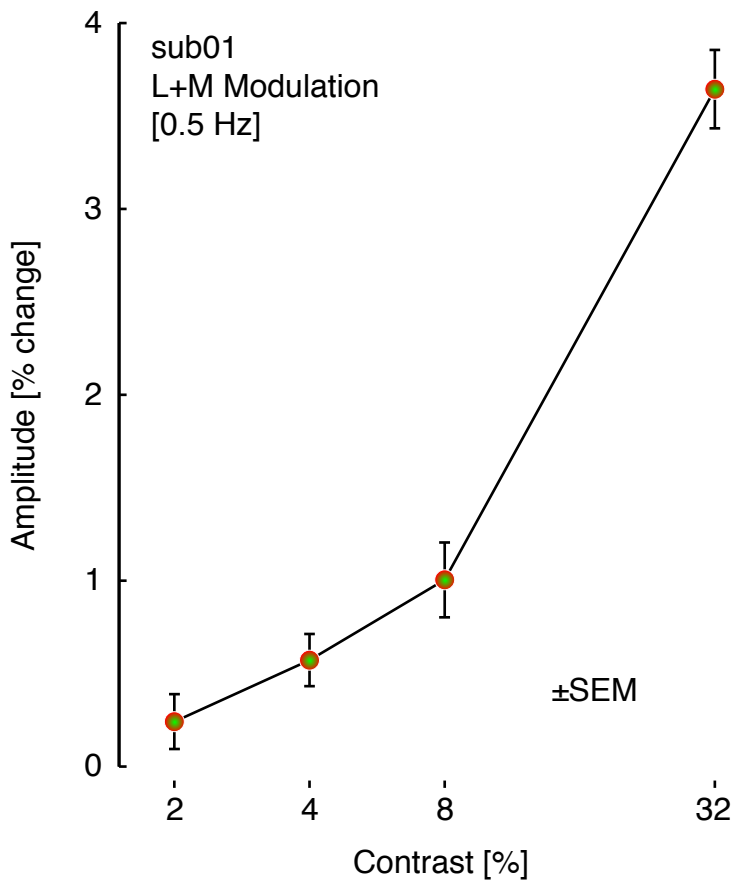


Figure 1.10: L+M contrast response function.

The pupil response to a 0.5-Hz modulation of L+M-directed stimulation was obtained for subject 01 at a range of contrast levels between 1% and 32% contrast. The contrast response function is notable for the absence of a compressive nonlinearity in the low-contrast regime, and in fact the observed nonlinearity is somewhat expansive. Phase was essentially uniform across contrast variation, with all responses within 0.15π radians of the mean phase across all responses. This indicates that a small amount of inadvertent contrast on L and M cones in our nominally melanopsin stimulus is unlikely to explain the measured melanopsin responses. The response of subject 01 to the 50% melanopsin-directed stimulus at 0.5 Hz was $\sim 1\%$ (Fig. 1.9). To produce a response of this size at this stimulation frequency, the splatter of the melanopsin-directed stimulus onto the L and M cones would have to be $\sim 8\%$. Taking ± 2 SD in the known variability in

the λ_{\max} of L and M cone [223], and the known variation in lens density and prereceptoral filtering at a given observer age [110], we calculate that the maximum splatter of the measured 50% melanopsin modulation used in these control studies onto L and M cones is 4.3% (maximum taken over the 95% confidence interval computed using the procedures described to produce the values provided in Table 1.1 for subject 01, but applied to the control modulations used here), and that the mean absolute expectation of splatter is 2.2%. Therefore, we consider it unlikely that inadvertent stimulation of L and M cones by our melanopsin stimulus is responsible for the responses observed from melanopsin-targeted stimulation at 0.5 Hz. At lower temporal frequencies of stimulation, where the size of the melanopsin-driven response rises with respect to that from L+M stimulation (Fig. 1.4 and Fig. 1.9), the possibility of inadvertent L+M stimulation as the source of apparent melanopsin response becomes ever less plausible.

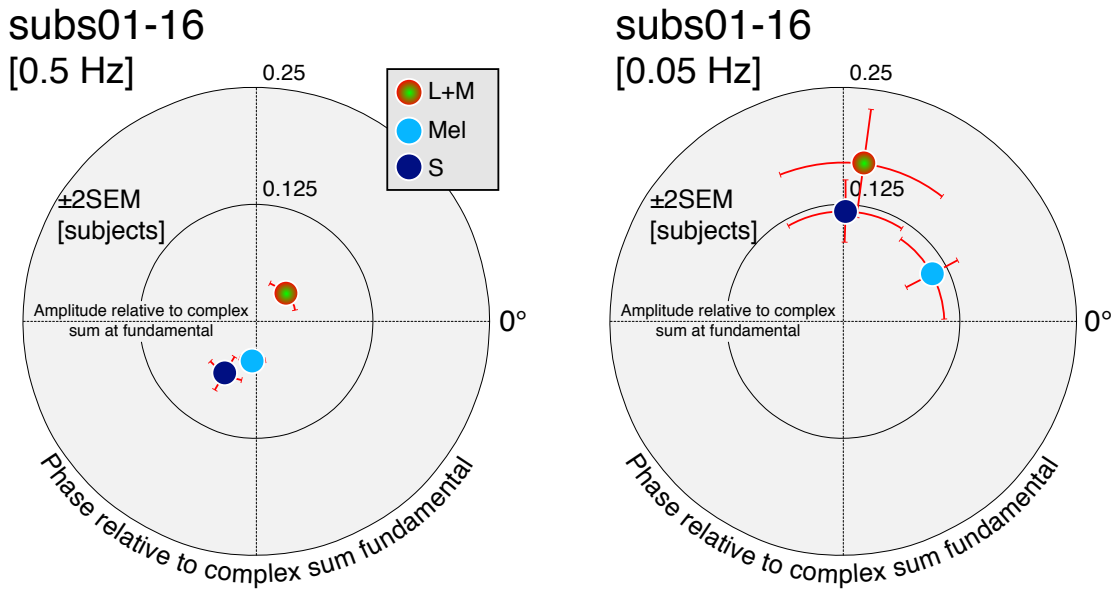


Figure 1.11: Pupil responses at the second harmonic.

Each panel shows the mean (over subjects) pupil response at the second harmonic of the stimulation frequency for 0.5 (Left) and 0.05 (Right) stimulation. Responses for L+M, melanopsin, and S are shown. In each panel, amplitude and phase are expressed relative to the complex sum of the response at the fundamental for these three modulation directions (the same convention as in Figs. 3 and 5).

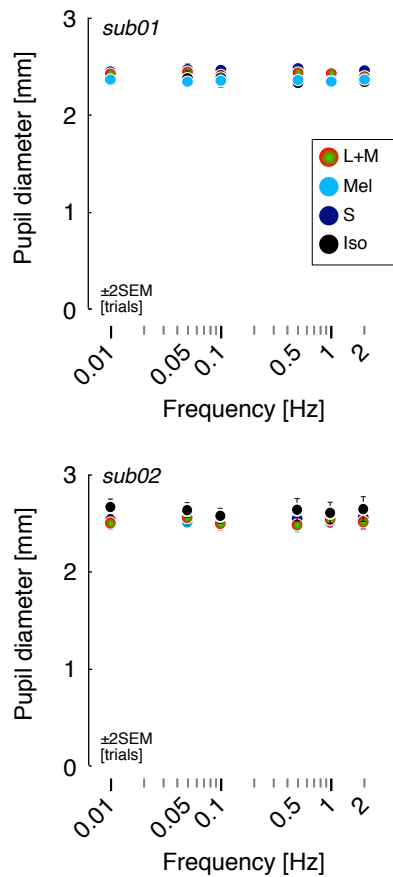


Figure 1.12: Mean pupil diameter does not depend on modulation direction or frequency.

Each panel shows the mean pupil diameter as a function of modulation frequency for one subject.

Pupil diameter for different modulation directions is indicated by the color of the plotted points.

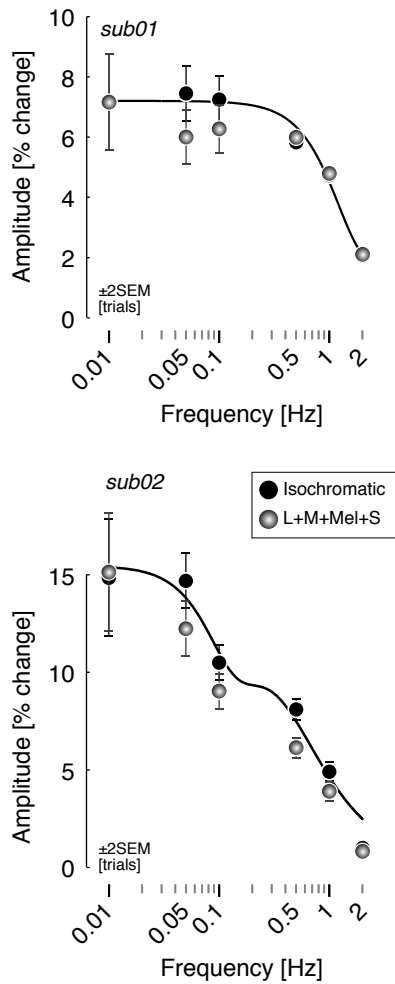


Figure 1.13: Isochromatic responses are approximated by the sum of photoreceptor specific responses.

Each panel compares, for one subject, the amplitude response at the fundamental measured to an isochromatic modulation—which nominally stimulates all photoreceptor classes with equal contrast and phase—and the complex sum of the responses to the L+M-, melanopsin-, and S-directed modulations. The agreement is good. The solid line is the fit of the two-filter linear model to the isochromatic modulation data, with parameters as provided in Table 1.2.

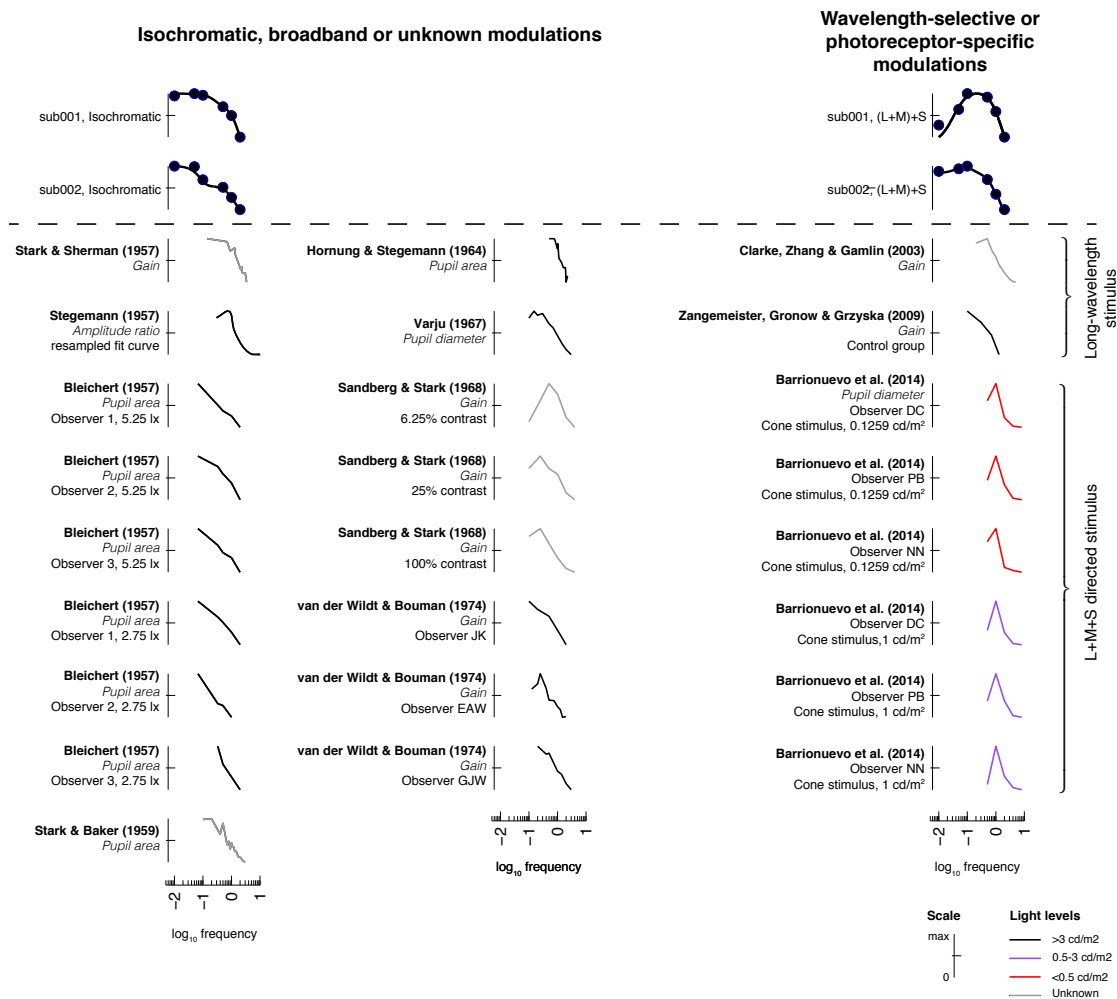


Figure 1.14: Observed isochromatic and cone-driven temporal transfer functions compared with prior reports.

Observed isochromatic and cone-driven temporal transfer functions compared with prior reports.

Pupil response temporal transfer functions reported previously in the literature were extracted in tabular form or reconstructed from graphical representations when tables were not available. The function extracted from each study was normalized to its maximum response. The italicized text for each study indicates the type of measurement made, and we did not correct for differences in dependent measure (e.g., pupil diameter vs. pupil area). If reported, the mean light level of each study included was converted into candelas per square meter and color-coded by range. TTFs

were reconstructed using Data Thief (<http://datathief.org/>) unless data were available in tabulated form [207, 215].

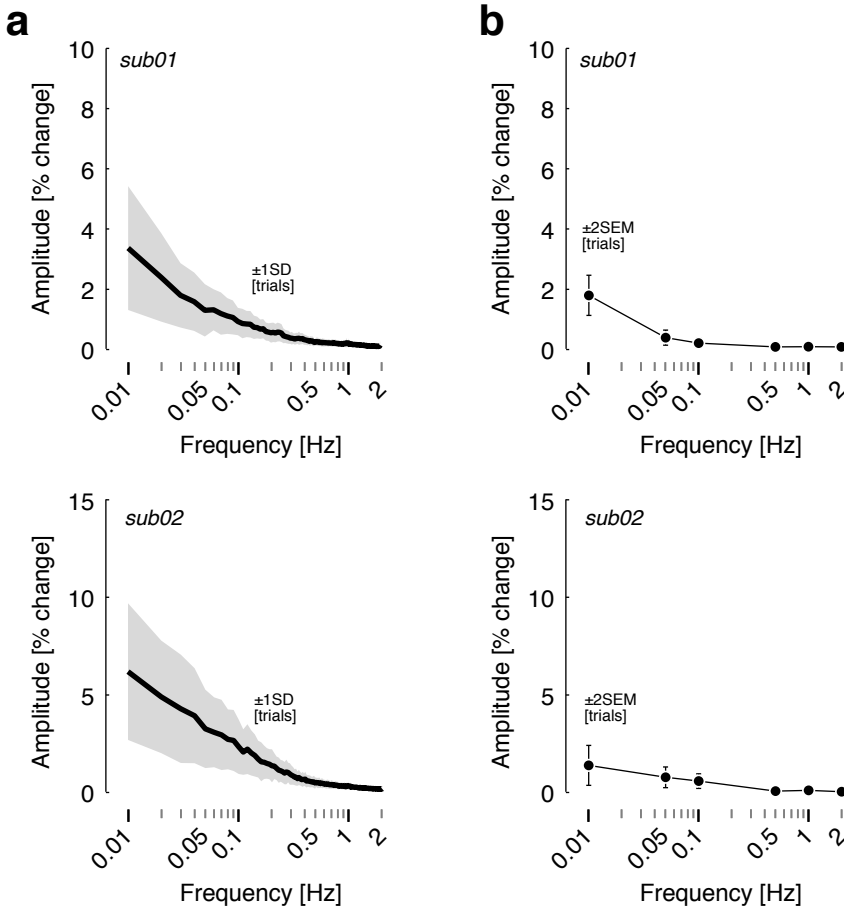


Figure 1.15: Noise properties of the measures.

(A) We obtained the average power spectrum of the residuals of the pupil measurements made during the 100-s trials for sub01 and sub02. For each trial, the amplitude of variation in pupil size at each frequency between 0.01 and 2 Hz was obtained by least-squares spectral fitting; a standard FFT could not be used because of missing time-series values in some trials (e.g., owing to blinks). Values corresponding to the frequency of the stimulus during the trial and all of its odd and even harmonics were excluded. The average of the measured amplitudes at each frequency across trials gives the power spectra shown. Intrinsic variation in pupil size over time (“pupil unrest”) increases at ever lower frequencies, similar to prior reports [225]. The intrinsic pupil noise inflates the variance of measurements of induced pupil response at low temporal frequencies

(reflected in the error bars of Fig. 1.3a) but will not affect the expectation of the amplitude if the phase of the noise is random (or if the stimulus phase is randomized). (B) We considered the possibility of a phase-locked pupil response evoked by the initiation of the trial itself, independent of the stimulus modulation. Trials from sub01 and sub02 were boot-strap-sampled to measure signal amplitude at a given frequency in a set of trials that did not have stimulation at the frequency being assessed. The number of trials sampled matched the number of trials obtained for each of the plot points shown in Fig. 1.3a, and boot-strap resampling with replacement was used to obtain the SE. A small effect was seen at 0.01 Hz, indicating some phase-locking of the noise at the lowest temporal frequency. This effect approaches zero at higher frequencies. This phase-locked noise could be present in the responses measured for sub01 and sub02 at 0.01 Hz. The phase of the evoked noise is such that correction for this component of the response would slightly raise the measured response amplitudes at 0.01 Hz for melanopsin and L+M stimulation for both subjects and leave the basic shape of these TTFs little changed. For S-driven responses, correction would lower the measured amplitude for sub01, making that TTF more band-pass and raise the amplitude for sub02, making that TTF more low-pass. Overall, such a correction would little alter the general forms of the TTFs observed across these two subjects.

Table 1.1: Uncertainty in photoreceptor isolation.

Modulation direction	Receptor	Age	Nominal contrast	Contrast, %, predicted spectra					Contrast, %, measured spectra				
				Target	Expected absolute	Minimum 95% [99%] CI	Maximum 95% [99%] CI	Target	Expected absolute	Minimum 95% [99%] CI	Maximum 95% [99%] CI		
L+M	L	21	50	53.08	52.91	52.17 [51.84]	53.51 [53.73]	57.34	57.16	56.35 [55.98]	57.81 [58.05]		
			43	53.08	53.23	52.38 [51.99]	53.94 [54.18]	57.34	57.49	56.56 [56.13]	58.27 [58.52]		
	M	21	50	47.38	46.78	45.10 [44.55]	48.42 [49.05]	51.31	50.68	48.88 [48.30]	52.43 [53.10]		
			43	47.38	48.14	46.32 [45.57]	49.82 [51.00]	51.31	52.12	50.18 [49.38]	53.91 [55.17]		
	S	21	0	2.78	3.34	1.54 [0.79]	4.98 [5.58]	3.6	4.15	2.35 [1.60]	5.78 [6.38]		
			43	2.78	2.02	0.07 [-1.16]	3.95 [4.68]	3.6	2.85	0.91 [-0.30]	4.78 [5.50]		
	Melanopsin-a	21	0	0	1.3	-4.16 [-5.41]	3.50 [5.12]	0.83	1.34	-3.55 [4.87]	4.53 [6.25]		
			43	0	1.43	-3.26 [-4.64]	4.94 [6.64]	0.83	1.91	-2.61 [-4.06]	6.05 [7.85]		
	Melanopsin-b	21	0	-2.34	2.74	-6.19 [-7.37]	1.01 [2.56]	-1.59	2.13	-5.64 [-6.88]	1.96 [3.60]		
			43	-2.34	1.99	-5.49 [-6.79]	2.26 [3.88]	-1.59	1.56	-4.90 [-6.27]	3.28 [4.99]		
Rods	Rods	21	N/A	15.09	14.44	10.20 [8.67]	18.56 [20.14]	16.93	16.23	11.71 [10.08]	20.62 [22.31]		
			43	15.09	15.99	11.61 [9.95]	20.37 [21.98]	16.93	17.87	13.20 [11.43]	22.54 [24.27]		
	Penumbra L	21	N/A	48.97	48.82	47.97 [47.59]	49.50 [49.74]	52.9	52.74	51.81 [51.39]	53.49 [53.75]		
			43	48.97	49.09	48.13 [47.69]	49.90 [50.15]	52.9	53.02	51.96 [51.48]	53.91 [54.18]		
	Penumbra M	21	N/A	43.91	43.3	40.67 [39.65]	45.54 [46.34]	47.59	46.93	44.13 [43.04]	49.32 [50.17]		
			43	43.91	44.66	42.05 [40.97]	46.89 [47.89]	47.59	48.37	45.59 [44.44]	50.76 [51.82]		
	Penumbra S	21	N/A	-5.11	4.63	-7.47 [-8.55]	-1.68 [-0.63]	-4	3.52	-6.44 [-7.56]	-0.50 [0.57]		
			43	-5.11	5.76	-8.68 [-9.75]	-2.79 [-1.67]	-4	4.66	-7.67 [-8.78]	-1.61 [-0.47]		
Melanopsin	L	21	0	-4.79	4.63	-5.22 [-5.45]	-3.87 [-3.52]	-1.73	1.54	-2.11 [-2.33]	-0.85 [-0.52]		
			43	-4.79	4.93	-5.67 [-5.92]	-4.05 [-3.63]	-1.73	1.89	-2.59 [-2.90]	-1.07 [-0.67]		
	M	21	0	2.81	3.43	1.52 [0.78]	5.45 [6.12]	6.83	7.49	5.47 [4.68]	9.62 [10.33]		
			43	2.81	2	0.01 [-1.27]	4.11 [4.99]	6.83	5.98	3.88 [2.54]	8.22 [9.15]		
	S	21	0	-6.84	8.2	-12.06 [-13.48]	-3.95 [-2.19]	-4.65	6.07	-10.11 [-11.59]	-1.62 [0.23]		
			43	-6.84	4.98	-9.54 [-11.28]	-0.39 [2.68]	-4.65	2.87	-7.49 [-9.30]	2.09 [5.26]		
	Melanopsin-a	21	50	49.88	47.77 [46.75]	51.50 [51.98]	55.88	55.75	53.60 [52.55]	57.41 [57.89]			
			43	50	49.96	47.50 [46.34]	51.91 [52.49]	55.88	55.85	53.33 [52.14]	57.85 [58.43]		
Penumbra	Melanopsin-b	21	50	49.81	49.6	47.63 [46.71]	51.17 [51.66]	55.66	55.44	53.42 [52.49]	57.04 [57.54]		
			43	49.81	49.9	47.63 [46.55]	51.78 [52.35]	55.66	55.76	53.44 [52.33]	57.69 [58.27]		
	Rods	21	N/A	35.79	36.06	32.31 [30.80]	39.65 [40.92]	41.21	41.48	37.60 [36.04]	45.19 [46.49]		
			43	35.79	35.33	31.24 [29.64]	39.21 [40.61]	41.21	40.74	36.51 [34.85]	44.75 [46.19]		
	Penumbra L	21	N/A	1.24	1.38	0.65 [0.40]	2.30 [2.71]	4.36	4.52	3.84 [3.59]	5.38 [5.77]		
			43	1.24	1.13	0.24 [-0.03]	2.18 [2.65]	4.36	4.23	3.39 [3.12]	5.21 [5.67]		
	Penumbra M	21	N/A	7.49	8.16	5.51 [4.59]	11.26 [12.48]	11.58	12.27	9.45 [8.46]	15.56 [16.84]		
			43	7.49	6.69	4.03 [2.98]	9.78 [11.05]	11.58	10.73	7.89 [6.80]	14.01 [15.35]		
	Penumbra S	21	N/A	12.86	11.75	5.28 [2.97]	17.96 [20.33]	15.44	14.28	7.42 [4.97]	20.88 [23.40]		
			43	12.86	14.33	7.81 [5.36]	20.73 [23.06]	15.44	16.99	10.07 [7.48]	23.79 [26.28]		
Standard S	L	21	0	1.1	1.1	1.02 [0.97]	1.13 [1.14]	0.67	0.66	0.62 [0.58]	0.68 [0.69]		
			43	1.1	1.09	0.99 [0.94]	1.15 [1.16]	0.67	0.67	0.60 [0.56]	0.70 [0.72]		
	M	21	0	-0.38	0.41	-0.67 [-0.77]	-0.17 [-0.08]	-0.92	0.95	-1.20 [-1.29]	-0.71 [-0.62]		
			43	-0.38	0.34	-0.61 [-0.71]	-0.08 [0.02]	-0.92	0.88	-1.15 [-1.25]	-0.63 [-0.53]		
	S	21	50	51.73	51.98	50.71 [50.16]	53.10 [53.51]	52.21	52.49	51.15 [50.58]	53.67 [54.11]		
			43	51.73	51.33	49.88 [49.28]	52.66 [53.10]	52.21	51.78	50.26 [49.61]	53.17 [53.64]		
	Melanopsin-a	21	0	0	0.65	-1.07 [-1.60]	2.33 [3.08]	0.06	0.69	-1.06 [-1.61]	2.44 [3.20]		
			43	0	0.71	-2.02 [-2.74]	1.26 [2.06]	0.06	0.7	-2.02 [-2.73]	1.36 [2.17]		
	Melanopsin-b	21	0	1.98	2.47	0.85 [0.28]	4.40 [4.16]	2.07	2.56	0.89 [0.30]	4.53 [5.31]		
			43	1.98	1.42	-0.17 [-0.94]	3.30 [4.12]	2.07	1.5	-0.14 [-0.91]	3.43 [4.26]		
Alternative S	Rods	21	N/A	-0.43	0.19	-0.70 [-0.92]	0.42 [0.63]	-0.63	0.33	-0.93 [-1.15]	0.28 [0.52]		
			43	-0.43	0.78	-1.33 [-1.94]	-0.12 [0.18]	-0.63	0.99	-1.56 [-2.18]	-0.29 [0.03]		
	Penumbra L	21	N/A	-0.05	0.06	-0.15 [-0.21]	-0.00 [0.01]	-0.39	0.4	-0.46 [-0.50]	-0.36 [-0.35]		
			43	-0.05	0.06	-0.17 [-0.24]	0.02 [0.04]	-0.39	0.38	-0.47 [-0.52]	-0.33 [-0.31]		
	Penumbra M	21	N/A	-1.44	1.49	-1.93 [-2.10]	-1.08 [-0.94]	-1.89	1.93	-2.35 [-2.52]	-1.53 [-1.39]		
			43	-1.44	1.38	-1.84 [-2.03]	-0.96 [-0.82]	-1.89	1.83	-2.28 [-2.46]	-1.42 [-1.28]		
	Penumbra S	21	N/A	49.95	50.35	47.28 [46.00]	53.26 [54.23]	50.01	50.42	47.33 [46.05]	53.37 [54.36]		
			43	49.95	49.34	46.08 [44.76]	52.37 [53.42]	50.01	49.39	46.12 [44.80]	52.44 [53.51]		
Standard S	L	21	0	-0.17	0.16	-0.23 [-0.27]	-0.12 [-0.12]	2.07	2.09	1.96 [1.90]	2.18 [2.19]		
			43	-0.17	0.18	-0.26 [-0.31]	-0.14 [-0.13]	2.07	2.03	1.90 [1.83]	2.13 [2.16]		
	M	21	0	-0.81	0.78	-0.87 [-0.90]	-0.70 [-0.67]	1.88	1.84	1.76 [1.70]	1.92 [1.96]		
			43	-0.81	0.82	-0.91 [-0.94]	-0.74 [-0.71]	1.88	1.84	1.76 [1.54]	1.82 [1.84]		
	S	21	50	54.49	55.44	52.22 [50.86]	58.35 [59.41]	64.46	65.45	62.06 [60.63]	68.52 [69.64]		
			43	54.49	53.16	49.65 [47.51]	56.58 [57.86]	64.46	63.07	59.36 [57.14]	66.68 [68.02]		
	Melanopsin-a	21	0	0	0.3	-0.22 [-0.41]	0.64 [0.78]	4.33	4.66	4.04 [3.82]	5.23 [5.45]		
			43	0	0.33	-0.78 [-1.27]	0.22 [0.48]	4.33	3.95	3.40 [2.81]	4.64 [4.98]		
Penumbra	Melanopsin-b	21	0	-0.2	0.24	-0.52 [-0.76]	0.79 [1.04]	4.32	4.71	3.87 [3.58]	5.59 [5.92]		
			43	-0.2	0.59	-1.19 [-1.80]	0.16 [0.52]	4.32	3.87	3.10 [2.42]	4.82 [5.27]		
	Rods	21	0	0.65	0.87	0.36 [0.18]	1.33 [1.47]	4.6	4.87	4.21 [3.95]	5.50 [5.70]		
			43	0.65	0.39	-0.08 [-0.43]	0.93 [1.16]	4.6	4.28	3.66 [3.23]	4.98 [5.29]		
	Penumbra L	21	N/A	-0.46	0.48	-0.57 [-0.62]	-0.43 [-0.41]	1.75	1.74	1.61 [1.54]	1.82 [1.84]		
			43	-0.46	0.45	-0.55 [-0.61]	-0.38 [-0.34]	1.75	1.75	1.60 [1.52]	1.84 [1.86]		
	Penumbra M	21	N/A	-1.58	1.61	-1.88 [-1.97]	-1.35 [-1.24]	1.03	1.03	0.84 [0.78]	1.21 [1.29]		
			43	-1.58	1.53	-1.80 [-1.91]	-1.26 [-1.16]	1.03	1.06	0.86 [0.80]	1.26 [1.33]		
	Penumbra S	21	N/A	42.11	42.95	37.53 [35.38]	48.38 [50.26]	51.67	52.57	46.79 [44.50]	58.35 [60.35]		
			43	42.11	40.93	35.27 [33.12]	46.46 [48.48]	51.67	50.42	44.39 [42.08]	56.31 [58.46]		

Contrast splatter, that is, contrast seen by nominally silenced photopigment classes, can arise because of (i) uncertainty about the spectral sensitivities of the photoreceptors and their preretinal filtering and (ii) imprecision in stimulus production. This table reports contrast statistics for each of

our modulation directions for each photoreceptor class, taken across a range of plausible biological variation in age-dependent, wavelength-specific prereceptoral filtering [via the age parameter of the CIE standard for cone fundamentals [200]] and in the wavelength of peak spectral sensitivity λ_{\max} of the photopigment classes, for both predicted and measured modulations (see also Fig. 1.7). For L, M, and S cones, λ_{\max} was assumed to be 558.9, 530.3, and 420.7 nm; for melanopsin, λ_{\max} was assumed to be 480 nm. Contrast splatter is given for both predicted spectra (left) and measured spectra (right). The target contrast is provided for subject age of 32 y and with the λ_{\max} values given above, which are the parameters for which the modulations used in the main experiment were designed, although here the field size is taken as 27.5°, whereas the modulations were designed for a field size of 10°. The maximum and minimum contrast was also found within the space of biological variation composed of 2 or 3 SDs in observer lens density [110] and λ_{\max} of the targeted photopigment [223]. Additionally, the mean absolute expectation of contrast was obtained by taking the probability weighted mean of contrast measurements within the space of lens density and λ_{\max} variation. These calculations were performed separately for the mean age of subjects 02–16 (21 y) and the age of subject 01 (43 y). Contrast was calculated for two sets of melanopsin spectral sensitivity estimates (see also Fig. 1.7). Melanopsin-a ($\lambda_{\max} = 480$ nm) was constructed using the Stockman–Sharpe nomogram [220], a field size of 10°, adjusting for prereceptoral filtering according to the CIE standard for cone fundamentals using the observer age parameter (20–80 y) [200], and assuming a peak optical density of 0.3. Melanopsin-b ($\lambda_{\max} = 480$ nm) constitutes a physiologically based [101] spectral sensitivity estimate of melanopsin, more appropriate for the stimulus conditions used, obtained using the Govardovskii nomogram [97], a field size of 27.5°, adjusting for lens transmittance according to the CIE standard for cone fundamentals using the observer age parameter (20–80 y) [200] but with filtering by the macular pigment excluded (as the central 5° of the stimulus was obscured), and assuming a peak optical density of 0.015. Importantly, the degree of splatter from the cone-directed modulations onto melanopsin yielded by the two

estimates is similar. Calculated contrast upon rods and penumbral L and M cones is also presented, although there are theoretical and empirical (Figs. S1, S3, and S4) reasons to believe that these photoreceptors do not contribute to our measured pupil responses. Rod spectral sensitivity was estimated using the Govardovskii nomogram [97], by taking $\lambda_{\max} = 500$ nm and peak optical density as 0.333; preretinal filtering according to the CIE standard was included. Penumbral cone sensitivity was estimated by assuming that the light seen by these cones was filtered through blood vessels of 5- μm thickness oxygenated at 85% using the spectral absorption of oxygenated and deoxygenated blood [226]. Cones and penumbral cones were assumed to be affected by self-screening to an estimate of the percentage of pigment bleached by the background spectrum with a photopic luminance of 800 cd/m², corresponding to approximately the mean photopic luminance of the background across sessions in the main experiments. In these splatter calculations we did not systematically explore the conjoint effect of age, nominal λ_{\max} , and photopigment bleaching on the splatter calculations. We separately considered the effect of photopigment bleaching in the range of 0–75% pigment bleached for L and M cones and 0–15% pigment bleached for S cones for a 21-y-old observer, with the nominal λ_{\max} of each cone class. Using the melanopsin-directed modulation, we found that the effect of photopigment bleaching is on the order of a few percent at most. The range in which splatter was affected by photopigment bleaching between 0 and 75% photopigment bleached (for L and M cones) and 0 and 15% (for S cones) was 4.4, 0.5, and 0.9% for L, M, and S cones, respectively. CI, confidence interval; N/A, not applicable.

Table 1.2: Two-filter linear model.

Subject	Direction	Center				Surround			
		Amplitude	Constant	Delay	Order	Amplitude	Constant	Delay	Order
		k_1	τ_1	$t_{0,1}$	n_1	k_2	τ_2	$t_{0,2}$	n_2
01	L+M	0.0381	0.2717	0.25	1	0.0139	0.5757	0.25	4
	S	-0.0061	0.2963	0.25	1	0.0050	0.4625	0.25	4
	Mel	0.0095	0.3073	0.25	1	-0.0130	1.2199	0.25	4
	Isochromatic	0.0179	0.0750	0.25	1	-0.0182	0.0750	0.25	4
02	L+M	0.0632	0.5742	0.23	1	0.0390	0.5742	0.23	4
	S	-0.0087	0.4672	0.23	1	-0.0200	1.3141	0.23	4
	Mel	0.0018	0.8340	0.23	1	-0.0390	0.8340	0.23	4
	Isochromatic	0.0562	0.3521	0.23	1	-0.0212	0.8155	0.23	4
Group (01–16)	L+M	0.0505	0.2717	0.25	1	0.0276	0.5757	0.25	4
	S	-0.0104	0.2963	0.25	1	0.0023	0.4625	0.25	4
	Mel	0.0133	0.3073	0.25	1	-0.0228	1.2199	0.25	4

Best-fitting parameters for the two-filter linear model (see *Discussion* and *SI Methods* for description of parameters).

SELECTIVE STIMULATION OF PENUMBRAL CONES REVEALS PERCEPTION IN
THE SHADOW OF RETINAL BLOOD VESSELS (Spitschan *et al.*, 2015)

Note: This chapter was published as Spitschan, et al. [2].

Abstract

In 1819, Johann Purkinje described how a moving light source that displaces the shadow of the retinal blood vessels to adjacent cones can produce the entopic percept of a branching tree. Here, we describe a novel method for producing a similar percept. We used a device that mixes 56 narrowband primaries under computer control, in conjunction with the method of silent substitution, to present observers with a spectral modulation that selectively targeted penumbral cones in the shadow of the retinal blood vessels. Such a modulation elicits a clear Purkinje-tree percept. We show that the percept is specific to penumbral L and M cone stimulation and is not produced by selective penumbral S cone stimulation. The Purkinje-tree percept was strongest at 16 Hz and fell off at lower (8 Hz) and higher (32 Hz) temporal frequencies. Selective stimulation of open-field cones that are not in shadow, with penumbral cones silenced, also produced the percept, but it was not seen when penumbral and open-field cones were modulated together. This indicates the need for spatial contrast between penumbral and open-field cones to create the Purkinje-tree percept. Our observation provides a new means for studying the response of retinally stabilized images and demonstrates that penumbral cones can support spatial vision. Further, the result illustrates a way in which silent substitution techniques can fail to be silent. We show that inadvertent penumbral cone stimulation can accompany melanopsin-directed modulations that are designed only to silence open-field cones. This in turn can result in visual responses that might be mistaken as melanopsin-driven.

Introduction

A fine network of retinal vessels supplies the inner retina with blood [227-229], with decreasing vessel diameter towards the fovea. This network lies in front of the photoreceptive layer of the retina, thus casting shadows onto a set of cone photoreceptors. As the blood vessels are thin, most of the retinal cone mosaic is in the open light field, receiving unobstructed, incident light (Fig. 2.1a). Cones positioned directly under the larger blood vessels lie in deep shadow and are termed *umbral cones*. Between these two regions lies the *penumbra*, in which cones experience partial shadow [230]. As the shadow of the vasculature is stabilized on the retina it is not perceived under normal viewing conditions [231].

In 1819, the Bohemian physiologist Johann Evangelist Purkinje (Czech spelling *Jan Evangelista Purkyně*) found that moving a candle across the visual field allows an observer to view their own retinal blood vessels. This method displaces the shadow of the blood vessels on the retina, breaking stabilization and producing the entopic percept that we now refer to as the Purkinje tree [232; see Fig. 2.2a, 233]. Visualization of the vasculature using kinetic techniques to move the shadow of the blood vessels has a rich history in vision science [234]. For example, Müller [235], Müller [236] used it to deduce the location of the photoreceptive layer in the retina and more recently it has found a variety of clinical applications [237-260].

Here we demonstrate a novel method for visualizing the Purkinje tree, one that does not involve stimulus motion. The three classes of cones (L, M, and S) differ in their spectral sensitivity (Fig. 2.1b). Light passing through hemoglobin is spectrally filtered. As a consequence, the cones that lie within the shadow of blood vessels have an altered spectral sensitivity relative to their open-field counterparts. The differential spectral sensitivity of open-field and penumbral cones allows these two populations to be selectively targeted using the method of silent substitution [113], with properly tailored spectral modulations. We report that selective stimulation of the penumbral L and M, but not S cones, elicits a clear percept of the retinal blood vessels.

Results

Using a digital spectral light modulator that produces a mixture of 56 narrowband primaries under computer control, we constructed sets of spatially-uniform spectral modulations that *a*) selectively stimulate penumbral cones (denoted as L*, M* and S*) while silencing open-field cones (denoted as L, M and S), *b*) selectively stimulate open-field cones while silencing the penumbral cones, and *c*) stimulate open-field and penumbral variants conjointly. Each set includes one modulation that targets L and M cones, and a second modulation that targets S cones (Fig 2.1C; Appendix). Approximately 3-5% contrast was available within the gamut of our device for selective and differential stimulation of the penumbral and open-field L and M cones. That is, to produce more than this amount of contrast we would have to produce power less than zero at some wavelengths and/or power that exceeded that maximum available from our device at others. Approximately 20% contrast was available for the S cone variants. All modulations had zero predicted contrast on melanopsin. Modulations were presented around a high-photopic background ($\sim 2000 \text{ cd/m}^2$, Fig. 2.1C) to saturate the rods. Table 2.1 provides the specific contrasts and background levels used for each modulation in each experiment. How we determined contrast is described in the Appendix (see Equations 2-4).

The output of the spectral light modulator was imaged onto a diffuser and viewed by observers through a custom eyepiece. The resulting stimulus configuration in all experiments was a spatially uniform annulus with a 27.5° outer diameter and with the central 5° obscured. Thin grid lines were etched into the diffuser to aid accommodation and fixation.

In informal observations, the three authors of this paper observed that when the penumbral L and M cone modulation was flickered at 8 or 16 Hz, a clear percept of the branching retinal blood vessels was produced within the stimulated portion of the visual field. This percept emerged at flicker onset, faded considerably over about a second, and could be restored if the flicker was halted and restarted. We do not have an explanation for the fading. Crucially, when viewing the

stimulus with the right eye, the vessels appeared to converge to a point on the right side of the visual field, and vice versa when viewed with the left eye. This mirror symmetry is consistent with the structure of the image of the blood vessels on the retina.

We asked a naïve observer (female, 29 years old) to draw her percept in response to a penumbral-cone directed spectral modulation. She viewed a 16 Hz square-wave modulation of penumbral L and M cones monocularly with each eye in turn (the modulation viewed by this observer differed from those studied further below in that it did not silence melanopsin and consequently allowed a larger penumbral cone contrast; see Appendix and Table 2.1). The observer viewed the modulation and drew her entoptic percept on a diagram that indicated both the obscured central 5° and the central grid lines superimposed on the uniform stimulus field (as shown in Fig. 2.2b; the circle shown corresponds to the size of the 27.5° diameter field). The observer freely switched between the drawing and viewing the stimulus. The sketches produced by this observer are notable for their general resemblance to a Purkinje tree and may be compared with her actual vasculature as obtained from ocular fundus photographs of her two eyes (Fig. 2.2c). The sketches capture the gross features of the larger blood vessels seen in the photos, with the larger vessels in the sketch emanating from the optic disk in both eyes and with smaller vessels shown branching from the larger ones. The implied location of the optic disks in the sketches (just inside the 13.75° eccentricity indicated by the circle) is consistent with their known anatomical positions in the retina [261]. A more detailed examination reveals that the correspondence between the sketches and photos is not exact; this may be a result of limits in the sketching ability of the observer. We also attribute to sketching imprecision the fact that the sketches extend slightly beyond the indicated outer diameter of the stimulus field; the Purkinje tree percepts were always confined to the part of the visual field that was stimulated.

Consistent with our own percepts, the sketched Purkinje tree corresponds only to the larger retinal blood vessels, similar in spatial structure to those observed when a moving penlight is

shown through the side of a closed eyelid. Finer vasculature extending in towards the fovea, which may be observed using other kinetic methods, was not visible using our method.

We conducted a rating experiment to measure three properties regarding the photoreceptor contributions to and temporal characteristics of the Purkinje-tree percept. First, we tested whether penumbral cone stimulation is necessary to produce the Purkinje-tree percept, or whether differential contrast between penumbral and open-field cones is both necessary and sufficient. Second, we considered that spatial contrast produced by the uniform spectral flicker is perfectly stabilized on the retinal surface, as the blood vessels move with the photoreceptors. Thus we predicted that the temporal dependence of the Purkinje-tree percept should have a bandpass shape similar to that found in measurements of temporal contrast sensitivity for retinally stabilized images [262, 263]. Finally, we expected the Purkinje-tree percept to be more robust for penumbral L and M cone flicker as compared to penumbral S cone flicker, given the reduced spatial resolution of the S cone mosaic.

The three authors viewed 2-second trials consisting of sinusoidal flicker modulations, with 250 ms cosine windowing at the beginning and end of each trial. Tones demarcated the start and end of each trial (Fig. 2.3a). The six spectral modulation directions depicted in Fig. 2.1C were shown. Each combination of modulation direction and frequency was presented five times, with trial order randomized. The observer was blind to the particular modulation direction and frequency presented on each trial. On every trial, the observer was asked to rate his percept using a 0-3 scale (0 = little or no spatial structure visible in the flicker; 1 = some spatial structure visible, but structure did not resemble the Purkinje-tree percept; 2 = faint or partial Purkinje-tree percept visible; 3 = strong Purkinje-tree percept). A rating of 3 corresponded to the strongest percepts we had observed in our apparatus. These were very salient, as in the sketch shown in Figure 2.2. On 21 out of 231 trials, no modulation at all was shown (blank trials), to provide a control for false positives.

Both the selective penumbral L and M cone and the open-field L and M cone modulations elicited a clear Purkinje-tree percept at 16 Hz in all three observers (Fig. 2.3b), with the strength of the percept falling off at lower and higher temporal frequencies. The control L and M cone modulation, which stimulated both open-field and penumbral L and M cones with similar contrast (much as would occur during natural viewing), did not elicit a Purkinje-tree percept. This confirms that time-varying differential contrast between open-field and penumbral cones is required to elicit a Purkinje-tree percept, and that this percept can be elicited by selective modulation of either penumbral or open-field cones.

The control L and M cone modulation did elicit faint percepts of spatial structure at temporal frequencies at and above 16 Hz, consistent with previous reports of flicker-induced visual field articulation at high frequencies [233, 264-268]. All observers noted that this percept was markedly different from that of the Purkinje tree. Blank trials did not lead to reported spatial structure (MS and GKA, all trials rated as 0; DHB 20 of 21 trials rated as 0, 1 trial rated as 1).

In contrast, selective stimulation of penumbral or open-field S cones did not produce a Purkinje-tree percept for any observer at any temporal frequency, although these modulations could produce some non-specific spatial structure at 16 and 32 Hz (Fig. 3C). Given the similarity of the temporal frequency dependence of the S cone ratings to those for L+M+L^{*}+M^{*}, it is possible that the S cone data are driven by residual contrast seen by L and M cones, as the precision of photoreceptor isolation is never perfect (see Appendix).

The trial-by-trial data for the rating experiment as well as the spectra of the modulations used are provided at <http://color.psych.upenn.edu/supplements/purkinjetree>. This site also provides the data for the supplemental rating experiment (see below) and the spectra of the modulation presented to our naïve observer.

Discussion

A variety of methods to visualize one's retinal vasculature have been described since Purkinje's original observation. These have included: the use of stimulus motion under special conditions, most notably moving a small spot of light across the pupil [269]; very brief flashes illuminating the retina through the sclera causing a brief shift in the retinal position of the shadow of the vasculature [270]; the motion of corpuscles flowing through the vasculature [240, 271-273]; long adaptation to dark, for example after lid closure during sleep [231, 274-279]; intense illumination [280, 281]; and pressure-induction [236, 271, 282]. These methods have been employed in a variety of studies that have determined the parameters needed to optimize entoptic visualization [238, 270, 283-287].

Here we demonstrate a novel method for visualizing the Purkinje tree. Differential modulation of the L and M cones inside and outside the partial shadow of the retinal blood vessels produces a strong percept of one's retinal vasculature, when viewed at 16 Hz. We formalized this observation through a rating experiment, as well as through the sketches of a naïve observer. Our method is conceptually distinct from earlier kinetic techniques for blood vessel visualization: what changes over time in our method is the spectrum of a spatially uniform stimulus. This change in spectrum, rather than spatial motion of the shadow, stimulates penumbral cones differentially from the neighboring open-field cones and leads to the characteristic Purkinje-tree percept. Because our method does not involve spatial modulation of the image impinging on the photoreceptors, it provides a new tool for studying percepts arising from retinally stabilized images. For example, future work could use this technique to investigate in detail the fading of the Purkinje tree percept that we observe for continuously flickering stimuli.

Interestingly, the possibility of a spectral stimulus modulation that selectively drives the penumbral cones was suggested 50 years ago by Cornsweet [288], who wrote:

"[I]t should be possible to provide a visual field in which the only thing that is changing is the stimulation of receptors behind blood vessels. This may be accomplished by showing the observer a field that is alternately lighted with 415 m μ [nm] and then with a mixture of two other wave lengths each of which is absorbed less strongly by blood, but so chosen that their mixture will match the 415 m μ [nm] light in regions not lying behind blood vessels." (p. 173)

The method we present here may be considered an implementation of Cornsweet's concept, albeit accomplished by a more complex spectral modulation than he envisioned. Our ability to construct an appropriate modulation is enabled by much more precise estimates of the cone fundamentals and their variation across the retina than were available in the 1960s [200, 289, 290].

We found that a temporal frequency of 16 Hz led to the strongest percept of the Purkinje tree, with weaker percepts at 8 and 32 Hz. These frequencies are somewhat higher than those reported by Sharpe [283] for visualization of the Purkinje tree using a kinetic method, and higher than the peak of the temporal contrast sensitivity functions for stabilized retinal images [262, 263]. In the former case differences might be expected because our stimulus does not involve any retinal motion, and in the latter because the temporal contrast sensitivity functions will depend on retinal location and the spatial structure of the stimulus as well as possibly the quality of image stabilization. Coppola and Purves [270] concluded from their kinetic-based studies of the Purkinje-tree percept that optimal stimulation frequencies were greater than 10 Hz. Our results are commensurate with this conclusion, although the data on which it is based were obtained for more central visualization of small capillaries rather than for the shadows of larger peripheral vasculature revealed by our method.

In a series of careful anatomical studies, Adams and Horton [230], Adams and Horton [291], Adams and Horton [292] demonstrated that the photoreceptors under retinal blood vessels have

a corresponding area of decreased cortical representation in the squirrel monkey visual cortex, akin to a local form of amblyopia. The altered cortical representation was present even for smaller vessels that produce only penumbral shadow, and the width of the reduced cortical representation was wider than the shadows themselves. We find that the selective stimulation of the penumbral cones results in a visible percept. Thus, the reduced cortical representation identified by Adams and Horton [230], Adams and Horton [291], Adams and Horton [292] is not so extreme as to render penumbral cones inoperative or to eliminate the possibility of spatial vision mediated by these cones.

Our result has practical implications for the study of visual processes. For example, there is current interest the melanopsin-containing intrinsically photosensitive retinal ganglion cells [10, 18, 21, 60, 63, 65, 67, 77, 90, 116, 119, 121, 130, 136, 163, 164, 204, 293-298]. Studies of melanopsin function in the mouse are facilitated by the use of transgenic photoreceptor knock-out models [49, 77, 293]. These techniques are obviously not available for studies of human observers. Because of the overlap in spectral sensitivity of the cones and melanopsin, functional isolation of melanopsin in humans has been approached using the method of silent substitution [1, 116-119]. As typically implemented, modulations that target melanopsin and silence the open-field cones will produce residual stimulation on the penumbral cones. In their recent paper, Horiguchi, et al. [164] calculated that such residual stimulation exceeds the cone detection threshold and noted the possibility that the effects of such stimulation might account for some of their psychophysical results, particularly the surprising observation that in the periphery observers could detect nominally cone-silent modulations at 40 Hz. We calculated that the nominally melanopsin-isolating direction in the study of Horiguchi, et al. [164] produced 1-2% contrast on penumbral cones. In our recent study of photoreceptor contributions to the pupillary light reflex [1], the primary melanopsin-directed modulation employed also produced residual stimulation of penumbral cones of similar magnitude. Our demonstration here that a small degree of selective penumbral cone contrast produces a clearly visible percept should prompt caution regarding the

interpretation of results obtained using silent substitution, particularly under conditions where penumbral-cones might plausibly mediate the measured response of interest. Similar warnings have been issues previously regarding variation of cone spectral sensitivity across the retina as a function of changes in pre-retinal filtering [299, 300] and with respect to individual variation in cone spectral sensitivities [164].

It is possible to produce spectral modulations that target melanopsin with about 20% contrast while nominally silencing both open-field and penumbral cones. Indeed, in a supplemental rating experiment, we found that controlling for the stimulation of penumbral cones reduces or removes the Purkinje-tree percept, which is otherwise visible for a melanopsin-directed modulation (Fig. 6). While even a small degree of penumbral cone contrast produces a prominent perceptual effect at 16 Hz, we have found that failure to control for this inadvertent stimulation has minimal effect upon measured pupil responses [1; Fig. 1.9, panel b] at low temporal frequencies. Consequently, the degree of attention needed to the effect of cones lurking in the vascular shadows will vary, depending upon the response being measured.

Detailed Methods and Supplemental Experiment

Subjects

The three authors of the study served as observers. All three are male, have corrected visual acuity of 20/20 or better and normal color vision as judged by Ishihara color plate screening [218]. At the time of data collection their ages were: MS 27, GKA 44, DHB 54. The research was conducted in accord with the principles of the Declaration of Helsinki and approved by the University of Pennsylvania Institutional Review Board. Informed written consent was obtained from all observers.

Apparatus

The apparatus is discussed in detail in Spitschan, et al. [1]. We used the method of silent substitution [113, 199] in combination with a spectral light modulator (OneLight VISX Spectra

Digital Light Engine), which produces light with arbitrary spectral power distributions. The theory of operation of the modulator is as follows: Light from a Xenon arc lamp passes through a slit, is collimated, then passed through a diffraction grating. This separates the light into individual narrowband wavelength components. Each component is then imaged onto a column of a digital light processing (DLP) chip (1,024 columns x 768 rows). Each row on this chip can be turned on or off independently in each column, thus allowing for the selective control over the exitant power in each wavelength band. Rather than addressing the 1,024 columns separately, we treated groups of 16 columns as single primaries, resulting in 56 independent nearly monochromatic primaries (after turning off 80 columns at the short wavelength end of the spectrum, and 48 columns at the long wavelength end of the spectrum, where there was too little light power for us to measure accurately). This grouping of columns provided us with $768 \times 16 = 12288$ discrete power levels for each primary; the spectral width of the primaries (~ 16 nm FWHM) was dominated by the spectral bandwidth of the optical system rather than the width of a column on the DLP chip, and there was little spectral shift with output power for our 56 primaries. The DLP chip can modulate rapidly. In the experiments reported here we use it in a mode where we control the emitted spectra at 256 Hz.

The monochromatic primaries leaving the DLP chip were mixed and transmitted through a fiber optic cable (FTIIG16860-40, total length 40 feet; Fiberoptics Technology, Inc.), passed through IR and UV blocking filters, and illuminated a diffuser within a custom-made eye piece. Observers viewed an image of the diffuser through a 25 mm focal length lens, resulting in a 27.5° spatially uniform field with the central 5° blocked by an opaque circular occluder mounted on the diffuser. The diffuser also contained then etched grid lines to facilitate accommodation and fixation by the observer.

The power at each wavelength for each of the 56 primaries was measured through the eyepiece using a spectroradiometer (PR-670 SpectraScan, Photo Research). Each primary was measured

at 16 power levels, which allowed us to characterize the nonlinearities between the device primary settings and the exitant light power. We verified that the light emitted from the spectral modulator with all mirrors turned on contained no appreciable power in the UV (200–380 nm) or NIR (780–1020 nm) wavelength ranges using fiber spectrometers (two customized Ocean Optics USB2000+ spectrometers with ILX-511B detector; wavelength ranges 180 nm–875 nm and 340–1025 nm, respectively; 3 m custom Ocean Optics fiber-optic cable). We calculated that the light power in the visible range of the spectrum (380–780 nm) was within light safety standards [301] and provide example code for light safety calculations in the Silent Substitution Toolbox (see below, <https://github.com/spitschan/SilentSubstitutionToolbox>).

Construction of Spectral Modulations

Because we have available 56 primaries, there are many physically distinct spectral modulations that can be produced by our device and that satisfy a set of specified photoreceptor-silencing constraints. To choose a specific modulation, we have developed general methods that allow us to trade off between several criteria. First, we wanted spectral modulation directions that maximized contrast on targeted photoreceptor classes, within the gamut limits of our stimulation device [114, 115]. Second, to the extent possible, we wanted the modulation to vary smoothly with respect to wavelength. This second requirement was imposed based on the intuition that small deviations between the desired modulation and that actually produced by the device will have a smaller effect on nominally-silenced photoreceptors for spectrally smooth modulations than will modulations that vary rapidly as a function of wavelength. Third, we wanted the contrasts produced by the modulations, particularly their ability to silence photoreceptor classes, to be robust with respect to uncertainty in our estimates of the spectral sensitivity of the nominally silenced photoreceptors. To choose modulations that are consistent with these criteria, we implemented a constrained numerical optimization procedure. We have made our software available under an open-source license (Silent Substitution Toolbox; <https://github.com/spitschan/SilentSubstitutionToolbox>). This provides a MATLAB

implementation, as well as methods for obtaining estimates of photoreceptor spectral sensitivities [in conjunction with software and data provided in the open-source Psychophysics Toolbox; 302, <http://psychtoolbox.org>] and methods for computing what we refer to as contrast splatter maps (see Precision of Photoreceptor Isolation section below). Our software takes advantage of the sequential quadratic programming (SQP) algorithm provided in the function *fmincon* in MATLAB's Optimization Toolbox.

To find desired modulations in the 56-dimensional device primary space, we divide the photoreceptor classes under consideration into three sets. We call these the targeted set, the silenced set, and the ignored set. We search over device primary settings to maximize the contrasts seen by the photoreceptor classes in the targeted set, subject to the constraints i) that the contrasts seen by the photoreceptors in the silenced set are zero and ii) that the device primary settings are within gamut. More specifically, we minimize the quantity

$$f = \sum_m (c_m - 1)^2 \quad (1)$$

where m indexes the photoreceptor classes in the targeted set and c_m is the contrast seen by the m^{th} class in the set. The quantity f is minimized when the contrasts in the targeted set are as close to 1 as can be obtained subject to the constraints described below. We generally seek spectral modulation directions for which equal positive and negative contrasts around the specified background may be obtained within gamut around the specified background, so that 1 is the maximum obtainable contrast. As a practical manner, our code enforces the device gamut constraints for both the positive and negative modulations during the numerical optimization.

The optimization also enforces a smoothness constraint on the modulations: the maximum absolute difference in spectral power between adjacent sample wavelengths was required to be below a specified criterion. The exact choice of criterion depends on the size of the wavelength

sampling step and the intensity of the spectral background, and it can be adjusted to tradeoff between maximal obtainable contrasts for the targeted set and the spectral smoothness of the obtained modulation spectra. This is a choice we make manually for each application of our procedures. For the modulations used in this paper, the wavelength sampling was 380 nm to 780 nm in 2 nm steps, the criterion was $10^{-1.5}$ watts/[m²·sr] relative to a background spectrum with total radiance of about 11.7 watts/[m²·sr].

To compute the contrasts for each photoreceptor class, we use device calibration information to compute the predicted spectrum from the device settings. This, together with specification of a background spectrum, allows the computation of contrasts. Typically, we chose the background spectrum $B(\lambda)$ to be that produced by the mixture of all primaries at half their maximum power. Suppose there are n classes of photoreceptor under consideration, whose spectral sensitivities

$S_n(\lambda)$ are known. We compute the receptor responses of each class to the background b_n as

$$b_n = \sum_n S_n(\lambda)B(\lambda)\delta\lambda \quad (2)$$

Similarly, for any other spectrum $M(\lambda)$, we compute the receptor responses m_n as

$$m_n = \sum_n S_n(\lambda)M(\lambda)\delta\lambda \quad (3)$$

This yields the contrast seen by each photoreceptor class between the between $M(\lambda)$ and $B(\lambda)$ as

$$c_n = \frac{m_n - b_n}{b_n} \quad (4)$$

To make the silent-substitution properties of the modulations robust to uncertainty about the spectral sensitivities of the specified photoreceptor classes, we add to the silenced set of photoreceptors not only the nominal versions of the silenced photoreceptor classes but also variants of the nominal versions that represent individual variation. Effectively, the set of silenced photoreceptors provides a basis that spans a larger space of silenced photoreceptor sensitivities. For example, if we are silencing the open-field cones, we have the option of adding to the silenced set variants of the open-field cones computed with higher and lower lens densities than the nominal versions. Whether this is desirable to do again involves a tradeoff that we make manually. The more photoreceptor variants we add to the silenced set, the more robust the modulations but the lower the maximum contrast achievable for the targeted set. We make this tradeoff through examination of the maximum achievable contrasts and of “contrast splatter maps”, which are described below. For the modulations used in this paper, we did not in the event add additional photoreceptor classes to the silenced set, because we wanted to produce as much differential contrast as possible between penumbral and open-field cones. In other work [1], we have found it beneficial to increase robustness in the manner described here.

Sometimes it is desirable not to maximize the contrast for the photoreceptor classes in the maximized set, but rather to produce modulations that have specified target contrasts for each class in this set. For example, for the supplemental experiment reported in this paper we produced modulations that had the same 20% contrast on melanopsin with and without stimulating the penumbral cones. This is achieved in our software by replacing the objective function that seeks to maximize the contrast of the classes in the maximized set with a modified objective function that seeks to bring these contrasts as close as possible to a set of specified

target contrasts t_m . Specifically, in this case the optimization routine seeks to minimize the sum of squared deviations

$$f = \sum_m (c_m - t_m)^2 \quad (5)$$

between the predicted contrasts c_m and the targeted contrasts t_m for the members of the targeted set. In practice, we generally begin by finding the maximum available contrast on classes in the maximized set and then choosing targeted contrasts based on this information.

The contrasts of the photoreceptor classes in the ignored set are disregarded in the optimization. For example, when we compute modulations for use in studies at high photopic light levels, we often place the rod spectral sensitivities in the ignored set. The reader may note that this could also be accomplished simply by not specifying the ignored classes in the set of photoreceptor spectral sensitivities under consideration. We find the code more transparent if we allow for explicit specification of what classes are ignored, as this allows use of a single set of receptor sensitivities across multiple calls to the optimization routine. The calculation of a given desired spectral modulation takes <400 ms in MATLAB on a current (2014) desktop computer.

Estimates of Photoreceptor Sensitivities

Spectral sensitivities of the open-field L, M and S cones at the cornea were calculated using the CIE 2006 parametric model and incorporate pre-retinal filtering due to lens, ocular media and macular pigment using the age, pupil size and field size dependences of that model [200]. Pre-retinal filtering for all spectral sensitivities was computed using the actual age of each observer and the appropriate field size (27.5°). Although the CIE standard specifies a very small but non-zero amount of macular pigment density outside the central 5°, the contribution of macular pigment filtering to the cone fundamentals for our stimulus configuration is minimal. We adjusted the peak optical density of the cone photopigments depending on the expected proportion of bleached photopigment [303, 304] for the retinal illuminance of our rod-saturating background stimulus. For the psychophysical rating task (observers MS, GKA, DHB), we assumed a pupil diameter of 3 mm in computing retinal illuminance, corresponding to the natural light-adapted

pupil. For the sketch drawing, we assumed a pupil diameter of 4.7 mm, which is slightly higher than the expected light-adapted pupil size for that light level [Table 1; 305].

We obtained spectral sensitivities for the penumbral cones by assuming that hemoglobin acts as a pre-retinal filter. We calculated the hemoglobin transmittance spectrum as follows, following the calculations of Horiguchi, et al. [164]. We obtained estimates of the molar extinction coefficients ϵ of oxyhemoglobin (HbO_2) and deoxyhemoglobin (Hb) expressed in [$\text{cm}^{-1}/(\text{moles/liter})$] [226]. To convert this to the absorptivity, we multiplied by the constant 2.303 and the molar concentration of

$\frac{150 \text{ g Hb/liter}}{64,500 \text{ g Hb/mole}}$ [226], giving the *absorptivity* oxyhemoglobin and deoxyhemoglobin, given by

coefficients A_{HbO_2} and A_{Hb} , expressed per μm . We assumed an optical path length through the vessels of 11.5 μm for penumbral cones, thus obtaining *absorptance* coefficients $a_{\text{HbO}_2} = 11.5A_{\text{HbO}_2}$ and $a_{\text{Hb}} = 11.5A_{\text{Hb}}$. This diameter corresponds to the size of venules or smaller arterioles. We combined these to get overall absorptance as follows. We assumed that oxyhemoglobin makes up 95% of the hemoglobin in arteries and 75% of the hemoglobin in veins at room air oxygenation following the oxygen-hemoglobin dissociation curve of adult hemoglobin [306], and took the average between these two to set the fraction of oxygenated hemoglobin at

85%. The overall absorptance was computed as $0.85a_{\text{HbO}_2} + 0.15a_{\text{Hb}}$ and the transmittance was then obtained as $10^{-(0.85a_{\text{HbO}_2} + 0.15a_{\text{Hb}})}$.

We constructed the spectral sensitivity of melanopsin along the lines of a recently proposed standard for ‘melanopic’ sensitivity [102] by shifting the Govardovskii nomogram [97] to have its peak spectral sensitivity λ_{\max} at 480 nm, consistent with previous reports of the peak spectral sensitivity of melanopsin [56, 100, 101]. We assumed an optical density of 0.015 [205]. For melanopsin, pre-retinal filtering was incorporated as for the cones, except for filtering due to

macular pigment, which was omitted altogether because the melanopsin-containing retinal ganglion cells lie in front of the macular pigment layer.

Precision of Photoreceptor Isolation

To estimate the uncertainty of the method of silent substitution given our apparatus, we calculated *contrast splatter*, which is the expected amount of contrast on nominally silenced photoreceptor classes for a given modulation around a given background. This was done by calculating contrast across variants of photoreceptor sensitivity obtained by shifts in the assumed wavelength of photopigment peak absorbance (λ_{\max}) and varying observer lens density using age as the parameter describing lens density according to the CIE formula [200]. Shifts of photopigment absorbance were accomplished by using the Stockman-Sharpe nomogram, which provides a formula that yields the full photopigment spectral absorbance spectrum given a specified wavelength of peak absorbance λ_{\max} [289]. A calculation was performed for each photoreceptor class in which we varied λ_{\max} by ± 10 nm and let the age parameter vary between 20 and 60 years. In estimating the spectral sensitivities of the photoreceptor variants, we did not recalculate the estimate of fraction of cone photopigment bleached for each variant. Figure 2.4 shows the results of the splatter calculation. In panel A, for example, the top two pseudocolor plots show the computed contrast splatter map for each variant of the open-field L cones and penumbral L cones, for a 27 year old observer (MS), for the L and M penumbral cone modulation. Computed contrast matches the nominal values (0% for open-field L cones; 4.2% for penumbral L cones) for the targeted λ_{\max} (558.9 nm) and observer age (27), and deviates from the nominal values for other L cone variants.

Using estimates of the variability of λ_{\max} and lens density in the population of normal color observers, we then constructed 95% and 99% confidence ellipses for these parameters, based on the assumption that variability is normally and independently distributed for both λ_{\max} and lens density. We also calculated the expected absolute contrast splatter, which is the expected

absolute value of the deviation between obtained and targeted contrast for the silenced photoreceptors, based on the same assumption. We assumed standard deviations of 1.5, 0.9 and 0.8 nm for L, M and S cone λ_{\max} variation around the nominal values [223]. We extracted the standard deviation of the veridical measurement residuals vs. chronological age from a two-component lens density model [110] and found that the standard deviation of the predicted age parameter of lens density due to individual variation is 7 years. For nominally silent photoreceptor classes, the expected absolute contrast splatter does not exceed 1.23% for any observer, modulation direction, and photopigment absorbance variant (Table 2.1). Additional contrast splatter may arise because of limitations of stimulus control. We periodically assess this via direct measurement of the spectra produced by our stimulus device, and find that it is of the same order as the contrast splatter we expect from uncertainty in photoreceptor sensitivities.

We considered the possibility that the modulation that nominally drove open-field and penumbral cones together ($L+M+L^*+M^*$) in practice elicited substantial differential contrast between the open-field and penumbral cones. To test this, we constructed contrast splatter maps for this modulation (Fig. 2.4, panel C) for the 27 year old observer (MS). For each photoreceptor variant we then plotted the contrast seen by the penumbral L and M cones against the contrast seen by their open-field counterparts (Fig. 4, panel D). We find that the contrasts seen by the open-field and penumbral cones are similar to each other across all of the photoreceptor variants, indicating that this key property of the modulation is highly robust with respect to variation in photoreceptor spectral sensitivity. The differential contrast of penumbral cones relative to open-field cones for our penumbral L and M modulation is similarly robust (Fig. 2.4, panel B).

Fundus Photos

The fundus photographs for our naïve observer (Fig. 2.2c, Fig. 2.5) were obtained using a NIDEK Microperimetry device (MP1). For visualization purposes, the retinal vasculature (Fig. 2.2c overlay) was manually extracted from the photograph with Adobe Photoshop using a combination

of image feature selection techniques, and the contrast and color balance of the photos was adjusted for visualization purposes. A raw version of the fundus photos is provided in Figure 2.5.

Supplemental Experiment

In a supplemental experiment, we tested whether a melanopsin-directed modulation designed to silence open-field but not penumbral cones can elicit percepts of the Purkinje tree, and whether this is due to contrast seen by penumbral cones (Fig. 2.6). Observers viewed two melanopsin-directed modulations. The *Melanopsin A* modulation was constructed using a target contrast for melanopsin of 20% with open-field L, M and S cones silenced. Stimulus contrast was not constrained for penumbral cones, however, and this resulted in a *Melanopsin A* modulation that produced ~2-3% contrast on penumbral L and M cones and ~10% contrast on penumbral S cones (Table 2.1). The *Melanopsin B* modulation was constructed again using a target contrast of 20% for melanopsin, but with both open-field and penumbral cones silenced. As control modulations, we added the L and M penumbral cone directed modulation and a modulation stimulating both sets of L and M cones together while silencing the other photopigments. These latter two modulations were as in our main experiment.

The rating methods, background light level, and stimulus temporal properties were the same as in our main experiment, and the three authors again served as observers. Each combination of modulation direction and frequency was presented five times, with trial order randomized. On 14 out of 154 trials, no modulation at all was shown (blank trials).

We replicated the visibility of the Purkinje tree for selective penumbral L and M cone stimulation (Figs. 2.3 and 2.6), finding a maximum visibility rating at 16 Hz, dropping sharply at frequencies lower than 8 Hz and higher than 32 Hz. As in the main experiment, our open-field and penumbral L and M cone modulation elicits some spatial structure at frequencies higher than 16 Hz, but no Purkinje tree. Crucially, the *Melanopsin A* modulation elicited Purkinje-tree percepts similar to those produced by the penumbral L and M cone modulation. When penumbral cones were

silenced but melanopsin driven at the same contrast (*Melanopsin B*), the Purkinje-tree percept was considerably reduced, with some observer variability in the degree of reduction. We speculate that the individual variability results from individual differences in the residual penumbral cone contrast produced by the *Melanopsin B* modulation. Out of the 14 blank trials, observers MS and GKA rated all of them as 0; observer DHB rated one trial out of the blank trials as 1, and 13 as 0.

Acknowledgements

We wish to thank Jessica Morgan and Grace Han for acquiring the fundus photographs of our naïve observer. This work was supported by NIH Grant 1 R01 EY020516 (GKA), R01 EY10016 (DHB), P30 EY001583 (Core Grant for Vision Research) and Deutscher Akademischer Austauschdienst (MS).

Figures

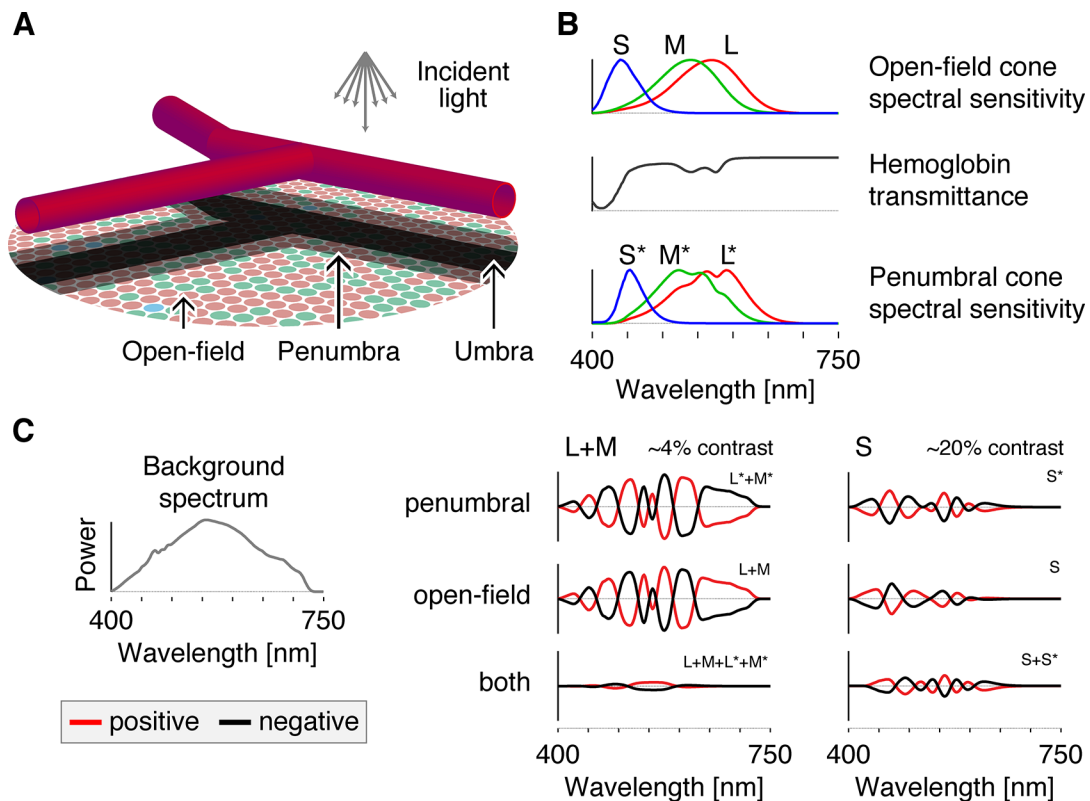


Figure 2.1: Spectral sensitivities and apparatus.

A: Schematic diagram of the retina showing the shadows cast by the retinal blood vessels lying in front of the photoreceptive layer of the retina. B: The spectral sensitivities of the open-field cones (*upper panel*) are filtered by the hemoglobin transmittance spectrum (*middle panel*), resulting in wavelength-specific changes of the cone spectral sensitivities (*lower panel*). C: All modulations are carried out around a rod-saturating background whose spectrum is shown at the left. On the right are plotted the spectral modulations that target each of the indicated cone class(es), with the targeted class(es) indicated at the upper right of each individual plot. The amplitudes of these modulations are varied sinusoidally in time between the plotted positive (red) and negative (black) modulations and are then added to the background spectrum to produce the stimuli seen by the observer.

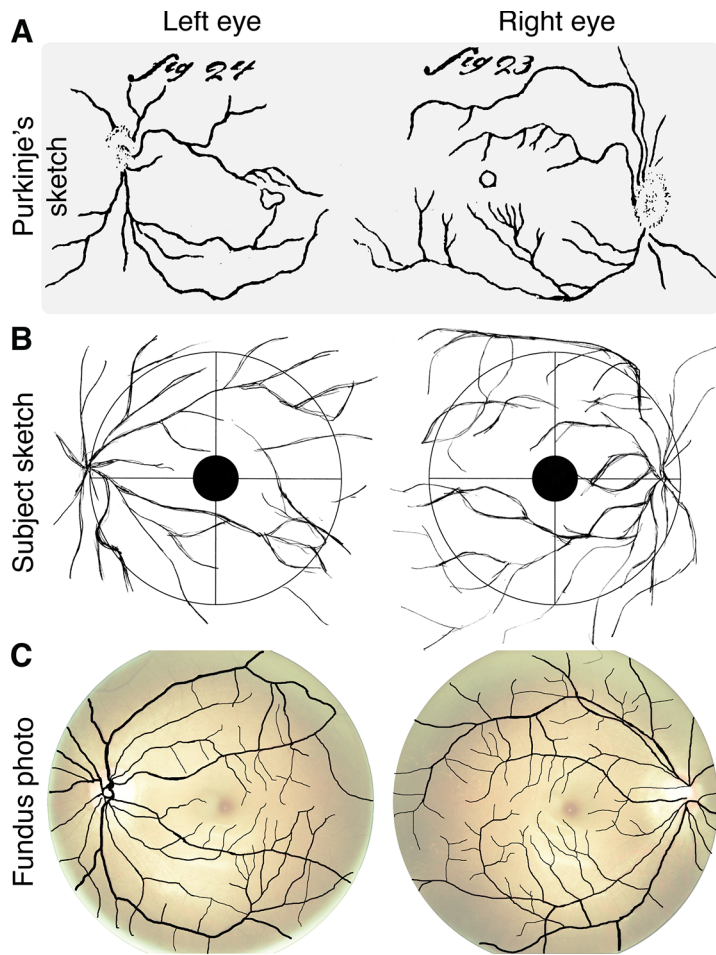


Figure 2.2: Purkinje-tree percepts.

A: Sketch of entoptic visualization of retinal blood vessels from Purkinje ([7]; Figs 23 and 24). B: Sketch produced by a naïve observer in our study while viewing penumbral cone directed flicker at 16 Hz. C: Fundus photographs with overlaid extracted retinal blood vessels (see detailed methods). The contrast and brightness of the fundus photographs were adjusted, and then made transparent for visualization purposes (see Fig. 2.5 for raw fundus photographs). The fundus photos were obtained after the observer produced her sketches.

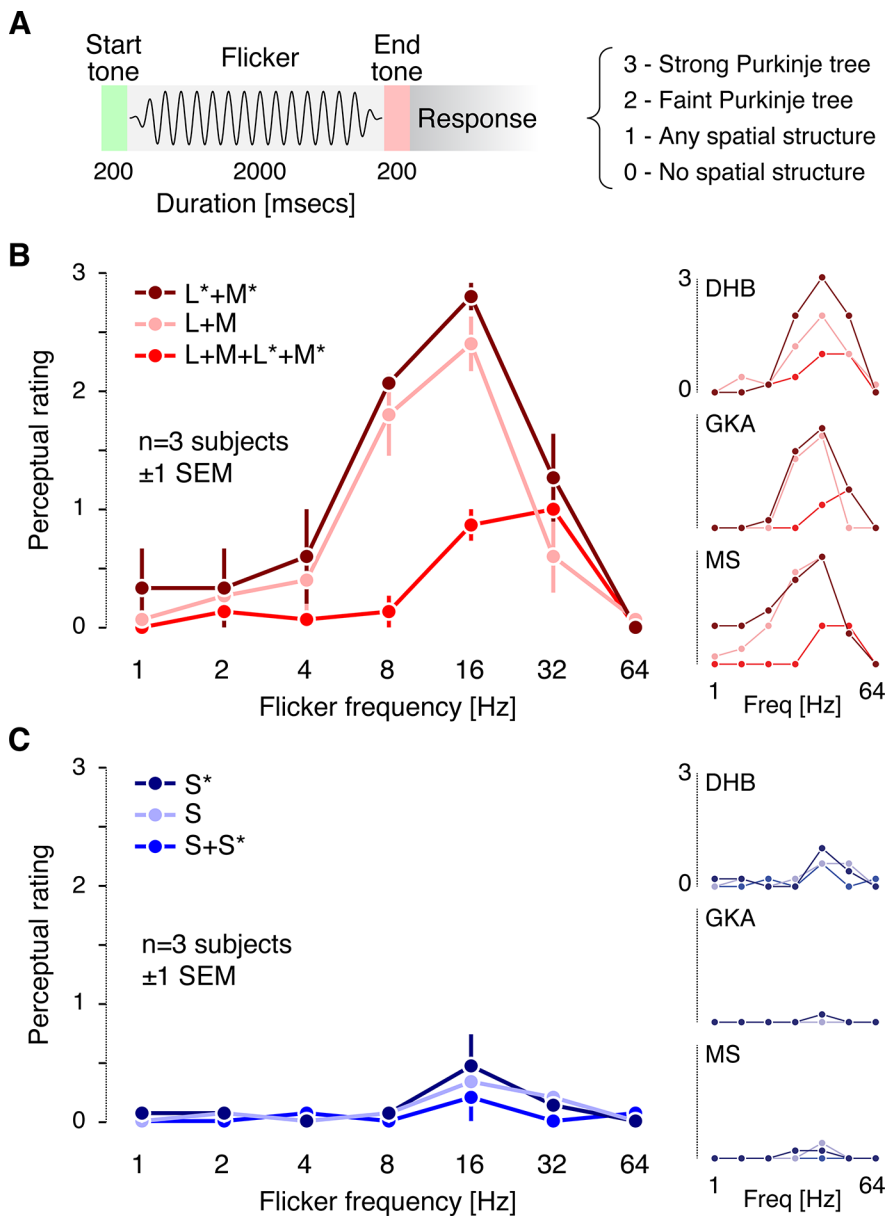


Figure 2.3: Psychophysical rating results.

A: Time course of a single trial of the rating experiment and summary of the perceptual rating scale (see main text for more detailed description). B: Average ratings across the three observers for the L and M cone directed modulations. L*+M*, penumbral L and M cone modulation; L+M, open-field L and M cone modulation; L+M+L*+M*, modulation visible to both open-field and penumbral L and M cones. Individual observer ratings are shown to the right. C: Average ratings

across the three observers for the S cone directed modulations. S^* , penumbral S cone modulation; S, open-field S cone modulation; $S+S^*$, modulation visible to both open-field and penumbral S cones. Individual observer ratings are shown to the right.

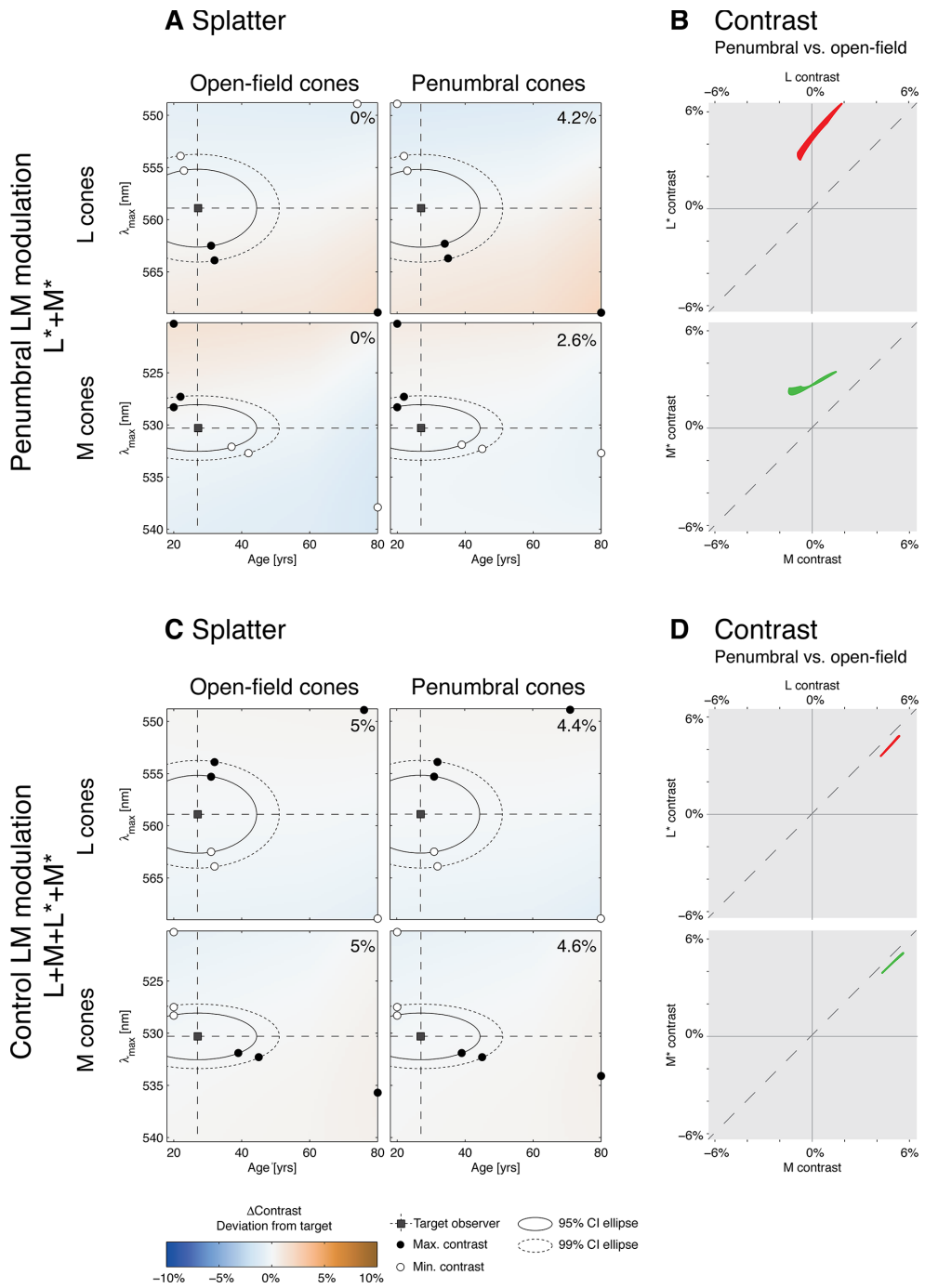


Figure 2.4: Contrast splatter.

A: Contrast splatter calculations for the penumbral L and M cone (L^*+M^*) modulation (27 year old observer). Separate splatter maps for open-field and penumbral L and M cones are provided.

Each point in a splatter map indicates in pseudocolor the contrast that will be seen by a variant of the nominal cone spectral sensitivity, as indicated by its position on the age and λ_{\max} axes. The color scale is provided at the bottom of the figure, with negative contrast splatter indicating contrast splatter that is 180° out-of-phase with the nominal stimulus modulation. The open square indicates age and λ_{\max} of the nominal cone spectral sensitivity, while the solid and dashed ellipses indicate the 95% and 99% confidence ellipses for variation around the nominal sensitivity. Open and closed circles on each ellipse show the variant with the minimum and maximum contrast splatter on the ellipse. Open and closed circles on the edges of the map represent the variant with minimum and maximum contrast splatter over the whole range of variants computed. The nominal contrast of the modulation for each cone type is provided in the upper right of each map. B: Comparison of contrast seen by the penumbral vs. open-field L cones across the entire range of photoreceptor variants studied in panel A (top plot) and similarly for the M cones (bottom plot). C: Contrast splatter maps for the modulation that stimulated both penumbral and open-field L and M cones together (27 year old observer). Same format as panel A. D: Same type of comparison as shown in panel B, obtained from the splatter maps shown in panel C.

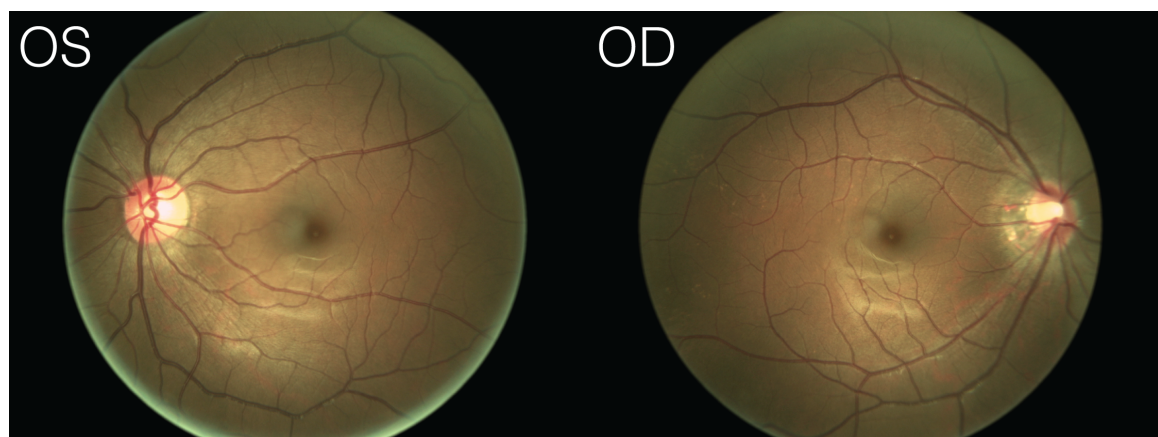


Figure 2.5: Raw fundus photographs.

Unedited fundus photographs (OS = left eye, OD = right eye) obtained for our naïve observer.

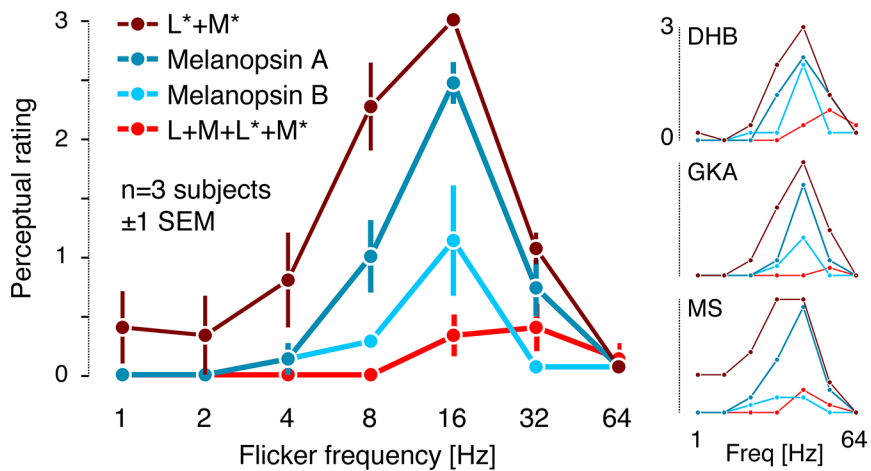


Figure 2.6: Rating data from the supplemental experiment.

Average ratings across the three observers. L^*+M^* , penumbral L and M cone modulation; Melanopsin A, melanopsin-directed modulation that did not silence penumbral cones; Melanopsin B, melanopsin-directed modulation with penumbral cones silenced; $L+M+L^*+M^*$, modulation visible to both open-field and penumbral L and M cones. Individual observer ratings are shown to the right.

Table 2.1: Modulations and contrast values.

Direction	Task	Observer		Chromaticity		Pupil diameter [mm]		Target contrast [%] (Expected absolute contrast splatter [%])								
		Age [yrs]	ID	Mean luminance [cd/m ²]	x	y	Assumed	Expected	L	M	S	L*	M*	S*	Mel	Rods
L*+M*	Psychophysical rating task (n = 3) Main data	27	MS	1950	0.38	0.43	3	3.22	0.00 (0.12)	0.00 (0.10)	0.00 (0.32)	4.24	2.64	0.00 (0.67)	0.00 (0.39)	2.53 (2.52)
		44	GKA					3.06	0.00 (0.11)	0.00 (0.10)	0.00 (0.34)	4.18	2.58	0.00 (0.69)	0.00 (0.41)	2.66 (2.65)
		54	DHB					2.97	0.00 (0.11)	0.00 (0.11)	0.00 (0.37)	4.15	2.54	0.00 (0.79)	0.00 (0.44)	2.75 (2.75)
	L+M	27	MS					3.22	4.06	2.87	0.00 (0.31)	0.00 (0.05)	0.00 (0.08)	0.00 (0.65)	0.00 (0.30)	-1.30 (1.28)
		44	GKA					3.06	3.89	2.95	0.00 (0.32)	0.00 (0.01)	0.00 (0.06)	0.00 (0.66)	0.00 (0.28)	-0.99 (0.98)
		54	DHB					2.97	3.71	3.07	0.00 (0.34)	0.00 (0.04)	0.00 (0.05)	0.00 (0.73)	0.00 (0.26)	-0.49 (0.48)
	L+M+L*+M*	27	MS					3.22	5.00	5.00	0.00 (0.03)	4.44	4.57	0.00 (0.05)	0.00 (0.13)	1.89 (1.90)
		44	GKA					3.06	5.00	5.00	0.00 (0.03)	4.44	4.57	0.00 (0.05)	0.00 (0.14)	1.91 (1.91)
		54	DHB					2.97	5.00	5.00	0.00 (0.03)	4.45	4.57	0.00 (0.06)	0.00 (0.14)	1.91 (1.93)
S*	Psychophysical rating task (n = 3) Main data	27	MS					3.22	0.00 (0.04)	0.00 (0.03)	0.00 (0.89)	0.00 (0.05)	20.00	0.00 (0.16)	-0.43 (0.43)	
		44	GKA					3.06	0.00 (0.05)	0.00 (0.04)	0.00 (1.06)	0.00 (0.06)	20.00	0.00 (0.21)	-0.68 (0.68)	
		54	DHB					2.97	0.00 (0.06)	0.00 (0.06)	0.00 (1.34)	0.00 (0.07)	20.00	0.00 (0.26)	-0.88 (0.88)	
S	Psychophysical rating task (n = 3) Main data	27	MS					3.22	0.00 (0.02)	0.00 (0.02)	20.00	0.00 (0.01)	0.00 (0.01)	0.00 (0.69)	0.00 (0.08)	0.47 (0.46)
		44	GKA					3.06	0.00 (0.04)	20.00	0.00 (0.04)	0.00 (0.04)	0.00 (0.03)	0.00 (0.91)	0.00 (0.17)	1.06 (1.06)
		54	DHB					2.97	0.00 (0.11)	0.00 (0.08)	19.81	0.00 (0.12)	0.00 (0.07)	0.00 (1.23)	0.00 (0.33)	2.18 (2.18)
S+S*	Psychophysical rating task (n = 3) Main data	27	MS					3.22	0.00 (0.04)	0.00 (0.02)	20.00	0.00 (0.05)	20.00	0.00 (0.03)	-0.12 (0.12)	
		44	GKA					3.06	0.00 (0.04)	20.00	0.00 (0.04)	0.00 (0.04)	20.00	0.00 (0.17)	-0.17 (0.17)	
		54	DHB					2.97	0.00 (0.04)	0.00 (0.02)	20.00	0.00 (0.05)	20.00	0.00 (0.20)	-0.20 (0.21)	
Melanopsin A	Psychophysical rating task (n = 3) Supplementary data	27	MS					3.22	0.00 (0.20)	0.00 (0.20)	0.00 (0.66)	2.93	2.43	10.06	20.00	12.78 (12.76)
		44	GKA					3.06	0.00 (0.20)	0.00 (0.21)	0.00 (0.68)	2.85	2.35	9.03	20.00	12.75 (12.75)
		54	DHB					2.97	0.00 (0.20)	0.00 (0.25)	0.00 (0.79)	2.81	2.30	8.49	20.00	12.74 (12.68)
Melanopsin B	Psychophysical rating task (n = 3) Supplementary data	27	MS					3.22	0.00 (0.21)	0.00 (0.18)	0.00 (0.44)	0.00 (0.24)	0.00 (0.21)	0.00 (0.80)	20.00	11.86 (11.85)
		44	GKA					3.06	0.00 (0.21)	0.00 (0.19)	0.00 (0.45)	0.00 (0.23)	0.00 (0.22)	0.00 (0.79)	20.00	11.80 (11.80)
		54	DHB					2.97	0.00 (0.21)	0.00 (0.23)	0.00 (0.49)	0.00 (0.23)	0.00 (0.26)	0.00 (0.88)	20.00	11.77 (11.72)
L*+M* +Melanopsin	Sketch	29	HW	2200	0.38	0.43	4.7	3.16	0.00 (0.60)	0.00 (0.97)	0.00 (0.78)	7.73	5.58	0.00 (2.67)	41.35 (41.05)	27.35 (28.05)

The table provides detailed information on the photoreceptor contrast expected for each of our stimulus modulations. Expected absolute contrast splatter was calculated according to the method outlined in the appendix. L*+M*, penumbral L and M cone modulation; L+M, open-field L and M cone modulation; L+L*+M*, modulation visible to both open-field and penumbral L and M cones; S*, penumbral S cone modulation; S, open-field S cone modulation; S+S*, modulation visible to both open-field and penumbral S cones. Individual observer ratings are shown to the right; Melanopsin A, melanopsin-directed modulation that did not silence penumbral cones; Melanopsin B, melanopsin-directed modulation with penumbral cones silenced; L*+M*+Melanopsin, penumbral L and M cone modulation ignoring melanopsin. Bold contrast values indicate the targeted photoreceptors. Italic contrast values indicate contrast not controlled for. Expected pupil diameter calculated using the unified formula for light-adapted pupil size from Watson and Yellott [36] assuming a 27.5° field and monocular illumination. This choice affects calculated retinal illuminance and thus the estimated fraction of cone pigment bleached used to construct cone spectral sensitivities. It would have been better to use a 3 mm pupil for observer HW, but the effect of the larger assumed pupil size is small (see [Appendix](#)).

doi:10.1371/journal.pone.0124328.t001

HUMAN VISUAL CORTEX RESPONSES TO RAPID CONE AND MELANOPSIN
DIRECTED FLICKER (Spitschan *et al.*, 2016)

Note: This chapter was published as Spitschan, et al. [3].

Abstract

Signals from cones are recombined in post-receptoral channels (luminance, L+M; red-green, L–M; blue-yellow; S–[L+M]). The melanopsin-containing retinal ganglion cells are also active at daytime light levels and recent psychophysical results suggest that melanopsin contributes to conscious vision in humans. Here, we measured BOLD fMRI responses to spectral modulations that separately targeted the post-receptoral cone channels and melanopsin. Responses to spatially uniform (27.5° field size, central 5° obscured) flicker at 0.5, 1, 2, 4, 8, 16, 32 and 64 Hz were recorded from areas V1, V2/V3, motion-sensitive area MT, and the lateral occipital complex (LOC). In V1 and V2/V3, higher temporal sensitivity was observed to L+M+S (16 Hz) as compared to L–M flicker (8 Hz), consistent with psychophysical findings. Area MT was most sensitive to rapid (32 Hz) flicker of either L+M+S or L–M. We find S cone responses only in areas V1 and V2/V3 (peak frequency: 4–8 Hz). In addition, we studied an L+M modulation and found responses that were effectively identical at all temporal frequencies to those recorded for the L+M+S modulation. Finally, we measured the cortical response to melanopsin-directed flicker, and compared this response to control modulations that addressed stimulus imprecision and the possibility of stimulation of cones in the shadow of retinal blood vessels (penumbral cones). For our stimulus conditions, melanopsin flicker did not elicit a cortical response exceeding that of the control modulations. We note that failure to control for penumbral cone stimulation could be mistaken for a melanopsin response.

Significance Statement

The retina contains cone photoreceptors as well as ganglion cells that contain the photopigment melanopsin. Cones provide brightness and color signals to visual cortex. Melanopsin influences circadian rhythm and the pupil, but its contribution to cortex and perception is less clear. We measured the response of human visual cortex with functional MRI, using spectral modulations tailored to separately stimulate the cones and melanopsin. We find that cortical responses to cone signals vary systematically across visual areas. Differences in temporal sensitivity for achromatic, red-green, and blue-yellow stimuli generally reflect the known perceptual properties of vision. We find that melanopsin signals do not produce a measurable response in visual cortex at temporal frequencies between 0.5 and 64 Hz at daytime light levels.

Introduction

In humans, signals originating in the short (S), middle (M) and long-wavelength (L) cones of the retina provide chromatic and luminance information [194]. The L and M cones are summed (L+M) to form a luminance channel and differenced (L-M) to form a ‘red-green’ chromatic pathway, while signals from S cones are opposed to the sum of L and M cones to create a ‘blue-yellow’ chromatic pathway [307] (Figure 3.1a).

The luminance and chromatic pathways differ in their temporal sensitivity as measured by psychophysics. The chromatic pathways have maximal temporal sensitivity at lower frequencies than the luminance pathway [308, 309], although the exact shape of the temporal contrast sensitivity functions depends on the spatial frequency [263, 310], mean luminance [311, 312], and eccentricity of the stimulus [313].

Functional magnetic resonance imaging (fMRI) has also been used to study the temporal properties of the post-receptoral mechanisms. For example, Engel, et al. [314] found strong Blood Oxygen Level Dependent (BOLD) responses to L-M flicker in areas V1 and V2 for flicker between 1 and 10 Hz, while responses to S-directed flicker were reduced at 10 Hz. They found

similarities in the temporal dependence of the BOLD response and psychophysical results for stimuli at 1 and 4 Hz, while at 10 Hz the relative response to L-M flicker in V1 and V2 was larger than psychophysics would predict.

Recent discoveries in the biology of the retina lead us to revisit these findings. Melanopsin is a light sensitive molecule expressed in some retinal ganglion cells, rendering them *intrinsically photosensitive*. The melanopsin-containing, intrinsically photosensitive ganglion cells (ipRGCs) also receive synaptic inputs from rods and cones, thus combining signals from the inner and outer retina. A major projection of the ipRGCs is to brainstem and hypothalamic sites, where they influence pupil response [1, 63, 116, 293] and circadian rhythm [60]. The ipRGCs project as well to the lateral geniculate nucleus [34, 90, 163, 295], and recent studies suggest that humans are able to perceive variation in melanopsin contrast as variation in brightness [162, 163].

This raises the possibility that prior studies of psychophysical and fMRI cone temporal sensitivity include a contribution of melanopsin-mediated signals, as the spectral sensitivity of melanopsin overlaps extensively with that of the cones (Figure 3.1b). While the responses of the ipRGCs are notably delayed and prolonged [34], these cells are capable of more rapid signaling. As stimulus intensity rises, the ipRGCs manifest initial transient responses that peak between 200 and 2000 msec [205]. Recent studies have raised the possibility that humans are able to perceive rapid melanopsin stimulation. For example, subjects were able to detect cone-silent flicker at rod saturating light levels in the visual periphery up to 40 Hz [164].

Here, we used functional MRI in conjunction with cone-directed, spatially uniform flicker to measure the temporal sensitivity profiles of the visual cortex representation of cone and melanopsin signals. Using a digital spectral device with 56 effective primaries [2], we constructed cone-directed modulations while controlling for activation of melanopsin. We measured cortical temporal transfer functions for the fMRI response to these modulations presented at logarithmically spaced flicker rates between 0.5 and 64 Hz. We then constructed a modulation

that targeted melanopsin while controlling for activation of the cones. We examined the perceptual properties of this modulation, and its ability to drive neural and pupil responses. Cortical responses to this stimulus were compared to those from control modulations that accounted for imprecision in our stimulus specification.

Materials & Methods

Subjects. Three male subjects (aged 43, 26 and 28 years; subjects S01, S02, and S03; the former two are authors of this study) participated in the fMRI experiments. These three primary subjects and twelve additional subjects (8 male, 4 female; age = $30 \pm 2\text{SD}$ years; subjects S04-15), participated in perceptual nulling and pupillometry experiments. The data from one additional subject who participated in the nulling and pupillometry experiments was discarded because of poor pupil tracking. All subjects had corrected-to-normal acuity of 20/40 or better and normal color vision [218]. The research was approved by the University of Pennsylvania Institutional Review Board and conducted in accord with the principles of the Declaration of Helsinki. All subjects gave informed written consent.

Visual stimuli

Digital light synthesis and silent substitution. We used the method of silent substitution with a digital light synthesis engine (OneLight Spectra) to stimulate targeted photoreceptors. Our device produces stimulus spectra as mixtures of 56 independent, ~ 16 nm full-width half-max primaries under digital control, and can modulate between these spectra at a rate up to 256 Hz. In the fMRI experiments, we used a refresh rate of 256 Hz, while in the pupillometry experiments we used a refresh rate of 64 Hz. Details regarding the device, stimulus generation, and estimates of precision may be found in Spitschan, et al. [2]. Our estimates of photoreceptor spectral sensitivities were as described in Spitschan, et al. [2] and account for the size of the visual field and subject age. Cone spectral sensitivity adjustments for photopigment bleaching were made for all modulations except those used in BOLD fMRI Experiment 1.

All stimuli were modulations around a common, rod-saturating background (Figure 3.1C; chromaticity $x = 0.40$, $y = 0.43$). Background luminance was $3,700 \text{ cd/m}^2$ in BOLD fMRI experiment 1, $3,000 \text{ cd/m}^2$ in perceptual nulling and pupillometry and $2,900 \text{ cd/m}^2$ in BOLD fMRI experiment 2. Modulations were between positive and negative spectra designed to increase and decrease excitation of the targeted photoreceptor(s) and produced sinusoidally-modulated contrast relative to the background. The spectra are designed such that excitations in “silenced” photoreceptors are held constant. The maximum contrast available upon the targeted photoreceptor(s) is limited by the degree of spectral overlap of the photoreceptors, the gamut of the device, and the chromaticity of the background. Several different modulations were studied as part of the BOLD fMRI and pupillometry studies (Fig 3.1D; Table 2.1).

Modulations studied in BOLD fMRI Experiment 1. We measured visual cortex responses to seven different photoreceptor-directed modulations at a range of temporal frequencies. A set of cone-directed stimuli targeted L, M and S cones with equal contrast (L+M+S, 45% contrast), a red-green chromatic channel (L-M, 10% contrast), S cones (45% contrast), and L and M cones in isolation (L+M, 45% contrast). A melanopsin directed modulation (Mel, 17% contrast) was also studied. This modulation was designed to stimulate melanopsin and to silence not only the cones with their expected spectral sensitivities, but also those cones that have (effectively) altered spectral sensitivity as a consequence of being shadowed by larger retinal blood vessels [2]. We designate these “penumbral” cones that receive hemoglobin-filtered light with an asterisk (i.e., L* indicates L-cones in the shadow of blood vessels). A rapid (8-16 Hz) melanopsin directed modulation that does not silence the penumbral cones produces an entopic percept of the branching retinal blood vessels [2].

A primary concern in studies of this kind is that inadvertent contrast upon the nominally silenced classes of photoreceptors might produce cortical responses that are mistakenly attributed to the action of the targeted photoreceptor class or classes. We have estimated that this undesired

photoreceptor contrast “splatter”—which can arise from biological variability, misspecification of the cone fundamentals, and imperfections in device control—is on the order of a few percent in our stimulus system [2]. We examined two control modulations in BOLD fMRI Experiment 1 to address the contribution of contrast splatter from various sources. A scaled (2% contrast) version of the L+M stimulus was selected to correspond to the uncertainty present in our silencing of photoreceptors. Therefore, the cortical response to a cone-directed modulation at this contrast level provides a threshold for “stimulus noise” in our BOLD fMRI measurements of wide-field photoreceptor directed flicker. We also measured the cortical response that can arise from isolated stimulation of penumbral cones. A modulation was constructed that selectively targeted the L* and M* cones with 2% and 1% contrast (respectively) while silencing the L, M, and S cones, as well as melanopsin [see 2]. We refer to this as the 2% L*+M* modulation.

Modulations studied during pupillometry. We measured the pupil response to slow (0.1 Hz) spectral modulations. Data were collected from all subjects using cone (L+M+S; 32% contrast) and melanopsin (Mel*; 32% contrast) directed modulations. The Mel* modulation was designed to silence the cones but not their penumbral variants, as the slow modulation studied for pupillometry does not produce a percept of the retinal blood vessels. In earlier work we have shown that the pupil response to a melanopsin modulation is not appreciably altered by the silencing of the penumbral cones [1, Figure 1.9b]. These modulations were tailored for each subject during a psychophysical calibration session (nulling procedure, described below) to remove residual chromatic and (in the case of the melanopsin modulation) luminance components.

In addition to these two modulations, the three primary subjects also were studied with a light flux modulation (32% contrast).

Modulations studied in BOLD fMRI Experiment 2. Four additional modulations were examined at a single temporal frequency (4 Hz) during BOLD fMRI scanning for the three primary subjects.

Immediately prior to scanning, each subject conducted the psychophysical nulling procedure upon the 17% contrast penumbral-cone silent Mel stimulus. The chromatic and luminance nulling values for each subject were noted. During scanning, the subject was presented with the same, un-nulled Mel modulation used in BOLD fMRI Experiment 1, as well as their individualized, perceptually nulled Mel modulation. The difference between the nulled and un-nulled Mel modulations constituted a third modulation condition, allowing measurement of the cortical response to the inadvertent cone contrast present in the un-nulled Mel stimulus. Finally, a high-contrast (90%) light flux modulation was included as a positive control.

Psychophysical calibration (nulling). In informal observations, we noted that although the melanopsin-directed and L+M+S-directed modulations theoretically silence post-receptoral cone opponent mechanisms, both melanopsin and L+M+S modulations produced reddish-greenish changes in color appearance for most of our subjects. We considered the most likely cause of these change to be differential contrast splatter onto the L and M cones. As human vision is highly sensitivity to L-M modulations [315], not much residual contrast is required to produce a perceptually visible color change. Although contrast splatter is not the only possible explanation for a perceived color change in response to our melanopsin modulation (e.g., melanopsin could in principle contribute to perceptual redness) we sought to measure the putative cone splatter using a psychophysical nulling procedure.

For the melanopsin-directed modulation, subjects were asked to null luminance and red-green color appearance changes. For the L+M+S-directed modulation, subjects nulled only the red-green changes. Luminance nulling was realized by alternating the positive or negative excursions of the modulation spectra with the background spectrum in a square-wave fashion at 30 or 40 Hz pulsed for 1 second (40 Hz for S01-03; 30 Hz for S04-S05). Subjects were then instructed to add or subtract (nominal) L+M+S contrast using a response pad until the flicker was minimally visible. Red-green nulling was realized by presenting the positive or negative modulation spectra

as 500 ms steps from the background, while subjects were asked to remove the red-green appearance by adding or subtracting (nominal) L–M contrast to the modulation spectra. In pilot experiments, we also examined nulling blue-yellow appearance by adding or subtracting (nominal) S cone contrast. We found that our subjects did not perform this task reliably in our initial attempts and so did not further pursue blue-yellow nulling.

Subjects nulled the positive and negative excursions of the melanopsin-directed and L+M+S-directed modulations independently. In any given nulling trial (i.e., melanopsin-directed positive, melanopsin-directed positive, L+M+S-directed positive, L+M+S-directed negative), subjects nulled luminance and red-green in alternation (melanopsin trials) or red-green only (L+M+S trials) until no more change was made. The ‘nulled’ modulation spectra were then averaged across the positive and negative arms to obtain an average ‘nulled’ modulation. These nulled subject-specific modulations were then used in the pupillometry experiment and in fMRI Experiment 2.

Eye piece and pupil dilation. The stimulus was viewed within an MRI compatible eye piece that provided a circular, uniform field of 27.5° diameter. The central 5° diameter was obscured to avoid variation in photoreceptor spectral sensitivity across the visual field caused by the presence of the foveal macular pigment (CIE, 2006). Grid marks (vertical, horizontal, and two annular) were present to assist the subject in maintaining fixation at the center of the stimulus field. Pupil dilation was achieved with 0.5% proparacaine hydrochloride as a local anesthetic followed by 1% tropicamide. In BOLD fMRI Experiment 1, subjects viewed the stimulus with their pharmacologically dilated eye through an artificial pupil (4.7 mm); the pupillometry, perceptual nulling, and BOLD fMRI Experiment 2 employed pharmacological dilation but did not employ an artificial pupil. For these experiments, the pupil diameter was taken to be 4.7 mm for purposes of computing the amount of cone photopigment bleaching to be used in correction of cone spectral sensitivities. A patch was worn over the unstimulated eye during fMRI scanning.

BOLD functional MRI

Experimental design. During BOLD fMRI Experiment 1, subjects viewed photoreceptor-directed modulations flickering sinusoidally at different frequencies (0.5, 1, 2, 4, 8, 16, 32 and 64 Hz; Figure 1E). During each of many scanning runs of 588 seconds, a single photoreceptor directed modulation was studied. Each scanning run was composed of multiple, 12 second blocks during which the modulation was presented at a particular temporal frequency, and the order of presented frequencies was counterbalanced within a run. Within each block, the sinusoidal profile of the flicker was ramped on and off using a 3 second cosine ramp. Each run included blocks in which only the static background spectrum was presented; these periods served as the reference condition in data analysis. The subject adapted to the background spectrum for 10-15 minutes at the start of each session during collection of anatomical images, and was returned to the background spectrum between scanning runs. Scanning was conducted for each subject during three separate sessions. During the first session, we examined stimulus frequencies between 2 and 64 Hz (2 runs each for L+M, L-M, S, L^{*}+M^{*} and scaled L+M, and 3 runs for melanopsin-directed), in the second session we probed stimulus frequencies 0.5, 1 and 2 Hz (2 runs each for L+M, L-M, S, and scaled L+M, 3 runs for melanopsin-directed), and in the third session, we examined the L+M+S modulation for the entire range of frequencies (2 runs per frequency set).

The design of BOLD fMRI Experiment 2 was the same as Experiment 1, except that a single modulation frequency (4 Hz) was used, and the four modulation types were intermixed in a single scan in a counter-balanced order.

Attention task. Subjects performed a detection task during scanning. During each 12 second block, there was a 33% probability of a brief (250 msec) interruption during which the stimulus would transition to a static presentation of a lower luminance (~50% reduced) background. The target events were constrained so as not to occur during the first and last 2 seconds of the block. Subjects were asked to report these brief dimming events by pressing a button on a keypad. If

the subject did not detect the dimming of the stimulus, we assumed that the 12s block was invalid and did not include these blocks in further analyses.

fMRI acquisition and data analysis

Data acquisition. We collected echoplanar (EPI) blood oxygen level dependent (BOLD) fMRI data on a 3T Siemens Trio using a 32-channel array coil at a TR of 3 seconds, with 2 mm isotropic voxels over 34 oblique axial slices (TE = 30 ms, FA = 90°). The imaging slab was centered over the occipital pole. A high-resolution anatomical image (3D MPRAGE) (160 slices, 1 mm isotropic voxels, TR = 1.62 s, TE = 3.09 ms, TI = 950 ms, FOV= 250 mm, FA = 15°) was acquired for each subject at the start of each scan. Magnitude and phase B0 maps were also collected (52 slices, TR = 1.2 s, TE 1 = 4.06 ms, TE 2 = 6.52 ms, FA = 60°).

Preprocessing. fMRI data processing in volumetric space was carried out using FEAT (FMRI Expert Analysis Tool; v6.00, part of FSL). Motion correction relative to the mid-point reference image of the 4D BOLD data was carried out using FSL's MCFLIRT. B0 unwarping was carried out within FSL using the FUGUE tool.

Regression. The data from each scanning run were modeled separately. Each modulation frequency across blocks was modeled with a separate square wave regressor relative to the static background blocks. Blocks in which the subject failed to detect the attention target were modeled with a separate, nuisance regressor; this was an infrequent occurrence (a total of 4/438, 4/473, 21/438 blocks missed by subjects S01, S02, and S03, respectively). An additional regressor of no interest modeled the occurrence of the attention target as a delta function. These regressors were convolved with a double-gamma hemodynamic response function. Motion outlier volumes were identified using the root mean-squared intensity difference of each volume to a reference volume (threshold 75th percentile + 1.5 interquartile range; FSL tool *fsl_motion_outliers*) and modeled as nuisance regressors in the form of a delta function. In the first level analysis, a

volumetric map of the response (expressed as percentage BOLD fMRI signal change) was obtained for each stimulus regressor of interest for each run.

For each of the cortical regions of interest (described below), we obtained the response for a given stimulus frequency by averaging the response across voxels in that area. Within subject, we obtained mean response across runs and hemispheres, and also the average across subjects. The set of the responses across frequencies constitutes the temporal transfer function.

Registration. T1 structural image volumes were segmented into white and grey matter, and flattened and inflated with FreeSurfer. Volumetric, voxel-wise maps of regressor weights were first registered to the subject anatomy, which was in turn co-registered to the *fsaverage_sum* standard space. The registration of the EPI slab volume to anatomy was performed using Advanced Normalization Tools (ANTs, <http://stnava.github.io/ANTs/>) and *bbregister* (FreeSurfer) as follows: The EPI slab reference image was registered to FreeSurfer anatomy using boundary-based linear registration. The registered EPI slab scout image was then binarized to create a binary mask for the anatomy, thus creating a corresponding slab anatomical image. We then used diffeomorphic registration in ANTs to map functional runs to the masked partial FOV anatomy, which was co-registered to the whole-brain anatomy. This procedure was performed for every run, which had a characteristic reference image. In this data set, we found that using diffeomorphic registration outperformed boundary-based registration based on visual inspection.

Definition of regions of interest (ROI). We defined the cortical location of visual areas V1, V2 and V3 using an anatomically informed template of retinotopic organization [316]. We restricted the regions of interest to the eccentricity range of 3 to 13° (unilateral eccentricity) to correspond to the visual extent of our stimulus, with a 1° inner margin around the centrally occluded spot. As we found similar responses in areas V2 and V3, we averaged the data from these two regions.

The scanning sessions included runs that served as functional localizers. To identify the MT complex, subjects viewed a circular field of static or moving random dot stimuli (white dots on black background) that alternated every 15 seconds. To identify the lateral occipital complex, subjects viewed 15 second blocks of presentations of pictures of faces, buildings, general objects, and scrambled objects (1 second per picture). The LOC was identified by the contrast of objects with scrambled objects. These localizer stimuli were presented using an un-calibrated LCD projector (Sanyo SXGA projector, 4200 lumens) with a Buhl long-throw lens for projection on a Mylar screen, and viewed by the subjects via a mirror mounted on the head coil in the scanner. The functional localizers were analyzed for each subject using the same processing pipeline as described above. After combining hemispheres and runs, we identified statistically significant voxels for these contrasts in FreeSurfer (cluster-wise p value threshold <0.01) for each subject. We then constructed a common region of interest for the group of three subjects by selecting vertices in which at least 2 of the 3 subjects had significant responses to the motion (MT) or object (LOC) stimuli, respectively.

Missing volumetric data. In some scans for some subjects, the position of the imaging slab was too superior or inferior, causing dorsal or ventral regions of the visual areas within our target eccentricity range to be incompletely imaged. As signal artifacts arise at the edge of the imaging slab due to head motion, we elected to identify and remove the data from the runs and regions in which this partial imaging occurred. For subject S01, we discarded data from 6/28 of the runs in V2d (left hemisphere), 12/28 of V2d (right hemisphere), 7/28 of V3d (left hemisphere) and 28/28 of V3d (right hemisphere). For subject S02, we discarded data from 6/28 of the runs in V1d (left hemisphere), 21/28 of V1d (right hemisphere), 9/28 of V2d (left hemisphere), 24/28 of V2d (right hemisphere), 24/28 of V3d (left hemisphere), and 24/28 of V3d (right hemisphere). For subject S03, we discarded 11/28 runs of the data from V3d (left hemisphere) and 11/28 runs of the data from V3d (right hemisphere).

Pupil measurements

The approach used to make these measurements has been described in detail previously [1]. A brief description follows.

Viewing geometry. Subjects viewed stimuli through the eyepiece and visual stimulation set-up described above (see *Visual stimuli*), while the consensual pupillary response of the unstimulated eye was measured using an infrared eye tracker (Video Eye Tracker, sampling rate 50 Hz; Cambridge Research Systems, Cambridge, UK). The pupil detection algorithm supplied in the Video Eye Tracker Toolbox was used, and further processing was performed off-line. For consistency, the three main subjects, who also took part in the fMRI experiments (S01, S02 and S03) viewed the stimulus with their right eye while their left eye was tracked, while the additional twelve subjects viewed the stimulus with their left eye, while their right eye was tracked. As noted above, the stimulated eye was pharmacologically dilated.

Procedure. After adapting to the mean background for at least 5 minutes, subjects viewed sinusoidal, cosine-windowed (at onset only; 3 sec) stimulus modulations at 0.1 Hz in a counterbalanced order with randomized phase (0°, 90°, 180° or 270°). During each 45 second trials per run, the stimuli would either be melanopsin-directed (Mel*, 32% contrast) or L+M+S-directed (32% contrast). The three primary subjects (S01, S02, and S03) also had trials in which a light flux (32% contrast) modulation was presented. The melanopsin-directed and L+M+S-directed modulations were individually nulled in chromaticity and brightness (melanopsin-directed) or only chromaticity (L+M+S-directed) by each subject (see *Psychophysical calibration* above). Subjects S01-S03 took part in two runs of 27 trials each (9 trials each of L+M+S, melanopsin-directed and light-flux), yielding a total of 18 repeats for each stimulus modulation direction. Subjects S04-15 took part in three runs of 24 trials each (12 trials each of L+M+S and melanopsin-directed), yielding a total of 36 repeats for each stimulus modulation direction. Subjects initiated each trial with a button press.

Data analysis. Raw traces of pupil diameter were smoothed and resampled using a 7th-order polynomial Savitzky-Golay filter. Missed pupillary samples due to blinks or eye movements were identified using a ‘spike detection’ algorithm (2SD from mean pupil size or 20% overall within a 10-sample window). Trials with more than 10% of invalid samples were discarded altogether. The first 5 s of each 45 s trial were removed from the data. Amplitude and phase of the pupillary responses to the sinusoidal stimuli were obtained by fitting sine and cosine waves to the average response for a given condition at the stimulation frequency (0.1 Hz) using least-squares spectral fitting. The stimulus phase jitter used in the experiment was accounted for when averaging responses across trials. The standard error (SEM) of the amplitude and phase values was estimated using a bootstrap procedure, in which trials were re-sampled randomly with replacement and amplitude and phase obtained from each set of resampled trials using the same method applied to the actual trials. The SD of the bootstrapped values was then used as the SEM.

Results

Responses to whole-field, cone-directed flicker

We measured the cortical temporal transfer functions between 0.5 and 64 Hz for flicker that targeted the L+M+S, L–M, and S cone pathways, while silencing melanopsin (Figure 3.2a). We studied three primary subjects in detail over several fMRI sessions, and found consistent responses across these subjects (see inset panels in Figure 3.2).

For the L+M+S direction (Figure 3.2a, left panels) we found a bandpass response that increased in peak frequency between area V1 (~16 Hz) and the extrastriate areas LOC and MT (~32 Hz). In the L–M direction, a more broadband response was observed that also increased in frequency of peak sensitivity between area V1 (8–16 Hz) and area MT (32 Hz), but not LOC (Figure 3.2a, center panels). The S cone stimulus in general elicited a lower amplitude response and a broad,

bandpass structure between 2 and 8 Hz in areas V1 and V2/V3 (Figure 3.2a, right panels). We did not find measurable S cone responses in areas LOC or MT.

An L+M cone directed stimulus is sometimes used to examine the cortical representation of the luminance pathway [314, 317]. While this is an effective stimulus for the luminance pathway, it also has the property of producing negative loading upon the blue-yellow mechanism and thus a chromatic percept. We considered the possibility that the cortical response to an L+M modulation would resemble a linear combination of the responses to the L+M+S and the S stimuli. We measured the cortical temporal transfer function to an L+M directed stimulus. Interestingly, the cortical response to the L+M modulation (Fig 2b) was effectively identical to that evoked by L+M+S directed flicker. This was the case even in areas V1 and V2/V3, where a substantial S cone driven response is measured when an S cone modulation is presented in isolation.

The failure of a simple additive combination of post-receptoral channel responses to account for the results is illustrated by the dashed line in Fig 2b. The measured temporal transfer function for the S cone directed stimulus was subtracted from the function obtained for the L+M+S stimulus. This predicted response function does not resemble the measured response to the L+M modulation in areas V1 and V2/V3, the areas where we observed a non-zero response to the S cone directed stimulus.

Psychophysical measurement of apparent cone contrast within a melanopsin directed modulation

In informal observations, we noted that the melanopsin directed modulation had a red-green chromatic component, despite being nominally cone silent. We characterized the perceptual properties of melanopsin-directed modulation in terms of apparent cone contrast using a psychophysical nulling procedure. Red-Green (L-M) contrast was measured using a 0.5 Hz melanopsin-directed modulation, while luminance (L+M+S) contrast was measured using rapid flicker (30 or 40 Hz depending on subject).

Across fifteen subjects (Figure 3.3a), slightly less than 2.5% chromatic (L–M) contrast was on average required to null red-green from the melanopsin modulation; an increase in un-nulled melanopsin contrast was seen as reddish and a decrease in melanopsin contrast as greenish, with this difference reflected in the sign of the nulling contrast obtained for the positive and negative arms. A similar degree of luminance (L+M+S) contrast on average was removed from the Mel modulation to null the cone flicker component. There was modest variation in these measures across subjects. Our three primary subjects had nulling values that were typical of the larger studied population.

We note that our psychophysical nulling does not render the nulled melanopsin modulations completely invisible at low temporal frequencies. This may be the result of imperfect nulling (as could be the case either because of nulling variability or if there are retinal inhomogeneities in cone spectral sensitivities) or could represent a subtle contribution of melanopsin to perceived brightness. We do not consider this issue further in this paper.

The chromatic and luminance percept in the un-nulled melanopsin directed stimulus could be a consequence of melanopsin stimulation itself, or the result of inadvertent contrast upon cones due to imperfect spectral silencing. In support of the later view, we measured a similar degree of chromatic content within the nominally achromatic L+M+S modulation (the positive arm of the un-nulled L+M+S modulation appeared greenish and vice versa for the negative arm; Figure 3.3b). While we consider it *a priori* unlikely that melanopsin stimulation itself is responsible for the measured chromatic and luminance components, we cannot discount this possibility completely. Therefore, we examined the neural response both to the un-nulled melanopsin directed stimulus (fMRI experiment 1) and to both the un-nulled and nulled melanopsin directed stimulus (fMRI experiment 2). We also adopted the strategy of comparing the amplitude of response to the melanopsin directed stimuli to the response produced by control stimuli consisting of low contrast cone directed modulations, with complementary instantiations of this strategy implemented in the

two experiments. A neural response to the melanopsin modulation greater than that evoked by the control stimuli and not eliminated by the psychophysical nulling might reasonably be interpreted as resulting from melanopsin stimulation itself, and not from inadvertent cone contrast.

Visual cortex responses to melanopsin flicker and control conditions

We tested if flicker directed at melanopsin produces a measurable cortical response. In the first set of measurements, we used an un-nulled 17% contrast melanopsin modulation. Seventeen percent contrast was the maximum available with our device given our choice of background, and the requirement to nominally silence both the L, M and S cones and their counterparts shadowed by retinal blood vessels (the penumbral cones, L*, M* and S*). Silencing of the penumbral cones is necessary, as rapid flicker of a melanopsin-directed modulation that does not do so produces a structured, entopic percept of the retinal blood vessels [2]. Such an entopic percept could itself produce a cortical response and confound our measurement of the response to melanopsin, a possibility we explicitly address in a later control measurement.

Minimal responses to the 17% melanopsin-directed stimulus were found across visual areas and temporal frequencies (Figure 3.4a). Within area V1 there was the suggestion of a band-pass pattern of responses, with the largest average response found for the 4 Hz stimulus. In the other visual areas, the average response did not exceed zero by appreciably more than 1 SEM at any temporal frequency. We considered the possibility that the small measured response in area V1 was the result of inadvertent cone contrast. To address this possibility, we measured cortical responses to a low-contrast (2%) L+M control modulation. We found that the cortical response to this control modulation was of small but consistently positive amplitude across the studied cortical regions (Figure 3.4b), although it had no systematic structure over temporal frequency. We regard the BOLD responses to this control modulation as the degree of measured response that might be attributed to inadvertent cone contrast. Importantly, the response evoked by the

melanopsin modulation did not reliably exceed the upper limb of the ± 1 SEM confidence interval for the response to the low-contrast control cone modulation at any frequency in any visual area.

The largest candidate response to the melanopsin modulation was found for 4 Hz flicker in primary visual cortex (V1). We examined this stimulus condition in greater detail in an additional BOLD fMRI study (fMRI experiment 2). A high-contrast, light flux modulation at 4 Hz served as a positive control and evoked a robust response within V1 cortex (Figure 3.5). Instead of using a fixed degree of cone contrast as a control for inadvertent cone stimulation, we measured immediately prior to scanning the L+M+S and L-M contrast needed to produce a psychophysical null of the 17% contrast, penumbral-cone silent melanopsin modulation for each subject. The nulling cone contrast was then presented as a 4 Hz control modulation to the subject. On average, this low contrast (1-2%) cone flicker produced a small, positive V1 response. We repeated the measure of V1 cortical response to the 4 Hz, un-nulled 17% contrast melanopsin-directed modulation. The measured response was smaller than that evoked by the cone contrast control, and indeed did not differ from zero in this replication. Finally, we created a nulled 17% contrast melanopsin modulation for each subject based on his psychophysical nulling. When presented at 4 Hz, this modulation also failed to produce a V1 response different from zero.

In sum, our studies did not identify a reliable visual cortex response to melanopsin directed flicker with 17% contrast at any frequency between 0.5 and 64 Hz. Attempts to replicate the small response initially observed at 4 Hz in area V1 failed. Cortical responses to these stimuli did not differ from the BOLD fMRI response to the static background spectrum, and were smaller than the cortical response to a small degree of cone contrast.

Pupil response to a slow, nulled melanopsin modulation

Rapid, melanopsin-directed flicker did not evoke cortical responses for the three subjects studied using fMRI. We used measurements of the pupil to confirm that it is possible to evoke a melanopsin-driven visual response in these subjects, and also to compare their melanopsin-

driven response to that of a larger sample of subjects. As the melanopsin directed stimulus was not designed to silence the penumbral cones in this experiment, a larger stimulus contrast upon melanopsin was available; it was not necessary to silence the penumbral cones as selective stimulation of these photoreceptors with a slow modulation does not produce a visible percept, and does not alter the measured pupil response [1]. Fifteen subjects viewed slow (0.1 Hz) 32% contrast, non-penumbral cone silent melanopsin directed and 32% contrast L+M+S directed stimuli during measurement of their consensual pupil response (Figure 3.6a). These stimuli were perceptually nulled for each subject as described above. Across subjects, a measurable pupil response to the melanopsin modulation was observed, and found to be of different phase than that evoked by the L+M+S modulation, consistent with prior reports [1, 119].

The pupillometry measures obtained on the three primary subjects also included a 32% light flux modulation. This modulation is simply a scaling of the entire background spectrum, and as such produces equal contrast on both the cones and melanopsin. Accordingly, a larger pupil response was obtained for the light flux modulation as compared to the cone only (L+M+S) modulation in these three subjects (Figure 3.6b). While a relatively small pupil response to the nulled melanopsin modulation was obtained for one subject (S01) on this occasion, this subject did have an appropriately enhanced response to the light flux stimulus and has had a measurable pupil response to un-nulled melanopsin-directed stimuli in our earlier study [1; subject S01 in the present study was subject sub001 in that study], both with and without silencing penumbral cones.

These measures confirm that melanopsin-directed stimuli, even after removal of measured cone contrast, are capable of driving a pupil response, despite the inability of these stimuli to evoke a reliable cortical response when modulated rapidly. We do note that the noisiness of the pupil response prevented us from measuring a reliable pupil response to our 17% contrast melanopsin directed modulation. We return to this limitation of our work in the discussion.

Visual cortex responses to penumbral cone flicker

The absence of a cortical response to melanopsin-directed sinusoidal flicker in our data may be contrasted with the results of a recent psychophysical study by Horiguchi, et al. [164] that reported a possible contribution of melanopsin to flicker detection in the periphery—but not the fovea—at frequencies as high as 40 Hz. Recently, we found that 8-16 Hz spectral flicker that selectively targets the penumbral cones (L^* and M^* , but not S^*) elicits a Purkinje-tree percept, in which the subject sees the spatial structure of their own retinal vasculature within the uniform stimulus field [2]. We have also determined that inadvertent stimulation of penumbral cones in a nominally melanopsin isolating stimulus can produce the percept [2], suggesting a possible mechanism for the high-temporal-frequency result of Horiguchi, et al. [164].

We examined the neural correlates of this entopic perceptual phenomenon, evoked with a modulation that selectively targeted the penumbral L and M cones (L^*+M^*) with ~2% contrast across a range of flicker frequencies. Across visual areas, penumbral cone flicker produced a consistent pattern of temporal responses, peaking in the 8-16 Hz range (Figure 3.7). This corresponds to the frequency that maximally evokes a spatially structured, Purkinje-tree percept in uniform penumbral cone flicker [2].

Discussion

Our measurements provide the cortical temporal transfer functions for spatially uniform stimulation of the melanopsin and post-receptoral cone mechanisms. The stimuli separate the cones and melanopsin, while silencing (for the melanopsin measurements) the penumbral cones that experience spectral filtering from retinal blood vessels (Table 2.1). We made these measurements between 0.5 and 64 Hz—matching the primary operating range of human perception—for both early cortical visual areas and higher level dorsal and ventral extrastriate regions.

Post-receptoral cone mechanisms

For the high luminance, spatially uniform stimuli we have studied, psychophysical temporal sensitivity is band-pass, with a notable decline in sensitivity for slow temporal modulations [263, 310]. Chromatic stimuli shift temporal sensitivity to lower frequencies [309], a phenomenon that appears as early as the retinal ganglion cells [318].

Our fMRI results are concordant with these findings. Within V1, sensitivity to achromatic (L+M+S) flicker peaks at or above 16 Hz, while for chromatic modulations of either L-M or S, the peak response is at 8 Hz or lower. Prior neuroimaging studies that compared luminance and L-M chromatic sensitivity did not observe such a separation of temporal sensitivity [314, 319, 320]. This difference in results may relate to our use of a bright, spatially uniform stimulus presented in the periphery, compared to the stimuli used in prior studies. Our results are in agreement with prior fMRI findings of peak S cone driven responses at lower temporal frequencies [314, 319].

We also studied L+M flicker. While this modulation does not stimulate S cones, it nonetheless activates the blue-yellow post-receptoral mechanism in addition to the luminance pathway. Interestingly, cortical responses to the L+M modulation are essentially identical in shape and amplitude to those evoked by the L+M+S modulation, even in cortical regions with a substantial S-cone driven response [but see 314]. As the L+M+S response is larger than the S driven response at all frequencies (at the 45% contrast level studied), this non-linear combination of neural response is consistent with a winner-takes-all mechanism [321, 322].

An increase in peak temporal sensitivity occurs between V1 and higher extrastriate visual areas. Within area MT, peak sensitivity shifts to 32 Hz, consistent with prior studies [319, 320]. Within the LOC (a form sensitive visual area) the shift in temporal sensitivity is found only for stimuli activating the luminance pathway (L+M+S and L+M). Generally, sensitivity to lower temporal frequencies would be expected within the LOC [323]. The responses to rapid L+M+S flicker in area LOC may reflect entopic visual phenomenon [264, 265]. In informal observations, we

experience a reticulated, geometric pattern within the uniform stimulus field for 16 and 32 Hz L+M+S flicker, but not for L–M and S cone modulations. In a prior study, we found that this entopic percept is evoked to a greater extent by L+M flicker as compared to S cone flicker [2].

We did not measure an S cone driven response in either area MT or LOC. Previous studies have demonstrated S cone responses in area MT using high contrast, spatially structured, moving or flickering stimuli in humans with fMRI [317, 319, 320, 324] and in monkeys with electrophysiology [325] and fMRI [326]. The difference with our results might be due to the spatially-structured stimuli employed in these studies (compared with our spatially uniform stimulus), but we note that Jayakumar, et al. [327] found units driven by S cones in Monkey MT with spatially uniform stimuli. We are unaware of a prior study of S cone driven responses within area LOC. Mullen, et al. [328] found responses to spatially structured, blue-yellow stimuli within ventral area VO (immediately anterior to hV4) but did not examine the more lateral, object responsive region LOC.

Melanopsin responses and the challenge of photopigment isolation

We find no reliable visual cortex response to rapid penumbral cone-silent melanopsin-directed flicker with 17% contrast. Given the generally slow response properties of the ipRGCs, we would have predicted a low-pass response to melanopsin contrast. Our data do not support the existence of a melanopsin driven response in visual cortex to flicker at 0.5 Hz and above. With the higher contrast (32%) that can be achieved without silencing penumbral cones, a melanopsin directed stimulus modulated slowly (0.1 Hz) does elicit a measurable pupil response.

With few exceptions [90, 297] studies of the ipRGCs in rodents and primates have used a spatially uniform stimulus as we have. The ipRGCs have broad dendritic arbors and correspondingly wide receptive fields [34], suggesting sensitivity to low spatial frequencies. As spatially uniform flicker evokes robust responses in area V1 for all post-receptoral cone pathways, we consider it unlikely that this property of our stimulus is responsible for the absence of a melanopsin-driven response in our data.

It is of course possible that a small response to our melanopsin directed stimuli within visual cortex went undetected in our study. The possible size of such a response is bounded by our results, with 17% melanopsin contrast producing cortical responses no larger than those produced by ~2% cone contrast.

Melanopsin signals may also be present at different locations along the visual pathways or under different stimulus conditions. In rodents [23, 295, 329] and primates [34, 35], ipRGCs are known to project to the lateral geniculate nucleus, a site that was not imaged in this study. Melanopsin signals may also drive visual cortex neurons at a lower temporal frequencies [295], under different light level conditions [330], or indirectly through interaction with cone signals [90].

A particular challenge of measuring a melanopsin driven response in humans is the need to isolate stimulation of this photopigment from incidental stimulation of the cones. The technique of silent substitution requires precise device control and specification of the effective spectral sensitivities of the photopigments, which are in turn influenced by numerous biological factors, including allelic variation, lens density, macular pigment, and photopigment bleaching. Inevitable imperfections in stimulus specification produce undesired, “splatter” contrast on the cones. As the visual system is extremely sensitive to even small degrees of differential cone contrast [331], this splatter may be expected to produce neural (and perceptual) responses that confound a measurement of melanopsin effects.

In this study we addressed two sources of systematic bias in photoreceptor isolation. First, subjects consistently perceived positive melanopsin contrast as reddish and containing a luminance component. While melanopsin stimulation has been reported to produce a perception of brightness at long time scales [163], the luminance effect measured here was in 30-40 Hz flicker, and thus unlikely to be mediated by melanopsin [1; but see Horiguchi et al., 2013, 34, 60, 63]. We suspect (but cannot prove) that the chromatic and luminance percepts produced by the melanopsin stimulus reflect a small error in our assumed cone fundamentals [specifically, the

photopigment optical density nomograms; 200] and/or a systematic error in our spectral calibrations. To account for possible cone intrusion, we evaluated cortical response to the melanopsin directed stimulus against the responses to low-contrast cone modulations. The cone component of the melanopsin stimulus may also be nulled (as in our second BOLD fMRI experiment), with the assumption that the chromatic and luminance effects are not themselves a manifestation of melanopsin activity.

Melanopsin stimulus specificity can also fail because of the penumbral cones. Our recent psychophysical studies show that inadvertent contrast on penumbral L and M cones can arise with modulations designed to target melanopsin, producing a Purkinje tree percept [2]. Here, we studied a modulation that targeted melanopsin with 17% contrast while silencing both the cones and their penumbral variants. While no reliable cortical response was found for rapid flicker of the penumbral-cone-silent melanopsin modulation, we did observe a measurable response to flicker that selectively targeted the penumbral L and M cones (L^*+M^*) with only 1-2% contrast. Indeed, in a meeting abstract [4] we mistakenly attributed to melanopsin the cortical response to penumbral cone flicker.

We cannot rule out the possibility that a response in visual cortex would be evoked with greater melanopsin contrast (as might be achieved using a background of different chromaticity), or for that matter at different overall light levels or at lower temporal frequencies than the ones we studied. We can be confident, however, that our BOLD fMRI measurements of cone temporal sensitivity are uncontaminated by melanopsin stimulation.

While cortical responses are not isomorphic to perception, we take our current results as consistent with an account that humans do not perceive rapid melanopsin flicker, but that inadvertent stimulation of the penumbral cones might be mistaken for this percept. Such an effect might explain prior reports of human perception of rapid melanopsin-directed flicker [120, 164].

Acknowledgements

This work was supported by NIH Grant 1 R01 EY020516 (GKA), R01 EY10016 (DHB), R01 EY024681 (GKA and DHB), P30 EY001583 (Core Grant for Vision Research), P30 NS045839 (Neuroscience Neuroimaging Center Core Grant), and Deutscher Akademischer Austauschdienst (MS). The authors thank Fred Letterio for technical assistance; Tanya Kurtz, Jacqueline Meeks, Patricia O'Donnell, and Joan Sparano for assistance with scanning; and Picanha Grill for motivation.

Figures

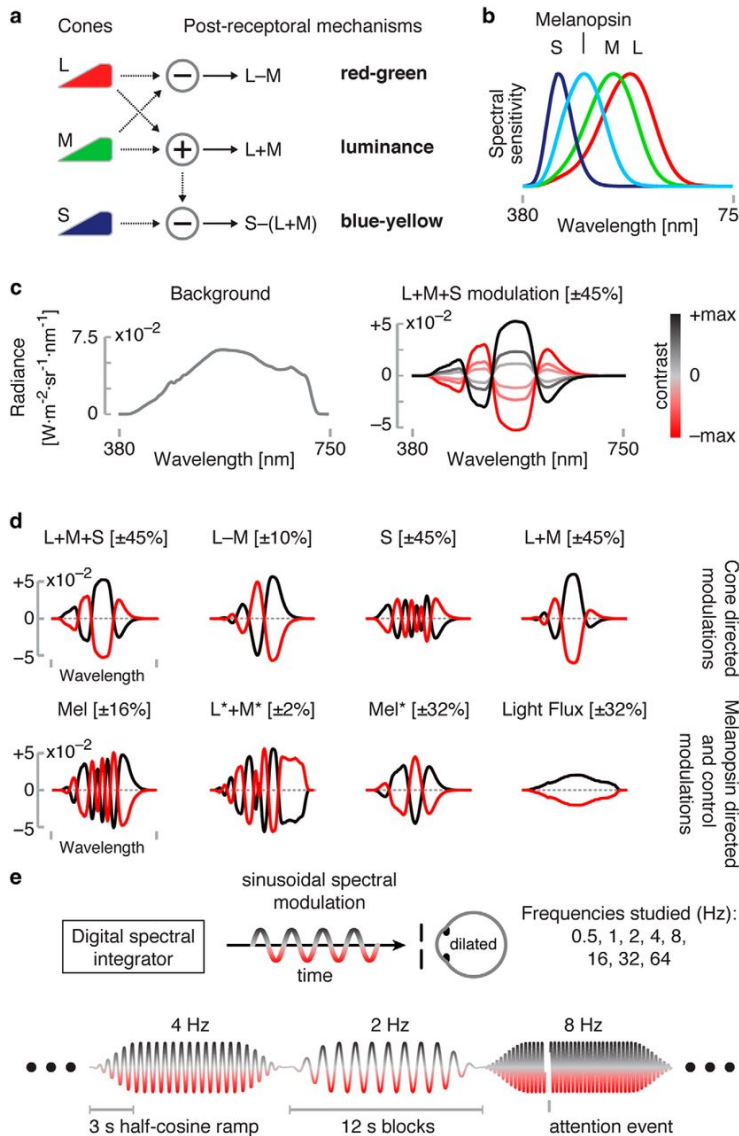


Figure 3.1: Overview and experimental design.

Overview and experimental design. **a**, Postreceptoral mechanisms arising from additive and opponent combination of cone signals. **b**, Spectral sensitivities of the L, M, and S cones and melanopsin. **c**, Left, Our stimuli all used a common, neutral background with the spectral power distribution shown. Right, Modulation spectra were added to the background. The L + M + S modulation is illustrated. Modulation spectra varied sinusoidally between an extreme positive

(black line) and negative (red line) modulation. **d**, The maximal positive and negative modulations for each set of targeted photoreceptor(s) studied. Maximal contrast values are given in square brackets. Wavelength axis is as in **c**. **e**, Schematic of experimental apparatus and design. The subject viewed sinusoidal spectral modulations produced by the digital spectral integrator through an artificial pupil with a pharmacologically dilated eye. During fMRI scanning, different stimulus frequencies targeting a given class of photoreceptor(s) were presented in 12 s blocks. The sinusoidal flicker was ramped at the start and end of each block by a 3 s half-cosine. The stimulus was occasionally interrupted by an attention event.

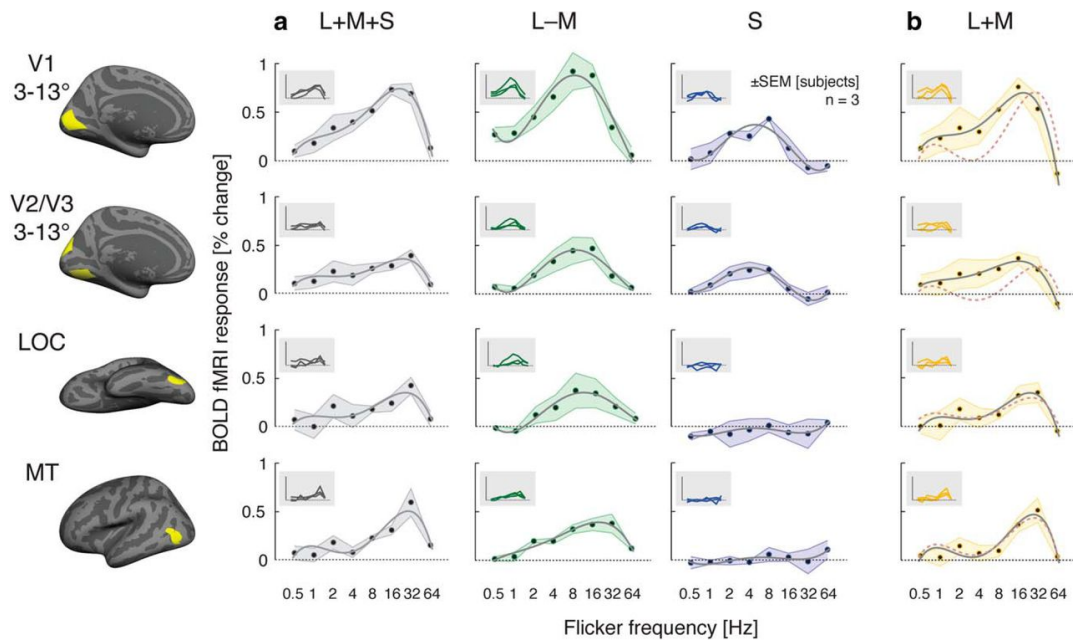


Figure 3.2: Temporal transfer functions for the postreceptoral cone pathways.

a, Temporal transfer functions for L + M + S, L – M, and S. The shaded region indicates ± 1 SEM across the three subjects. The solid line is a fourth-order polynomial fit to the data. Views for ROIs at left are medial for V1 and V2/V3, lateral for MT, and ventral for LOC. Insets provide the response profile for each subject. **b**, Temporal transfer functions for L + M. The dashed red line is the difference of the L + M + S and S temporal transfer functions scaled to best (least-squares) match the L + M modulation.

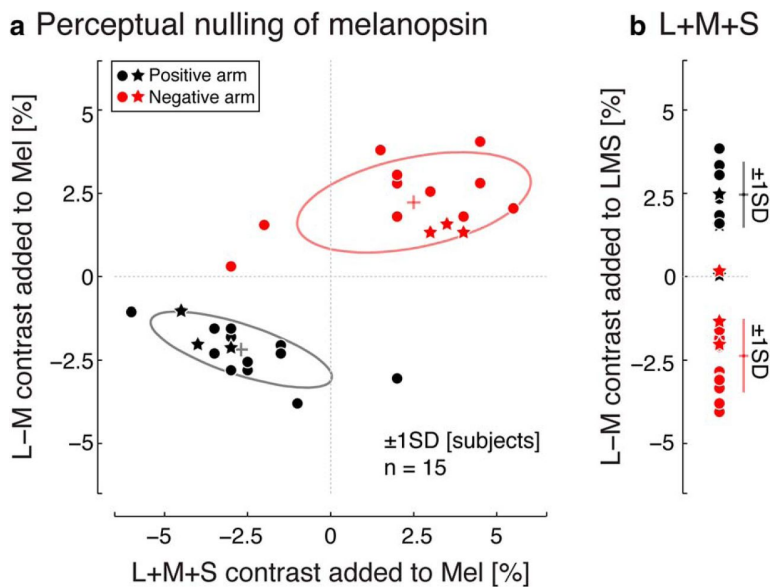


Figure 3.3: Psychophysical nulling.

a, Perceptual nulling data for a positive (black points) and negative (red points) 32% melanopsin (Mel*; nonpenumbral-cone silent) modulation in a population of subjects ($n = 15$). Primary subjects (S01, S02, and S03) are indicated with a star symbol. Some plot points are overlapping. Ellipse indicates ± 1 SD across subjects. **b**, Perceptual nulling data for a 32% cone-directed (L + M + S) modulation in the same population of 15 subjects. Error bars indicate ± 1 SD across subjects.

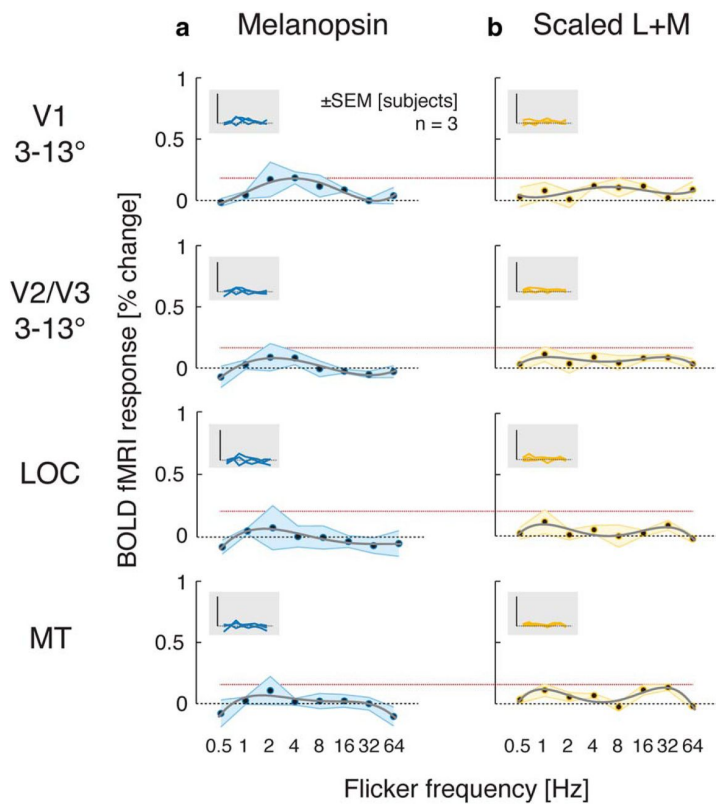


Figure 3.4: Temporal transfer functions for melanopsin-directed (a) and cone control flicker (b).

Same format as Figure 3.2. Dotted red horizontal lines indicate the peak response (+1 SEM) for the scaled (2% contrast) L + M modulation for each area.

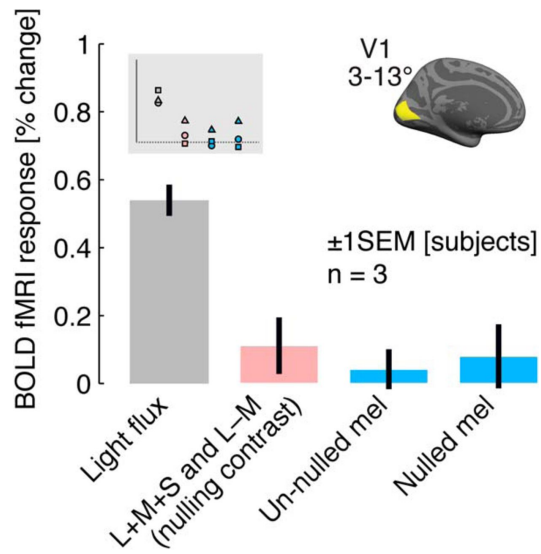
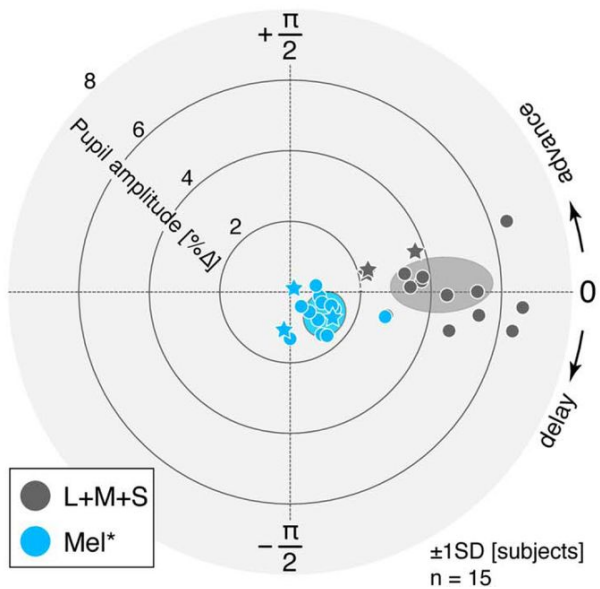


Figure 3.5: V1 response to melanopsin and control modulations.

BOLD amplitudes shown as average across the two V1 hemispheres and across V1 vertices in the relevant eccentricity range (inset) for a set of 4 Hz modulations.

a Pupil response to 0.1 Hz modulations



b Pupil response to 0.1 Hz modulations for primary subjects

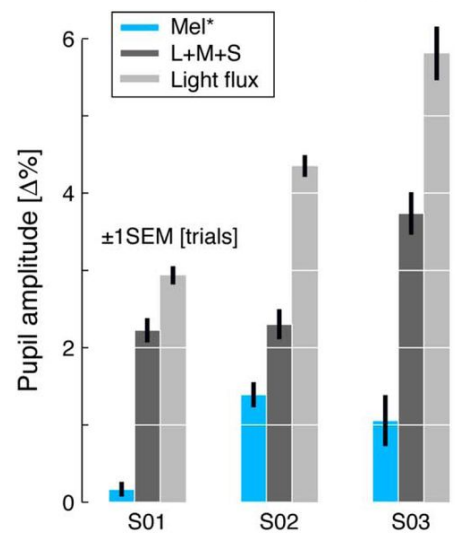


Figure 3.6: Pupil response to 0.1 Hz modulations.

a, Polar plot of pupil responses (0.1 Hz modulation frequency) in 15 subjects. Radial eccentricity indicates pupil amplitude; angle in the polar plots indicates phase of the pupil response. Primary subjects (S01, S02, and S03) are indicated with a star symbol. **b**, Amplitude of pupil responses, including a light flux modulation, for the three primary subjects.

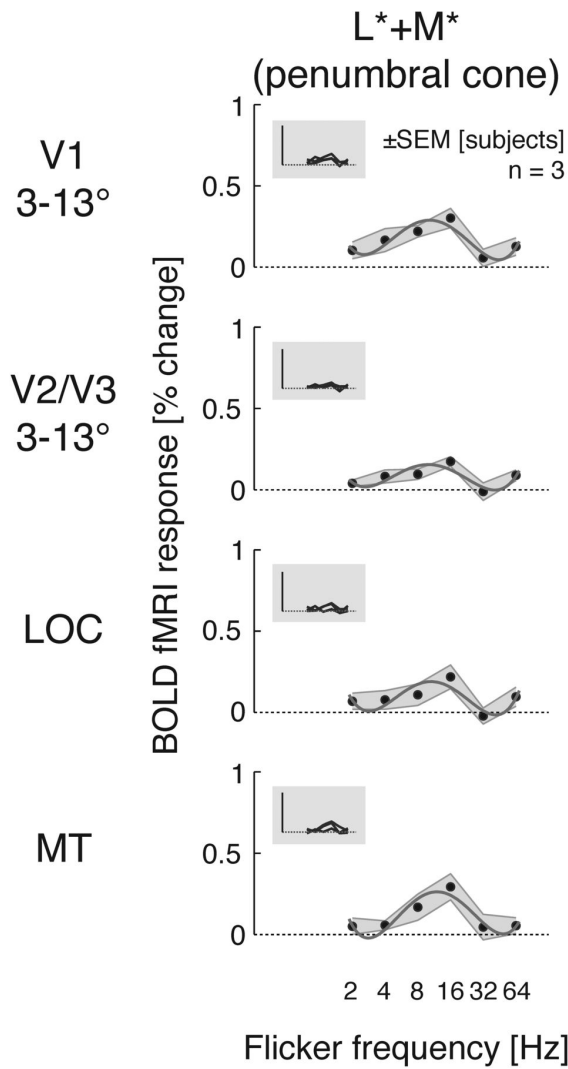


Figure 3.7: Temporal transfer functions for penumbral cone ($L^* + M^*$)-directed flicker.

Temporal transfer functions for penumbral cone ($L^* + M^*$)-directed flicker. Same format as Fig. 3.2.

Table 3.1: Predicted contrasts of the modulations.

	$L + M + S$ ($\pm 45\%$)	$L - M$ ($\pm 10\%$)	S ($\pm 45\%$)	$L + M$ ($\pm 45\%$)	$L + M$ ($\pm 2\%$)	Mel ($\pm 17\%$)	$L^* + M^*$ ($\pm 2\%$)	Mel^* ($\pm 32\%$)	Light flux (32%)
L	45%	10%	0%	45%	2%	0%	0%	0%	32%
M	45%	-10%	0%	45%	2%	0%	0%	0%	32%
S	45%		0%	45%	0%	0%	0%	0%	32%
Mel	0%		0%	0%	0%	17%	0%	32%	32%
Rods	17%	-10%	0%	17%	1%	10%	3%	20%	32%
L^*	42%		14%	42%	2%	0%	2%	2%	32%
M^*	43%		-7%	42%	2%	0%	1%	2%	32%
S^*	38%		0%	36%	0%	0%	0%	7%	32%

Values are given as contrasts of the modulations targeted to a 32-year-old subject (spectral power distributions are shown in Figure 1). Bolded numbers indicate contrast that was targeted for the respective modulation direction; italic numbers indicate contrast that was not specifically controlled. Modulation names designated with an asterisk produce differential spatial contrast on penumbral cones and thus a Purkinje tree percept if flickered rapidly.

GENERAL DISCUSSION

The preceding dissertation presents three research articles containing studies, the goal of which was to measure and characterize sensitivity to melanopsin stimulation in humans. To summarize:

- a) In *Chapter 1*, the temporal properties of the photoreceptor contributions to the human pupillary light response were measured with a silent substitution methodology. It was found that under conditions of careful photoreceptor isolation, the photoreceptor contributions were dissociable in the temporal domain. Joint stimulation of L+M cones resulted in a band-pass fashion with a peak at 1 Hz. Stimulation of melanopsin in isolation revealed a low-pass shape for the melanopsin-driven pupillary light response. Similarly, S cones contribute to the pupillary light response in slow temporal regime, but crucially with opposite sign. Taken together, S cones oppose a hypothesized joint ‘brightness’ signal between melanopsin and the L and M cones. This finding is consistent with S cone opponency and positive L and M cone input into intrinsically photosensitive retinal ganglion cells (ipRGCs) in macaque retinae.
- b) In *Chapter 2*, the psychophysical properties of the penumbral cones were studied. These are cones that are located in the shadow of the retinal blood vessels, thus experiencing a hemoglobin-filtered version of the stimulus. We demonstrate that using a multi-spectral silent substitution paradigm, these cones can be selectively stimulated and upon such stimulation, the subject sees their own retinal vasculature as an entoptic percept. We demonstrate that efforts to measure the melanopsin in humans in isolation can lead to the artefactual stimulation of penumbral cones which might be mistaken for a genuine signal from melanopsin.
- c) In *Chapter 3*, the properties of human visual cortical areas were studied using the silent substitution methodology. Sinusoidal stimuli targeting the post-receptoral channels (L+M, S, L-M) and melanopsin (with and without controlling for penumbral cones) were presented in a

wide range of frequencies (0.5–64 Hz). Characteristic temporal transfer functions were found for these modulation responses; melanopsin was not found to evoke a cortical response.

The three research studies presented here represent but a first step towards an understanding of how blue light affects human physiology. With the discovery of melanopsin only dating back less than 20 years, many questions remain in this open territory. In the following, a few areas of open and hopefully upcoming investigation will be highlighted, acknowledging the historical context of the research presented in this dissertation.

1. *Primate ipRGCs*: The functional properties of the two identified ipRGC subtypes in primates are not well understood. No *in vivo* electrophysiology studies have followed the seminal paper by Dacey, et al. [34]. Further studies characterizing the synaptic inputs, the temporal and spatial properties, and the functional significance of primate ipRGCs would contribute to our understanding of melanopsin function.
2. *Melanopsin-mediated retinal adaptation and melanopsin-cone interactions*. An adaptive effect of melanopsin activation on cone sensitivity has been found to exist in the rodent retina [89, 90]. There is evidence that melanopsin regulates the sensitivity of human ERG responses [88]. A complete picture of the adaptive properties of melanopsin is at present not available. Furthermore, how melanopsin interacts with cones in driving the pupillary light reflex and other non-image-forming functions such as acute melatonin suppression is not well understood.
3. *Melanopsin genetics*. Recent work has shown complexity in the genetic determinants of melanopsin in rodents (two isoforms; [11-13]) and humans (SNPs; [14-17]). How genetic variants of melanopsin could affect melanopsin-mediated function will be an active area of investigation.

4. *Projections of ipRGCs.* This work has shown that there is no measurable cortical response to melanopsin stimulation (0.5-64 Hz) in primary visual cortex (V1) and higher visual areas as measured with BOLD fMRI (see Chapter 4). Future work will investigate the neural responses to high-contrast melanopsin stimuli in other brain regions, and the response of human visual cortex to pulses of melanopsin contrast.
5. *Spectral properties of natural scenes.* An ongoing project investigates the match of the spectral and temporal properties of natural scenes to the spectral sensitivity and kinetics of the melanopsin photopigment using a database of natural spectra collected under conditions of minimal light pollution.

More work remains to be done; it is to be hoped that the findings presented here will be of use to many.

REFERENCES

1. Spitschan, M., Jain, S., Brainard, D.H., and Aguirre, G.K. (2014). Opponent melanopsin and S-cone signals in the human pupillary light response. *Proceedings of the National Academy of Sciences of the United States of America* *111*, 15568-15572. doi:10.1073/pnas.1400942111.
2. Spitschan, M., Aguirre, G.K., and Brainard, D.H. (2015). Selective stimulation of penumbral cones reveals perception in the shadow of retinal blood vessels. *PloS One* *10*, e0124328. doi:10.1371/journal.pone.0124328.
3. Spitschan, M., Datta, R., Stern, A.M., Brainard, D.H., and Aguirre, G.K. (2016). Human visual cortex responses to rapid cone and melanopsin-directed flicker. *Journal of Neuroscience* *36*, 1471-1482. doi:10.1523/JNEUROSCI.1932-15.2016.
4. Spitschan, M., Luu, L., Datta, R., Brainard, D.H., and Aguirre, G.K. (2014). Melanopsin-driven responses in the human brain. *Journal of Vision* *14*, 594-594. doi:10.1167/14.10.594.
5. Spitschan, M., Aguirre, G.K., and Brainard, D.H. (2014). Penumbral cones and Purkinje trees. *Journal of Vision* *14*, 22-22. doi:10.1167/14.15.22.
6. Aguirre, G., Spitschan, M., Jain, S., and Brainard, D.H. (2014). Opponent mechanisms of cone and melanopsin pupil control. *Neurology* *82*, S39.004.
7. Spitschan, M., Jain, S., Brainard, D.H., and Aguirre, G.K. (2013). Temporal properties of photopigment contributions to the pupillary light reflex. *Journal of Vision* *13*, P4-P4. doi:10.1167/13.15.39.
8. Wong, K.Y., Dunn, F.A., Graham, D.M., and Berson, D.M. (2007). Synaptic influences on rat ganglion-cell photoreceptors. *Journal of Physiology* *582*, 279-296. doi:10.1113/jphysiol.2007.133751.
9. Wong, K.Y. (2012). A retinal ganglion cell that can signal irradiance continuously for 10 hours. *Journal of Neuroscience* *32*, 11478-11485. doi:10.1523/JNEUROSCI.1423-12.2012.
10. Provencio, I., Rodriguez, I.R., Jiang, G., Hayes, W.P., Moreira, E.F., and Rollag, M.D. (2000). A novel human opsin in the inner retina. *J Neurosci* *20*, 600-605.
11. Pires, S.S., Hughes, S., Turton, M., Melyan, Z., Peirson, S.N., Zheng, L., Kosmaoglou, M., Bellingham, J., Cheetham, M.E., Lucas, R.J., et al. (2009). Differential expression of two distinct functional isoforms of melanopsin (Opn4) in the mammalian retina. *J Neurosci* *29*, 12332-12342. doi:10.1523/JNEUROSCI.2036-09.2009.
12. Jagannath, A., Hughes, S., Abdelgany, A., Pothecary, C.A., Di Pretoro, S., Pires, S.S., Vachtsevanos, A., Pilorz, V., Brown, L.A., Hossbach, M., et al. (2015). Isoforms of Melanopsin Mediate Different Behavioral Responses to Light. *Curr Biol* *25*, 2430-2434. doi:10.1016/j.cub.2015.07.071.
13. Hughes, S., Welsh, L., Katti, C., Gonzalez-Menendez, I., Turton, M., Halford, S., Sekaran, S., Peirson, S.N., Hankins, M.W., and Foster, R.G. (2012). Differential expression of melanopsin isoforms Opn4L and Opn4S during postnatal development of the mouse retina. *PLoS One* *7*, e34531. doi:10.1371/journal.pone.0034531.
14. Lee, S.I., Hida, A., Tsujimura, S., Morita, T., Mishima, K., and Higuchi, S. (2013). Association between melanopsin gene polymorphism (I394T) and pupillary light reflex is dependent on light wavelength. *Journal of Physiological Anthropology* *32*, 16. doi:10.1186/1880-6805-32-16.
15. Higuchi, S., Hida, A., Tsujimura, S., Mishima, K., Yasukouchi, A., Lee, S.I., Kinjyo, Y., and Miyahira, M. (2013). Melanopsin gene polymorphism I394T is associated with pupillary light responses in a dose-dependent manner. *PloS One* *8*, e60310. doi:10.1371/journal.pone.0060310.

16. Roecklein, K.A., Wong, P.M., Franzen, P.L., Hasler, B.P., Wood-Vasey, W.M., Nimgaonkar, V.L., Miller, M.A., Kepreos, K.M., Ferrell, R.E., and Manuck, S.B. (2012). Melanopsin gene variations interact with season to predict sleep onset and chronotype. *Chronobiology International* 29, 1036-1047. doi:10.3109/07420528.2012.706766.
17. Roecklein, K.A., Rohan, K.J., Duncan, W.C., Rollag, M.D., Rosenthal, N.E., Lipsky, R.H., and Provencio, I. (2009). A missense variant (P10L) of the melanopsin (OPN4) gene in seasonal affective disorder. *Journal of Affective Disorders* 114, 279-285. doi:10.1016/j.jad.2008.08.005.
18. Roecklein, K., Wong, P., Ernecoff, N., Miller, M., Donofry, S., Kamarck, M., Wood-Vasey, W.M., and Franzen, P. (2013). The post illumination pupil response is reduced in seasonal affective disorder. *Psychiatry Res* 210, 150-158. doi:10.1016/j.psychres.2013.05.023.
19. Lee, S.I., Hida, A., Kitamura, S., Mishima, K., and Higuchi, S. (2014). Association between the melanopsin gene polymorphism OPN4*Ile394Thr and sleep/wake timing in Japanese university students. *Journal of Physiological Anthropology* 33, 9. doi:10.1186/1880-6805-33-9.
20. Gooley, J.J., Lu, J., Chou, T.C., Scammell, T.E., and Saper, C.B. (2001). Melanopsin in cells of origin of the retinohypothalamic tract. *Nat Neurosci* 4, 1165. doi:10.1038/nn768.
21. Hattar, S., Liao, H.W., Takao, M., Berson, D.M., and Yau, K.W. (2002). Melanopsin-containing retinal ganglion cells: architecture, projections, and intrinsic photosensitivity. *Science* 295, 1065-1070. doi:10.1126/science.1069609.
22. Gooley, J.J., Lu, J., Fischer, D., and Saper, C.B. (2003). A broad role for melanopsin in nonvisual photoreception. *J Neurosci* 23, 7093-7106.
23. Hattar, S., Kumar, M., Park, A., Tong, P., Tung, J., Yau, K.W., and Berson, D.M. (2006). Central projections of melanopsin-expressing retinal ganglion cells in the mouse. *J Comp Neurol* 497, 326-349. doi:10.1002/cne.20970.
24. Baver, S.B., Pickard, G.E., Sollars, P.J., and Pickard, G.E. (2008). Two types of melanopsin retinal ganglion cell differentially innervate the hypothalamic suprachiasmatic nucleus and the olfactory pretectal nucleus. *Eur J Neurosci* 27, 1763-1770. doi:10.1111/j.1460-9568.2008.06149.x.
25. Delwig, A., Larsen, D.D., Yasumura, D., Yang, C.F., Shah, N.M., and Copenhagen, D.R. (2016). Retinofugal Projections from Melanopsin-Expressing Retinal Ganglion Cells Revealed by Intraocular Injections of Cre-Dependent Virus. *PLoS One* 11, e0149501. doi:10.1371/journal.pone.0149501.
26. Allen, A.E., Procyk, C.A., Howarth, M., Walmsley, L., and Brown, T.M. (2016). Visual input to the mouse lateral posterior and posterior thalamic nuclei: photoreceptive origins and retinotopic order. *J Physiol* 594, 1911-1929. doi:10.1113/JP271707.
27. Schmidt, T.M., Chen, S.K., and Hattar, S. (2011). Intrinsically photosensitive retinal ganglion cells: many subtypes, diverse functions. *Trends Neurosci* 34, 572-580. doi:10.1016/j.tins.2011.07.001.
28. Chen, S.K., Badea, T.C., and Hattar, S. (2011). Photoentrainment and pupillary light reflex are mediated by distinct populations of ipRGCs. *Nature* 476, 92-95. doi:10.1038/nature10206.
29. Schmidt, T.M., Alam, N.M., Chen, S., Kofuji, P., Li, W., Prusky, G.T., and Hattar, S. (2014). A role for melanopsin in alpha retinal ganglion cells and contrast detection. *Neuron* 82, 781-788. doi:10.1016/j.neuron.2014.03.022.
30. Estevez, M.E., Fogerson, P.M., Ilardi, M.C., Borghuis, B.G., Chan, E., Weng, S., Auferkorte, O.N., Demb, J.B., and Berson, D.M. (2012). Form and function of the M4 cell, an intrinsically photosensitive retinal ganglion cell type contributing to geniculocortical vision. *J Neurosci* 32, 13608-13620. doi:10.1523/JNEUROSCI.1422-12.2012.

31. Zhao, X., Stafford, B.K., Godin, A.L., King, W.M., and Wong, K.Y. (2014). Photoresponse diversity among the five types of intrinsically photosensitive retinal ganglion cells. *J Physiol* **592**, 1619-1636. doi:10.1113/jphysiol.2013.262782.
32. Baden, T., Berens, P., Franke, K., Roman Roson, M., Bethge, M., and Euler, T. (2016). The functional diversity of retinal ganglion cells in the mouse. *Nature* **529**, 345-350. doi:10.1038/nature16468.
33. Hannibal, J., Hindersson, P., Ostergaard, J., Georg, B., Heegaard, S., Larsen, P.J., and Fahrenkrug, J. (2004). Melanopsin is expressed in PACAP-containing retinal ganglion cells of the human retinohypothalamic tract. *Invest Ophthalmol Vis Sci* **45**, 4202-4209. doi:10.1167/iovs.04-0313.
34. Dacey, D.M., Liao, H.W., Peterson, B.B., Robinson, F.R., Smith, V.C., Pokorny, J., Yau, K.W., and Gamlin, P.D. (2005). Melanopsin-expressing ganglion cells in primate retina signal colour and irradiance and project to the LGN. *Nature* **433**, 749-754. doi:10.1038/nature03387.
35. Hannibal, J., Kankipati, L., Strang, C.E., Peterson, B.B., Dacey, D., and Gamlin, P.D. (2014). Central projections of intrinsically photosensitive retinal ganglion cells in the macaque monkey. *J Comp Neurol* **522**, 2231-2248. doi:10.1002/cne.23588.
36. Jusuf, P.R., Lee, S.C., Hannibal, J., and Grunert, U. (2007). Characterization and synaptic connectivity of melanopsin-containing ganglion cells in the primate retina. *Eur J Neurosci* **26**, 2906-2921. doi:10.1111/j.1460-9568.2007.05924.x.
37. Neumann, S., Haverkamp, S., and Auferkorte, O.N. (2011). Intrinsically photosensitive ganglion cells of the primate retina express distinct combinations of inhibitory neurotransmitter receptors. *Neuroscience* **199**, 24-31. doi:10.1016/j.neuroscience.2011.10.027.
38. Liao, H.W., Ren, X., Peterson, B.B., Marshak, D.W., Yau, K.W., Gamlin, P.D., and Dacey, D.M. (2016). Melanopsin-expressing ganglion cells in macaque and human retinas form two morphologically distinct populations. *J Comp Neurol*. doi:10.1002/cne.23995.
39. Dkhissi-Benyahya, O., Rieux, C., Hut, R.A., and Cooper, H.M. (2006). Immunohistochemical evidence of a melanopsin cone in human retina. *Invest Ophthalmol Vis Sci* **47**, 1636-1641. doi:10.1167/iovs.05-1459.
40. Peirson, S.N., Bovee-Geurts, P.H., Lupi, D., Jeffery, G., DeGrip, W.J., and Foster, R.G. (2004). Expression of the candidate circadian photopigment melanopsin (Opn4) in the mouse retinal pigment epithelium. *Brain Res Mol Brain Res* **123**, 132-135. doi:10.1016/j.molbrainres.2004.01.007.
41. Semo, M., Gias, C., Ahmad, A., and Vugler, A. (2014). A role for the ciliary marginal zone in the melanopsin-dependent intrinsic pupillary light reflex. *Exp Eye Res* **119**, 8-18. doi:10.1016/j.exer.2013.11.013.
42. Xue, T., Do, M.T., Riccio, A., Jiang, Z., Hsieh, J., Wang, H.C., Merbs, S.L., Welsbie, D.S., Yoshioka, T., Weissgerber, P., et al. (2011). Melanopsin signalling in mammalian iris and retina. *Nature* **479**, 67-73. doi:10.1038/nature10567.
43. Steinach, E. (1892). Untersuchungen zur vergleichenden Physiologie der Iris. *Pflüger, Archiv für die Gesammte Physiologie des Menschen und der Thiere* **52**, 495-525. doi:10.1007/bf01673612.
44. Barr, L., and Alpern, M. (1963). Photosensitivity of the Frog Iris. *J Gen Physiol* **46**, 1249-1265.
45. Brown-Séquard, E. (1847). Recherches expérimentales concernant l'action de la lumière et celle d'un changement de température sur l'iris, dans les cinq classes d'animaux vertébrés. *C R Acad Sci* **25**, 482-483, 508.
46. Sikka, G., Hussmann, G.P., Pandey, D., Cao, S., Hori, D., Park, J.T., Steppan, J., Kim, J.H., Barodka, V., Myers, A.C., et al. (2014). Melanopsin mediates light-dependent

- relaxation in blood vessels. *Proc Natl Acad Sci U S A* **111**, 17977-17982. doi:10.1073/pnas.1420258111.
47. Walker, M.T., Brown, R.L., Cronin, T.W., and Robinson, P.R. (2008). Photochemistry of retinal chromophore in mouse melanopsin. *Proc Natl Acad Sci U S A* **105**, 8861-8865. doi:10.1073/pnas.0711397105.
48. Shirzad-Wasei, N., and DeGrip, W.J. (2016). Heterologous expression of melanopsin: Present, problems and prospects. *Prog Retin Eye Res* **52**, 1-21. doi:10.1016/j.preteyeres.2016.02.001.
49. Panda, S., Nayak, S.K., Campo, B., Walker, J.R., Hogenesch, J.B., and Jegla, T. (2005). Illumination of the melanopsin signaling pathway. *Science* **307**, 600-604. doi:10.1126/science.1105121.
50. Qiu, X., Kumbalasiri, T., Carlson, S.M., Wong, K.Y., Krishna, V., Provencio, I., and Berson, D.M. (2005). Induction of photosensitivity by heterologous expression of melanopsin. *Nature* **433**, 745-749. doi:10.1038/nature03345.
51. Matsuyama, T., Yamashita, T., Imamoto, Y., and Shichida, Y. (2012). Photochemical properties of mammalian melanopsin. *Biochemistry* **51**, 5454-5462. doi:10.1021/bi3004999.
52. Shirzad-Wasei, N., van Oostrum, J., Bovee-Geurts, P.H., Wasserman, M., Bosman, G.J., and Degrip, W.J. (2013). Large scale expression and purification of mouse melanopsin-L in the baculovirus expression system. *Protein Expr Purif* **91**, 134-146. doi:10.1016/j.pep.2013.07.010.
53. Koyanagi, M., Kubokawa, K., Tsukamoto, H., Shichida, Y., and Terakita, A. (2005). Cephalochordate melanopsin: evolutionary linkage between invertebrate visual cells and vertebrate photosensitive retinal ganglion cells. *Curr Biol* **15**, 1065-1069. doi:10.1016/j.cub.2005.04.063.
54. Torii, M., Kojima, D., Okano, T., Nakamura, A., Terakita, A., Shichida, Y., Wada, A., and Fukada, Y. (2007). Two isoforms of chicken melanopsins show blue light sensitivity. *FEBS Lett* **581**, 5327-5331. doi:10.1016/j.febslet.2007.10.019.
55. Davies, W.I., Zheng, L., Hughes, S., Tamai, T.K., Turton, M., Halford, S., Foster, R.G., Whitmore, D., and Hankins, M.W. (2011). Functional diversity of melanopsins and their global expression in the teleost retina. *Cell Mol Life Sci* **68**, 4115-4132. doi:10.1007/s00018-011-0785-4.
56. Bailes, H.J., and Lucas, R.J. (2013). Human melanopsin forms a pigment maximally sensitive to blue light (lambda_{max} approximately 479 nm) supporting activation of G(q/11) and G(i/o) signalling cascades. *Proc Biol Sci* **280**, 20122987. doi:10.1098/rspb.2012.2987.
57. Spoida, K., Eickelbeck, D., Karapinar, R., Eckhardt, T., Mark, M.D., Jancke, D., Ehinger, B.V., Konig, P., Dalkara, D., Herlitze, S., et al. (2016). Melanopsin Variants as Intrinsic Optogenetic On and Off Switches for Transient versus Sustained Activation of G Protein Pathways. *Curr Biol*. doi:10.1016/j.cub.2016.03.007.
58. Newman, L.A., Walker, M.T., Brown, R.L., Cronin, T.W., and Robinson, P.R. (2003). Melanopsin forms a functional short-wavelength photopigment. *Biochemistry* **42**, 12734-12738. doi:10.1021/bi035418z.
59. Melyan, Z., Tarttelin, E.E., Bellingham, J., Lucas, R.J., and Hankins, M.W. (2005). Addition of human melanopsin renders mammalian cells photoresponsive. *Nature* **433**, 741-745. doi:10.1038/nature03344.
60. Berson, D.M., Dunn, F.A., and Takao, M. (2002). Phototransduction by retinal ganglion cells that set the circadian clock. *Science* **295**, 1070-1073. doi:10.1126/science.1067262.
61. Tu, D.C., Zhang, D., Demas, J., Slutsky, E.B., Provencio, I., Holy, T.E., and Van Gelder, R.N. (2005). Physiologic diversity and development of intrinsically photosensitive retinal ganglion cells. *Neuron* **48**, 987-999. doi:10.1016/j.neuron.2005.09.031.

62. Lucas, R.J., Douglas, R.H., and Foster, R.G. (2001). Characterization of an ocular photopigment capable of driving pupillary constriction in mice. *Nat Neurosci* 4, 621-626. doi:10.1038/88443.
63. Gamlin, P.D., McDougal, D.H., Pokorny, J., Smith, V.C., Yau, K.W., and Dacey, D.M. (2007). Human and macaque pupil responses driven by melanopsin-containing retinal ganglion cells. *Vision Res* 47, 946-954. doi:10.1016/j.visres.2006.12.015.
64. Markwell, E.L., Feigl, B., and Zele, A.J. (2010). Intrinsically photosensitive melanopsin retinal ganglion cell contributions to the pupillary light reflex and circadian rhythm. *Clin Exp Optom* 93, 137-149. doi:10.1111/j.1444-0938.2010.00479.x.
65. Feigl, B., and Zele, A.J. (2014). Melanopsin-expressing intrinsically photosensitive retinal ganglion cells in retinal disease. *Optom Vis Sci* 91, 894-903. doi:10.1097/OPX.0000000000000284.
66. Adhikari, P., Zele, A.J., and Feigl, B. (2015). The Post-Illumination Pupil Response (PIPR). *Invest Ophthalmol Vis Sci* 56, 3838-3849. doi:10.1167/iovs.14-16233.
67. McDougal, D.H., and Gamlin, P.D. (2010). The influence of intrinsically-photosensitive retinal ganglion cells on the spectral sensitivity and response dynamics of the human pupillary light reflex. *Vision Res* 50, 72-87. doi:10.1016/j.visres.2009.10.012.
68. Wagman, I.H., and Gullberg, J.E. (1942). The relationship between monochromatic light and pupil diameter the low intensity visibility curve as measured by pupillary measurements. *American Journal of Physiology* 137, 769-778.
69. Bouma, H. (1962). Size of the static pupil as a function of wavelength and luminosity of the light incident on the human eye. *Nature* 193, 690-691.
70. Kimura, E., and Young, R.S. (1995). Nature of the pupillary responses evoked by chromatic flashes on a white background. *Vision Res* 35, 897-906.
71. Alpern, M., and Campbell, F.W. (1962). The spectral sensitivity of the consensual light reflex. *J Physiol* 164, 478-507.
72. Young, R.S., and Alpern, M. (1980). Pupil responses to foveal exchange of monochromatic lights. *J Opt Soc Am* 70, 697-706.
73. Krastel, H., Alexandridis, E., and Gertz, J. (1985). Pupil increment thresholds are influenced by color opponent mechanisms. *Ophthalmologica* 191, 35-38.
74. Kimura, E., and Young, R.S. (1999). S-cone contribution to pupillary responses evoked by chromatic flash offset. *Vision Res* 39, 1189-1197.
75. Sperling, H.G., and Harwerth, R.S. (1971). Red-green cone interactions in the increment-threshold spectral sensitivity of primates. *Science* 172, 180-184.
76. King-Smith, P.E., and Carden, D. (1976). Luminance and opponent-color contributions to visual detection and adaptation and to temporal and spatial integration. *J Opt Soc Am* 66, 709-717.
77. Hattar, S., Lucas, R.J., Mrosovsky, N., Thompson, S., Douglas, R.H., Hankins, M.W., Lem, J., Biel, M., Hofmann, F., Foster, R.G., et al. (2003). Melanopsin and rod-cone photoreceptive systems account for all major accessory visual functions in mice. *Nature* 424, 76-81. doi:10.1038/nature01761.
78. Takahashi, J.S., DeCoursey, P.J., Bauman, L., and Menaker, M. (1984). Spectral sensitivity of a novel photoreceptive system mediating entrainment of mammalian circadian rhythms. *Nature* 308, 186-188.
79. Thapan, K., Arendt, J., and Skene, D.J. (2001). An action spectrum for melatonin suppression: evidence for a novel non-rod, non-cone photoreceptor system in humans. *J Physiol* 535, 261-267.
80. Brainard, G.C., Hanifin, J.P., Greeson, J.M., Byrne, B., Glickman, G., Gerner, E., and Rollag, M.D. (2001). Action spectrum for melatonin regulation in humans: evidence for a novel circadian photoreceptor. *J Neurosci* 21, 6405-6412.

81. Rea, M.S., Bullough, J.D., and Figueiro, M.G. (2001). Human melatonin suppression by light: a case for scotopic efficiency. *Neurosci Lett* 299, 45-48.
82. Reilly, C.E. (2001). Melatonin is suppressed by rod-based illuminance in humans. *J Neurol* 248, 352-353.
83. Zeitzer, J.M., Kronauer, R.E., and Czeisler, C.A. (1997). Photopic transduction implicated in human circadian entrainment. *Neuroscience Letters* 232, 135-138. doi:10.1016/s0304-3940(97)00599-5.
84. Hanifin, J.P., Stewart, K.T., Smith, P., Tanner, R., Rollag, M., and Brainard, G.C. (2006). High-intensity red light suppresses melatonin. *Chronobiol Int* 23, 251-268. doi:10.1080/07420520500521988.
85. Gooley, J.J., Rajaratnam, S.M., Brainard, G.C., Kronauer, R.E., Czeisler, C.A., and Lockley, S.W. (2010). Spectral responses of the human circadian system depend on the irradiance and duration of exposure to light. *Sci Transl Med* 2, 31ra33. doi:10.1126/scitranslmed.3000741.
86. Figueiro, M.G., Bullough, J.D., Parsons, R.H., and Rea, M.S. (2004). Preliminary evidence for spectral opponency in the suppression of melatonin by light in humans. *Neuroreport* 15, 313-316.
87. Najjar, R.P., Chiquet, C., Teikari, P., Cornut, P.L., Claustre, B., Denis, P., Cooper, H.M., and Gronfier, C. (2014). Aging of non-visual spectral sensitivity to light in humans: compensatory mechanisms? *PLoS One* 9, e85837. doi:10.1371/journal.pone.0085837.
88. Hankins, M.W., and Lucas, R.J. (2002). The primary visual pathway in humans is regulated according to long-term light exposure through the action of a nonclassical photopigment. *Curr Biol* 12, 191-198.
89. Allen, A.E., and Lucas, R.J. (2016). Using Silent Substitution to Track the Mesopic Transition From Rod- to Cone-Based Vision in Mice. *Invest Ophthalmol Vis Sci* 57, 276-287. doi:10.1167/iovs.15-18197.
90. Allen, A.E., Storchi, R., Martial, F.P., Petersen, R.S., Montemurro, M.A., Brown, T.M., and Lucas, R.J. (2014). Melanopsin-driven light adaptation in mouse vision. *Curr Biol* 24, 2481-2490. doi:10.1016/j.cub.2014.09.015.
91. Emanuel, Alan J., and Do, Michael Tri H. (2015). Melanopsin Tristability for Sustained and Broadband Phototransduction. *Neuron* 85, 1043-1055. doi:10.1016/j.neuron.2015.02.011.
92. Mure, L.S., Cornut, P.L., Rieux, C., Drouyer, E., Denis, P., Gronfier, C., and Cooper, H.M. (2009). Melanopsin bistability: a fly's eye technology in the human retina. *PLoS One* 4, e5991. doi:10.1371/journal.pone.0005991.
93. Mansfield, R.J.W. (1985). Primate photopigments and cone mechanisms. In *The Visual System*. (New York: Alan R. Liss).
94. Lamb, T.D. (1995). Photoreceptor spectral sensitivities: common shape in the long-wavelength region. *Vision Research* 35, 3083-3091.
95. Dartnall, H.J.A., and Goodeve, C.F. (1937). Scotopic luminosity curve and the absorption spectrum of visual purple. *Nature* 139, 409-411.
96. Partridge, J.C., and De Grip, W.J. (1991). A new template for rhodopsin (vitamin A1 based) visual pigments. *Vision Research* 31, 619-630.
97. Govardovskii, V.I., Fyhrquist, N., Reuter, T., Kuzmin, D.G., and Donner, K. (2000). In search of the visual pigment template. *Visual Neuroscience* 17, 509-528.
98. Gall, D., and Bieske, K. (2004). Definition and measurement of circadian radiometric quantities. In *Light and health – non-visual effects: proceedings of the CIE symposium '04* (Vienna, Austria: Commission internationale de l'éclairage), pp. 129-132.
99. Rea, M.S., Figueiro, M.G., Bierman, A., and Bullough, J.D. (2010). Circadian light. *J Circadian Rhythms* 8, 2. doi:10.1186/1740-3391-8-2.

100. Enezi, J., Revell, V., Brown, T., Wynne, J., Schlangen, L., and Lucas, R. (2011). A "melanopic" spectral efficiency function predicts the sensitivity of melanopsin photoreceptors to polychromatic lights. *J Biol Rhythms* *26*, 314-323. doi:10.1177/0748730411409719.
101. Brown, T.M., Allen, A.E., al-Enezi, J., Wynne, J., Schlangen, L., Hommes, V., and Lucas, R.J. (2013). The melanopic sensitivity function accounts for melanopsin-driven responses in mice under diverse lighting conditions. *PLoS One* *8*, e53583. doi:10.1371/journal.pone.0053583.
102. Lucas, R.J., Peirson, S.N., Berson, D.M., Brown, T.M., Cooper, H.M., Czeisler, C.A., Figueiro, M.G., Gamlin, P.D., Lockley, S.W., O'Hagan, J.B., et al. (2014). Measuring and using light in the melanopsin age. *Trends Neurosci* *37*, 1-9. doi:10.1016/j.tins.2013.10.004.
103. CIE (2015). Report on the First International Workshop on Circadian and Neurophysiological Photometry, 2013. (Vienna: CIE).
104. CIE (1932). Recueil des travaux et compte rendu des séances (huitième session, Cambridge – Septembre 1931), (Cambridge: Cambridge University Press).
105. CIE (1951). Recueil des travaux et compte rendu des séances (douzième session, Stockholm – Juin et Juillet 1951), (New York: Bureau Central de la C.I.E.).
106. Foster, R.G. (2005). Neurobiology: bright blue times. *Nature* *433*, 698-699. doi:10.1038/433698a.
107. Asakawa, K., and Ishikawa, H. (2015). Why do melanopsin-containing retinal ganglion cells have the greatest sensitivity to blue light? *Acta Ophthalmol* *93*, e308-309. doi:10.1111/aos.12574.
108. Barrionuevo, P.A., and Cao, D. (2014). Contributions of rhodopsin, cone opsins, and melanopsin to postreceptoral pathways inferred from natural image statistics. *J Opt Soc Am A Opt Image Sci Vis* *31*, A131-139. doi:10.1364/JOSAA.31.00A131.
109. Weale, R.A. (1988). Age and the transmittance of the human crystalline lens. *J Physiol* *395*, 577-587.
110. Xu, J., Pokorny, J., and Smith, V.C. (1997). Optical density of the human lens. *Journal of the Optical Society of America A: Optics, Image Science, and Vision* *14*, 953-960. doi:10.1364/JOSAA.14.000953.
111. Kessel, L., Lundeman, J.H., Herbst, K., Andersen, T.V., and Larsen, M. (2010). Age-related changes in the transmission properties of the human lens and their relevance to circadian entrainment. *J Cataract Refract Surg* *36*, 308-312. doi:10.1016/j.jcrs.2009.08.035.
112. Douglas, R.H., and Jeffery, G. (2014). The spectral transmission of ocular media suggests ultraviolet sensitivity is widespread among mammals. *Proc Biol Sci* *281*, 20132995. doi:10.1098/rspb.2013.2995.
113. Estévez, O., and Spekreijse, H. (1982). The "silent substitution" method in visual research. *Vision Research* *22*, 681-691. doi:10.1016/0042-6989(82)90104-3.
114. Viénot, F., Brettel, H., Dang, T.V., and Le Rohellec, J. (2012). Domain of metamers exciting intrinsically photosensitive retinal ganglion cells (ipRGCs) and rods. *Journal of the Optical Society of America A: Optics, Image Science, and Vision* *29*, A366-376. doi:10.1364/JOSAA.29.00A366.
115. Viénot, F., and Brettel, H. (2014). The Verriest Lecture: Visual properties of metamerics blacks beyond cone vision. *Journal of the Optical Society of America A: Optics, Image Science, and Vision* *31*, A38-46. doi:10.1364/JOSAA.31.000A38.
116. Tsujimura, S., Ukai, K., Ohama, D., Nuruki, A., and Yunokuchi, K. (2010). Contribution of human melanopsin retinal ganglion cells to steady-state pupil responses. *Proceedings: Biological Sciences* *277*, 2485-2492. doi:10.1098/rspb.2010.0330.

117. Vienot, F., Bailacq, S., and Rohellec, J.L. (2010). The effect of controlled photopigment excitations on pupil aperture. *Ophthalmic and Physiological Optics* 30, 484-491. doi:10.1111/j.1475-1313.2010.00754.x.
118. Tsujimura, S., and Tokuda, Y. (2011). Delayed response of human melanopsin retinal ganglion cells on the pupillary light reflex. *Ophthalmic and Physiological Optics* 31, 469-479. doi:10.1111/j.1475-1313.2011.00846.x.
119. Barrionuevo, P.A., Nicandro, N., McAnany, J.J., Zele, A.J., Gamlin, P., and Cao, D. (2014). Assessing rod, cone, and melanopsin contributions to human pupil flicker responses. *Investigative Ophthalmology and Visual Science* 55, 719-727. doi:10.1167/iovs.13-13252.
120. Cao, D., Nicandro, N., and Barrionuevo, P.A. (2015). A five-primary photostimulator suitable for studying intrinsically photosensitive retinal ganglion cell functions in humans. *J Vis* 15. doi:10.1167/15.1.27.
121. Kankipati, L., Girkin, C.A., and Gamlin, P.D. (2010). Post-illumination pupil response in subjects without ocular disease. *Investigative Ophthalmology and Visual Science* 51, 2764-2769. doi:10.1167/iovs.09-4717.
122. Feigl, B., Mattes, D., Thomas, R., and Zele, A.J. (2011). Intrinsically photosensitive (melanopsin) retinal ganglion cell function in glaucoma. *Invest Ophthalmol Vis Sci* 52, 4362-4367. doi:10.1167/iovs.10-7069.
123. Kankipati, L., Girkin, C.A., and Gamlin, P.D. (2011). The post-illumination pupil response is reduced in glaucoma patients. *Invest Ophthalmol Vis Sci* 52, 2287-2292. doi:10.1167/iovs.10-6023.
124. Munch, M., Leon, L., Collomb, S., and Kawasaki, A. (2015). Comparison of acute non-visual bright light responses in patients with optic nerve disease, glaucoma and healthy controls. *Sci Rep* 5, 15185. doi:10.1038/srep15185.
125. Rukmini, A.V., Milea, D., Baskaran, M., How, A.C., Perera, S.A., Aung, T., and Gooley, J.J. (2015). Pupillary Responses to High-Irradiance Blue Light Correlate with Glaucoma Severity. *Ophthalmology* 122, 1777-1785. doi:10.1016/j.ophtha.2015.06.002.
126. Kelbsch, C., Maeda, F., Strasser, T., Blumenstock, G., Wilhelm, B., Wilhelm, H., and Peters, T. (2016). Pupillary responses driven by ipRGCs and classical photoreceptors are impaired in glaucoma. *Graefes Arch Clin Exp Ophthalmol*. doi:10.1007/s00417-016-3351-9.
127. Kardon, R., Anderson, S.C., Damarjian, T.G., Grace, E.M., Stone, E., and Kawasaki, A. (2011). Chromatic pupillometry in patients with retinitis pigmentosa. *Ophthalmology* 118, 376-381. doi:10.1016/j.ophtha.2010.06.033.
128. Park, J.C., Moura, A.L., Raza, A.S., Rhee, D.W., Kardon, R.H., and Hood, D.C. (2011). Toward a clinical protocol for assessing rod, cone, and melanopsin contributions to the human pupil response. *Invest Ophthalmol Vis Sci* 52, 6624-6635. doi:10.1167/iovs.11-7586.
129. Kawasaki, A., Crippa, S.V., Kardon, R., Leon, L., and Hamel, C. (2012). Characterization of pupil responses to blue and red light stimuli in autosomal dominant retinitis pigmentosa due to NR2E3 mutation. *Invest Ophthalmol Vis Sci* 53, 5562-5569. doi:10.1167/iovs.12-10230.
130. Feigl, B., Zele, A.J., Fader, S.M., Howes, A.N., Hughes, C.E., Jones, K.A., and Jones, R. (2012). The post-illumination pupil response of melanopsin-expressing intrinsically photosensitive retinal ganglion cells in diabetes. *Acta Ophthalmol* 90, e230-234. doi:10.1111/j.1755-3768.2011.02226.x.
131. Kawasaki, A., Munier, F.L., Leon, L., and Kardon, R.H. (2012). Pupillometric quantification of residual rod and cone activity in leber congenital amaurosis. *Arch Ophthalmol* 130, 798-800. doi:10.1001/archophthalmol.2011.1756.

132. Kawasaki, A., Herbst, K., Sander, B., and Milea, D. (2010). Selective wavelength pupillometry in Leber hereditary optic neuropathy. *Clin Experiment Ophthalmol* 38, 322-324. doi:10.1111/j.1442-9071.2010.02212.x.
133. Moura, A.L., Nagy, B.V., La Morgia, C., Barboni, P., Oliveira, A.G., Salomao, S.R., Berezovsky, A., de Moraes-Filho, M.N., Chicani, C.F., Belfort, R., Jr., et al. (2013). The pupil light reflex in Leber's hereditary optic neuropathy: evidence for preservation of melanopsin-expressing retinal ganglion cells. *Invest Ophthalmol Vis Sci* 54, 4471-4477. doi:10.1167/iovs.12-11137.
134. Lorenz, B., Strohmayer, E., Zahn, S., Friedburg, C., Kramer, M., Preising, M., and Stieger, K. (2012). Chromatic pupillometry dissects function of the three different light-sensitive retinal cell populations in RPE65 deficiency. *Invest Ophthalmol Vis Sci* 53, 5641-5652. doi:10.1167/iovs.12-9974.
135. Leon, L., Crippa, S.V., Borruat, F.X., and Kawasaki, A. (2012). Differential effect of long versus short wavelength light exposure on pupillary re-dilation in patients with outer retinal disease. *Clin Experiment Ophthalmol* 40, e16-24. doi:10.1111/j.1442-9071.2011.02665.x.
136. Kardon, R., Anderson, S.C., Damarjian, T.G., Grace, E.M., Stone, E., and Kawasaki, A. (2009). Chromatic pupil responses: preferential activation of the melanopsin-mediated versus outer photoreceptor-mediated pupil light reflex. *Ophthalmology* 116, 1564-1573. doi:10.1016/j.ophtha.2009.02.007.
137. Herbst, K., Sander, B., Lund-Andersen, H., Wegener, M., Hannibal, J., and Milea, D. (2013). Unilateral anterior ischemic optic neuropathy: chromatic pupillometry in affected, fellow non-affected and healthy control eyes. *Front Neurol* 4, 52. doi:10.3389/fneur.2013.00052.
138. Tsika, C., Crippa, S.V., and Kawasaki, A. (2015). Differential monocular vs. binocular pupil responses from melanopsin-based photoreception in patients with anterior ischemic optic neuropathy. *Sci Rep* 5, 10780. doi:10.1038/srep10780.
139. Maynard, M.L., Zele, A.J., and Feigl, B. (2015). Melanopsin-Mediated Post-Illumination Pupil Response in Early Age-Related Macular Degeneration. *Invest Ophthalmol Vis Sci* 56, 6906-6913. doi:10.1167/iovs.15-17357.
140. Nissen, C., Ronnback, C., Sander, B., Herbst, K., Milea, D., Larsen, M., and Lund-Andersen, H. (2015). Dissociation of Pupillary Post-Illumination Responses from Visual Function in Confirmed OPA1 c.983A > G and c.2708_2711delTTAG Autosomal Dominant Optic Atrophy. *Front Neurol* 6, 5. doi:10.3389/fneur.2015.00005.
141. Collison, F.T., Park, J.C., Fishman, G.A., Stone, E.M., and McAnany, J.J. (2016). Two-color pupillometry in enhanced S-cone syndrome caused by NR2E3 mutations. *Documenta Ophthalmologica*. doi:10.1007/s10633-016-9535-0.
142. Brondsted, A.E., Sander, B., Haargaard, B., Lund-Andersen, H., Jennum, P., Gammeltoft, S., and Kessel, L. (2015). The Effect of Cataract Surgery on Circadian Photoentrainment: A Randomized Trial of Blue-Blocking versus Neutral Intraocular Lenses. *Ophthalmology* 122, 2115-2124. doi:10.1016/j.ophtha.2015.06.033.
143. Narita, A., Shirai, K., Kubota, N., Takayama, R., Takahashi, Y., Onuki, T., Numakura, C., Kato, M., Hamada, Y., Sakai, N., et al. (2014). Abnormal pupillary light reflex with chromatic pupillometry in Gaucher disease. *Ann Clin Transl Neurol* 1, 135-140. doi:10.1002/acn3.33.
144. Park, J.C., Moss, H.E., and McAnany, J.J. (2016). The Pupillary Light Reflex in Idiopathic Intracranial Hypertension. *Invest Ophthalmol Vis Sci* 57, 23-29. doi:10.1167/iovs.15-18181.
145. Zele, A.J., Feigl, B., Smith, S.S., and Markwell, E.L. (2011). The circadian response of intrinsically photosensitive retinal ganglion cells. *PLoS One* 6, e17860. doi:10.1371/journal.pone.0017860.

146. Munch, M., Leon, L., Crippa, S.V., and Kawasaki, A. (2012). Circadian and wake-dependent effects on the pupil light reflex in response to narrow-bandwidth light pulses. *Invest Ophthalmol Vis Sci* 53, 4546-4555. doi:10.1167/iovs.12-9494.
147. Herbst, K., Sander, B., Lund-Andersen, H., Broendsted, A.E., Kessel, L., Hansen, M.S., and Kawasaki, A. (2012). Intrinsic photosensitive retinal ganglion cell function in relation to age: a pupillometric study in humans with special reference to the age-related optic properties of the lens. *BMC Ophthalmol* 12, 4. doi:10.1186/1471-2415-12-4.
148. Adhikari, P., Pearson, C.A., Anderson, A.M., Zele, A.J., and Feigl, B. (2015). Effect of Age and Refractive Error on the Melanopsin Mediated Post-Illumination Pupil Response (PIPR). *Sci Rep* 5, 17610. doi:10.1038/srep17610.
149. Sharma, S., Baskaran, M., Rukmini, A.V., Nongpiur, M.E., Htoo, H., Cheng, C.Y., Perera, S.A., Gooley, J.J., Aung, T., and Milea, D. (2016). Factors influencing the pupillary light reflex in healthy individuals. *Graefes Arch Clin Exp Ophthalmol*. doi:10.1007/s00417-016-3311-4.
150. Joyce, D.S., Feigl, B., Cao, D., and Zele, A.J. (2015). Temporal characteristics of melanopsin inputs to the human pupil light reflex. *Vision Res* 107, 58-66. doi:10.1016/j.visres.2014.12.001.
151. Lei, S., Goltz, H.C., Chandrakumar, M., and Wong, A.M. (2014). Full-field chromatic pupillometry for the assessment of the postillumination pupil response driven by melanopsin-containing retinal ganglion cells. *Invest Ophthalmol Vis Sci* 55, 4496-4503. doi:10.1167/iovs.14-14103.
152. Lei, S., Goltz, H.C., Chandrakumar, M., and Wong, A.M. (2015). Test-retest reliability of hemifield, central-field, and full-field chromatic pupillometry for assessing the function of melanopsin-containing retinal ganglion cells. *Invest Ophthalmol Vis Sci* 56, 1267-1273. doi:10.1167/iovs.14-15945.
153. Herbst, K., Sander, B., Milea, D., Lund-Andersen, H., and Kawasaki, A. (2011). Test-retest repeatability of the pupil light response to blue and red light stimuli in normal human eyes using a novel pupillometer. *Front Neurol* 2, 10. doi:10.3389/fneur.2011.00010.
154. van der Meijden, W.P., te Lindert, B.H., Bijlenga, D., Coppens, J.E., Gomez-Herrero, G., Bruijel, J., Kooij, J.J., Cajochen, C., Bourgin, P., and Van Someren, E.J. (2015). Post-illumination pupil response after blue light: Reliability of optimized melanopsin-based phototransduction assessment. *Exp Eye Res* 139, 73-80. doi:10.1016/j.exer.2015.07.010.
155. Zhou, W., Lou, Y., Pan, B., and Huang, J. (2015). Reliability of Field Chromatic Pupillometry for Assessing the Function of Melanopsin-Containing Retinal Ganglion Cells. *Invest Ophthalmol Vis Sci* 56, 2519. doi:10.1167/iovs.15-16672.
156. Ba-Ali, S., Sander, B., Brondsted, A.E., and Lund-Andersen, H. (2015). Effect of topical anti-glaucoma medications on late pupillary light reflex, as evaluated by pupillometry. *Front Neurol* 6, 93. doi:10.3389/fneur.2015.00093.
157. Traustason, S., Brondsted, A.E., Sander, B., and Lund-Andersen, H. (2016). Pupillary response to direct and consensual chromatic light stimuli. *Acta Ophthalmol* 94, 65-69. doi:10.1111/aos.12894.
158. Munch, M., Kourtzi, P., Brouzas, D., and Kawasaki, A. (2016). Variation in the pupil light reflex between winter and summer seasons. *Acta Ophthalmol* 94, e244-246. doi:10.1111/aos.12966.
159. Ishikawa, H., Onodera, A., Asakawa, K., Nakadomari, S., and Shimizu, K. (2012). Effects of selective-wavelength block filters on pupillary light reflex under red and blue light stimuli. *Jpn J Ophthalmol* 56, 181-186. doi:10.1007/s10384-011-0116-1.
160. Fukuda, Y., Tsujimura, S., Higuchi, S., Yasukouchi, A., and Morita, T. (2010). The ERG responses to light stimuli of melanopsin-expressing retinal ganglion cells that are

- independent of rods and cones. *Neuroscience Letters* 479, 282-286. doi:10.1016/j.neulet.2010.05.080.
161. Fukuda, Y., Higuchi, S., Yasukouchi, A., and Morita, T. (2012). Distinct responses of cones and melanopsin-expressing retinal ganglion cells in the human electroretinogram. *Journal of Physiological Anthropology* 31, 20. doi:10.1186/1880-6805-31-20.
162. Zaidi, F.H., Hull, J.T., Peirson, S.N., Wulff, K., Aeschbach, D., Gooley, J.J., Brainard, G.C., Gregory-Evans, K., Rizzo, J.F., 3rd, Czeisler, C.A., et al. (2007). Short-wavelength light sensitivity of circadian, pupillary, and visual awareness in humans lacking an outer retina. *Current Biology* 17, 2122-2128. doi:10.1016/j.cub.2007.11.034.
163. Brown, T.M., Tsujimura, S., Allen, A.E., Wynne, J., Bedford, R., Vickery, G., Vugler, A., and Lucas, R.J. (2012). Melanopsin-based brightness discrimination in mice and humans. *Current Biology* 22, 1134-1141. doi:10.1016/j.cub.2012.04.039.
164. Horiguchi, H., Winawer, J., Dougherty, R.F., and Wandell, B.A. (2013). Human trichromacy revisited. *Proceedings of the National Academy of Sciences of the United States of America* 110, E260-269. doi:10.1073/pnas.1214240110.
165. Choi, J.Y., Oh, K., Kim, B.J., Chung, C.S., Koh, S.B., and Park, K.W. (2009). Usefulness of a photophobia questionnaire in patients with migraine. *Cephalalgie* 29, 953-959. doi:10.1111/j.1468-2982.2008.01822.x.
166. Robbins, M.S., and Lipton, R.B. (2010). The epidemiology of primary headache disorders. *Semin Neurol* 30, 107-119. doi:10.1055/s-0030-1249220.
167. Amini, A., Digre, K., and Couldwell, W.T. (2006). Photophobia in a blind patient: An alternate visual pathway. Case report. *J Neurosurg* 105, 765-768. doi:10.3171/jns.2006.105.5.765.
168. Noseda, R., Kainz, V., Jakubowski, M., Gooley, J.J., Saper, C.B., Digre, K., and Burstein, R. (2010). A neural mechanism for exacerbation of headache by light. *Nat Neurosci* 13, 239-245. doi:10.1038/nn.2475.
169. Main, A., Vlachonikolis, I., and Dowson, A. (2000). The wavelength of light causing photophobia in migraine and tension-type headache between attacks. *Headache* 40, 194-199.
170. Noseda, R., Bernstein, C.A., Nir, R.R., Lee, A.J., Fulton, A.B., Bertisch, S.M., Hovaguimian, A., Cestari, D.M., Saavedra-Walker, R., Borsook, D., et al. (2016). Migraine photophobia originating in cone-driven retinal pathways. *Brain*. doi:10.1093/brain/aww119.
171. Barnard, A.R., Hattar, S., Hankins, M.W., and Lucas, R.J. (2006). Melanopsin regulates visual processing in the mouse retina. *Current Biology* 16, 389-395. doi:10.1016/j.cub.2005.12.045.
172. Zhang, D.Q., Wong, K.Y., Sollars, P.J., Berson, D.M., Pickard, G.E., and McMahon, D.G. (2008). Intraretinal signaling by ganglion cell photoreceptors to dopaminergic amacrine neurons. *Proceedings of the National Academy of Sciences of the United States of America* 105, 14181-14186. doi:10.1073/pnas.0803893105.
173. Zhang, D.Q., Belenky, M.A., Sollars, P.J., Pickard, G.E., and McMahon, D.G. (2012). Melanopsin mediates retrograde visual signaling in the retina. *PloS One* 7, e42647. doi:10.1371/journal.pone.0042647.
174. Reitler, A.N., Chervenak, A.P., Dolikian, M.E., Benenati, B.A., Li, B.Y., Wachter, R.D., Lynch, A.M., Demertzis, Z.D., Meyers, B.S., Abufarha, F.S., et al. (2015). All spiking, sustained ON displaced amacrine cells receive gap-junction input from melanopsin ganglion cells. *Current Biology* 25, 2763-2773. doi:10.1016/j.cub.2015.09.018.
175. Cameron, M.A., Pozdnyev, N., Vugler, A.A., Cooper, H., Iuvone, P.M., and Lucas, R.J. (2009). Light regulation of retinal dopamine that is independent of melanopsin phototransduction. *European Journal of Neuroscience* 29, 761-767. doi:10.1111/j.1460-9568.2009.06631.x.

176. Joo, H.R., Peterson, B.B., Dacey, D.M., Hattar, S., and Chen, S.K. (2013). Recurrent axon collaterals of intrinsically photosensitive retinal ganglion cells. *Visual Neuroscience* 30, 175-182. doi:10.1017/S0952523813000199.
177. Wright, H.R., and Lack, L.C. (2001). Effect of light wavelength on suppression and phase delay of the melatonin rhythm. *Chronobiol Int* 18, 801-808.
178. Warman, V.L., Dijk, D.J., Warman, G.R., Arendt, J., and Skene, D.J. (2003). Phase advancing human circadian rhythms with short wavelength light. *Neurosci Lett* 342, 37-40.
179. Wright, H.R., Lack, L.C., and Kennaway, D.J. (2004). Differential effects of light wavelength in phase advancing the melatonin rhythm. *J Pineal Res* 36, 140-144.
180. Cajochen, C., Zeitzer, J.M., Czeisler, C.A., and Dijk, D.J. (2000). Dose-response relationship for light intensity and ocular and electroencephalographic correlates of human alertness. *Behav Brain Res* 115, 75-83.
181. Cajochen, C., Munch, M., Kobialka, S., Krauchi, K., Steiner, R., Oelhafen, P., Orgul, S., and Wirz-Justice, A. (2005). High sensitivity of human melatonin, alertness, thermoregulation, and heart rate to short wavelength light. *J Clin Endocrinol Metab* 90, 1311-1316. doi:10.1210/jc.2004-0957.
182. Lockley, S.W., Evans, E.E., Scheer, F.A., Brainard, G.C., Czeisler, C.A., and Aeschbach, D. (2006). Short-wavelength sensitivity for the direct effects of light on alertness, vigilance, and the waking electroencephalogram in humans. *Sleep* 29, 161-168.
183. Chellappa, S.L., Steiner, R., Blattner, P., Oelhafen, P., Gotz, T., and Cajochen, C. (2011). Non-visual effects of light on melatonin, alertness and cognitive performance: can blue-enriched light keep us alert? *PLoS One* 6, e16429. doi:10.1371/journal.pone.0016429.
184. Rahman, S.A., Flynn-Evans, E.E., Aeschbach, D., Brainard, G.C., Czeisler, C.A., and Lockley, S.W. (2014). Diurnal spectral sensitivity of the acute alerting effects of light. *Sleep* 37, 271-281. doi:10.5665/sleep.3396.
185. Sasseville, A., Martin, J.S., Houle, J., and Hebert, M. (2015). Investigating the contribution of short wavelengths in the alerting effect of bright light. *Physiol Behav* 151, 81-87. doi:10.1016/j.physbeh.2015.06.028.
186. Munch, M., Kobialka, S., Steiner, R., Oelhafen, P., Wirz-Justice, A., and Cajochen, C. (2006). Wavelength-dependent effects of evening light exposure on sleep architecture and sleep EEG power density in men. *Am J Physiol Regul Integr Comp Physiol* 290, R1421-1428. doi:10.1152/ajpregu.00478.2005.
187. Figueiro, M.G., and Rea, M.S. (2010). The effects of red and blue lights on circadian variations in cortisol, alpha amylase, and melatonin. *Int J Endocrinol* 2010, 829351. doi:10.1155/2010/829351.
188. Figueiro, M.G., and Rea, M.S. (2012). Short-wavelength light enhances cortisol awakening response in sleep-restricted adolescents. *Int J Endocrinol* 2012, 301935. doi:10.1155/2012/301935.
189. Gabel, V., Maire, M., Reichert, C.F., Chellappa, S.L., Schmidt, C., Hommes, V., Viola, A.U., and Cajochen, C. (2013). Effects of artificial dawn and morning blue light on daytime cognitive performance, well-being, cortisol and melatonin levels. *Chronobiol Int* 30, 988-997. doi:10.3109/07420528.2013.793196.
190. Tarttelin, E.E., Bellingham, J., Bibb, L.C., Foster, R.G., Hankins, M.W., Gregory-Evans, K., Gregory-Evans, C.Y., Wells, D.J., and Lucas, R.J. (2003). Expression of opsin genes early in ocular development of humans and mice. *Exp Eye Res* 76, 393-396.
191. Sekaran, S., Lupi, D., Jones, S.L., Sheely, C.J., Hattar, S., Yau, K.W., Lucas, R.J., Foster, R.G., and Hankins, M.W. (2005). Melanopsin-dependent photoreception provides earliest light detection in the mammalian retina. *Curr Biol* 15, 1099-1107. doi:10.1016/j.cub.2005.05.053.

192. Rao, S., Chun, C., Fan, J., Kofron, J.M., Yang, M.B., Hegde, R.S., Ferrara, N., Copenhagen, D.R., and Lang, R.A. (2013). A direct and melanopsin-dependent fetal light response regulates mouse eye development. *Nature* *494*, 243-246. doi:10.1038/nature11823.
193. Norton, T.T., and Siegwart, J.T., Jr. (2013). Light levels, refractive development, and myopia--a speculative review. *Exp Eye Res* *114*, 48-57. doi:10.1016/j.exer.2013.05.004.
194. Stockman, A., and Brainard, D.H. (2010). Color vision mechanisms. In {OSA Handbook of Optics}, 3rd Edition, M. Bass, ed. (New York: McGraw-Hill), pp. 11.11-11.104.
195. Kimura, E., and Young, R.S.L. (2010). Sustained pupillary constrictions mediated by an L- and M-cone opponent process. *Vision Research* *50*, 489-496. doi:10.1016/j.visres.2010.01.001.
196. Kimura, E., and Young, R.S. (1996). A chromatic-cancellation property of human pupillary responses. *Vision Research* *36*, 1543-1550.
197. Tsujimura, S., Wolffsohn, J.S., and Gilmartin, B. (2001). A linear chromatic mechanism drives the pupillary response. *Proceedings: Biological Sciences* *268*, 2203-2209. doi:10.1098/rspb.2001.1775.
198. Verdon, W., and Howarth, P.A. (1988). The pupil's response to short wavelength cone stimulation. *Vision Research* *28*, 1119-1128.
199. Donner, K.O., and Rushton, W.A. (1959). Retinal stimulation by light substitution. *Journal of Physiology* *149*, 288-302.
200. CIE (2006). Technical Report 170-1: Fundamental chromaticity diagram with physiological axes – Part 1. (Vienna: Central Bureau of the Commission Internationale de l'Éclairage).
201. Watson, A.B. (1986). Temporal sensitivity. In *Handbook of Perception and Human Performance*, Volume 1, K. Boff, L. Kaufman and J. Thomas, eds. (New York: Wiley), pp. 6-1-6-43.
202. Dacey, D.M., Crook, J.D., and Packer, O.S. (2014). Distinct synaptic mechanisms create parallel S-ON and S-OFF color opponent pathways in the primate retina. *Visual Neuroscience* *31*, 139-151. doi:10.1017/S0952523813000230.
203. Frank, J.W., Kushner, B.J., and France, T.D. (1988). Paradoxical pupillary phenomena. A review of patients with pupillary constriction to darkness. *Archives of Ophthalmology* *106*, 1564-1566.
204. Gooley, J.J., Ho Mien, I., St Hilaire, M.A., Yeo, S.C., Chua, E.C., van Reen, E., Hanley, C.J., Hull, J.T., Czeisler, C.A., and Lockley, S.W. (2012). Melanopsin and rod-cone photoreceptors play different roles in mediating pupillary light responses during exposure to continuous light in humans. *Journal of Neuroscience* *32*, 14242-14253. doi:10.1523/JNEUROSCI.1321-12.2012.
205. Do, M.T., Kang, S.H., Xue, T., Zhong, H., Liao, H.W., Bergles, D.E., and Yau, K.W. (2009). Photon capture and signalling by melanopsin retinal ganglion cells. *Nature* *457*, 281-287. doi:10.1038/nature07682.
206. Bleichert, A. (1957). Die Lichtreaktion der Pupille als Regelvorgang. *Albrecht von Graefes Archiv für Ophthalmologie Vereinigt mit Archiv für Augenheilkunde* *159*, 396-410. doi:10.1007/bf00684646.
207. Stark, L., and Sherman, P.M. (1957). A servoanalytic study of consensual pupil reflex to light. *Journal of Neurophysiology* *20*, 17-26.
208. Stegemann, J. (1957). Über den Einfluß sinusförmiger Leuchtdichteänderungen auf die Pupillenweite. *Pflügers Archiv für die Gesamte Physiologie des Menschen und der Tiere* *264*, 113-122. doi:10.1007/bf00363400.
209. Stark, L., and Baker, F. (1959). Stability and oscillations in a neurological servomechanism. *Journal of Neurophysiology* *22*, 156-164.

210. Hornung, J., and Stegemann, J. (1964). Ein nichtlineares kybernetisches Modell für die Pupillenreaktion auf Licht, (Köln/Obladen (Germany): Westdeutscher Verlag).
211. Varju, D. (1967). [Nervous reciprocal effect in the pupillomotoric pathway of man. I. Differences in pupillary reactions to monocular and binocular light stimulations]. *Kybernetik* 3, 203-214. doi:10.1007/BF00288550.
212. Sandberg, A., and Stark, L. (1968). Wiener G-function analysis as an approach to non-linear characteristics of human pupil light reflex. *Brain Research* 11, 194-211.
213. van der Wildt, G.J., and Bouman, M.A. (1974). Dependence of the Dynamic Behaviour of the Human Pupil System on the Input Signal. *Optica Acta: International Journal of Optics* 21, 59-74. doi:10.1080/713818835.
214. Clarke, R.J., Zhang, H., and Gamlin, P.D. (2003). Characteristics of the pupillary light reflex in the alert rhesus monkey. *Journal of Neurophysiology* 89, 3179-3189. doi:10.1152/jn.01131.2002.
215. Zangemeister, W.H., Gronow, T., and Grzyska, U. (2009). Pupillary responses to single and sinusoidal light stimuli in diabetic patients. *Neurology International* 1, e19. doi:10.4081/ni.2009.e19.
216. Lee, J., and Stromeier, C.F., 3rd (1989). Contribution of human short-wave cones to luminance and motion detection. *Journal of Physiology* 413, 563-593.
217. Stockman, A., MacLeod, D.I., and DePriest, D.D. (1991). The temporal properties of the human short-wave photoreceptors and their associated pathways. *Vision Research* 31, 189-208.
218. Ishihara, S. (1977). Tests for Colour-Blindness, (Tokyo: Kanehara Shuppen Company, Ltd.).
219. Aguilar, M., and Stiles, W.S. (1954). Saturation of the Rod Mechanism of the Retina at High Levels of Stimulation. *Optica Acta: International Journal of Optics* 1, 59-65. doi:10.1080/713818657.
220. Stockman, A., and Sharpe, L.T. (2000). The spectral sensitivities of the middle- and long-wavelength-sensitive cones derived from measurements in observers of known genotype. *Vision Research* 40, 1711-1737.
221. Alpern, M., and Pugh, E.N., Jr. (1974). The density and photosensitivity of human rhodopsin in the living retina. *Journal of Physiology* 237, 341-370.
222. Zwas, F., and Alpern, M. (1976). The density of human rhodopsin in the rods. *Vision Research* 16, 121-127.
223. Webster, M.A., and MacLeod, D.I. (1988). Factors underlying individual differences in the color matches of normal observers. *Journal of the Optical Society of America A: Optics and Image Science* 5, 1722-1735. doi:10.1364/JOSAA.5.001722.
224. Loewenfeld, I.E., and Lowenstein, O. (1993). The pupil: anatomy, physiology, and clinical applications, Volume I, 1st Edition, (Ames, IA/Detroit, MI: Iowa State University Press/Wayne State University Press).
225. Stark, L., Campbell, F.W., and Atwood, J. (1958). Pupil unrest: an example of noise in a biological servomechanism. *Nature* 182, 857-858.
226. Prahl, S. (1999). Optical absorption of hemoglobin. (Oregon Medical Laser Center).
227. Snodderly, D.M., Weinhaus, R.S., and Choi, J.C. (1992). Neural-vascular relationships in central retina of macaque monkeys (*Macaca fascicularis*). *Journal of Neuroscience* 12, 1169-1193.
228. Bird, A.C., and Weale, R.A. (1974). On the retinal vasculature of the human fovea. *Experimental Eye Research* 19, 409-417. doi:10.1016/0014-4835(74)90050-5.
229. Ashton, N. (1957). Retinal vascularization in health and disease: Proctor Award Lecture of the Association for Research in Ophthalmology. *American Journal of Ophthalmology* 44, 7-17. doi:10.1016/0002-9394(57)90426-9.

230. Adams, D.L., and Horton, J.C. (2003). The representation of retinal blood vessels in primate striate cortex. *Journal of Neuroscience* 23, 5984-5997.
231. Cornsweet, T.N. (1970). *Visual Perception*, (New York: Academic Press).
232. Purkinje, J. (1825). Beobachtungen und Versuche zur Physiologie der Sinne: Neue Beiträge zur Kenntnis des Sehens in subjectiver Hinsicht, (Berlin: G. Reimer).
233. Purkinje, J. (1819). Beobachtungen und Versuche zur Physiologie der Sinne: Beiträge zur Kenntnis des Sehens in subjectiver Hinsicht, (Prague: Johann Gottfried Calve).
234. Wade, N.J., and Brožek, J. (2001). Purkinje's vision: The dawning of neuroscience, (Mahwah, NJ: Lawrence Erlbaum Associates).
235. Müller, H. (1854). Ueber einige Verhältnisse der Netzhaut bei Menschen und Thieren. *Verhandlungen der Physikalisch-Medizinischen Gesellschaft zu Würzburg* 4, 96-100.
236. Müller, H. (1855). Ueber die entoptische Wahrnehmung der Netzhautgefäße, insbesondere als Beweismittel für die Lichtperception für die nach hinten gelegenen Netzhauptelemente. *Verhandlungen der Physikalisch-Medizinischen Gesellschaft zu Würzburg* 5, 411-447.
237. Walker, C.B. (1940). Use of the Purkinje figures as test for separated retina and other intraocular pathology. *American Journal of Ophthalmology* 23, 803-804. doi:10.1016/S0002-9394(40)92383-2.
238. Talbot, E.M., Murdoch, J.R., and Keating, D. (1992). The Purkinje vascular entoptic test: a halogen light gives better results. *Eye* 6, 322-325. doi:10.1038/eye.1992.64.
239. Suzuki, R. (1941). Die klinische Bedeutung der Purkinjeschen Aderfigur. I. Die grundlegende Forschung über das entoptische Gesichtsfeld. *Nippon Ganka Gakkai Zasshi [Acta Societatis Ophthalmologicae Japonicae]* 45, 590-621.
240. Scheerer, R. (1924). Die entoptische Sichtbarkeit der Blutbewegung im Auge und ihre klinische Bedeutung. *Klinische Monatsblätter für Augenheilkunde* 73, 67-107.
241. Pagenstecher, A.H. (1903). Ueber Staroperationen mit besonderer Berücksichtigung der Nachstaroperation. *Zeitschrift für Augenheilkunde* 10, 206-219.
242. Murillo-Lopez, F., Maumenee, A.E., and Guyton, D.L. (2000). Perception of Purkinje vessel shadows and foveal granular pattern as a measure of potential visual acuity. *Journal of Cataract and Refractive Surgery* 26, 260-265. doi:10.1016/S0886-3350(99)00341-7.
243. Kraupa, E. (1949). Ueber die Purkinje'schen Aderfiguren und die Doppelbeleuchtung in Ophthalmoskopie und Spaltlampenuntersuchung. *Ophthalmologica* 118, 318-320. doi:10.1159/000300734.
244. Goldmann, H. (1972). Examination of the fundus of the cataractous eye. *American Journal of Ophthalmology* 73, 309-320. doi:10.1016/0002-9394(72)90058-X.
245. Ehrich, W. (1961). Netzhautgefäßschattenfigur und Makulachagrin als entoptische Funktionsprüfung. *Documenta Ophthalmologica* 15, 371-425. doi:10.1007/bf00234354.
246. Ehrich, W. (1961). Entoptische Phänomene von klinischer Bedeutung. *Medizinische Klinik* 54, 31-32.
247. Ehrich, W. (1958). Methodische Richtlinien zur entoptischen Funktionsprüfung. *Klinische Monatsblätter für Augenheilkunde* 133, 396-401.
248. Comberg, D., and Ehrich, W. (1971). Welche Gesichtsfeldbereiche kann man mit der Netzhautgefäßschattenfigur erfassen? *Ophthalmologica* 162, 140-145. doi:10.1159/000306255.
249. Applegate, R.A., Bradley, A., van Heuven, W.A., Lee, B.L., and Garcia, C.A. (1997). Entoptic evaluation of diabetic retinopathy. *Investigative Ophthalmology and Visual Science* 38, 783-791.
250. Bowen, S.F. (1963). Retinal entoptic phenomena. *Archives of Ophthalmology* 69, 551. doi:10.1001/archopht.1963.00960040557003.

251. Atchison, D.A., and Applegate, R.A. (1997). Two new tests assist in the diagnosis of a small calibre vein occlusion. *Clinical and Experimental Optometry* *80*, 49-52. doi:10.1111/j.1444-0938.1997.tb04850.x.
252. Hilmantel, G., Applegate, R.A., van Heuven, W.A., Stowers, S.P., Bradley, A., and Lee, B.L. (1999). Entoptic foveal avascular zone measurement and diabetic retinopathy. *Optometry and Vision Science* *76*, 826-831.
253. Applegate, R.A., Bradley, A., and van Heuven, W.A. (1990). Entoptic visualization of the retinal vasculature near fixation. *Investigative Ophthalmology and Visual Science* *31*, 2088-2098.
254. Kluxen, G., and Wilden, E. (1987). An entoptic test in diabetic patients. *Diabetes Care* *10*, 800-801.
255. Eber, S.I. (1922). Autoophthalmoscopy — subjective examination of the retina. *American Journal of Ophthalmology* *5*, 973-974. doi:10.1016/s0002-9394(22)90950-x.
256. Drews, L.C. (1941). Autofundoscopy. *American Journal of Ophthalmology* *24*, 1403-1417. doi:10.1016/s0002-9394(14)77452-5.
257. Drews, L.C. (1943). Further observations on autofundoscopy (auto-ophthalmoscopy of Eber; Purkinje figure of Walker). *American Journal of Ophthalmology* *26*, 1143-1154. doi:10.1016/s0002-9394(43)90490-8.
258. Friedman, B. (1931). A test for retinal function in cataractous patients. *Archives of Ophthalmology* *5*, 636-637. doi:10.1001/archopht.1931.00820040132010.
259. Brodie, S.E. (1987). Evaluation of cataractous eyes with opaque media. *International Ophthalmology Clinics* *27*, 153-162. doi:10.1097/00004397-198702730-00004.
260. Goebel, K. (1922). Die Funktionsprüfung der zentralen Netzhautpartien auf entoptischem Wege. *Archiv für Augenheilkunde* *90*, 245-249.
261. Kolb, H. (1995). Facts and Figures Concerning the Human Retina. In *Webvision: The Organization of the Retina and Visual System*, H. Kolb, E. Fernandez and R. Nelson, eds. (Salt Lake City (UT)).
262. Kelly, D.H. (1964). Sine waves and flicker fusion. *Documenta Ophthalmologica* *18*, 16-35. doi:10.1007/bf00160561.
263. Kelly, D.H. (1979). Motion and vision II Stabilized spatio-temporal threshold surface. *Journal of the Optical Society of America* *69*, 1340. doi:10.1364/josa.69.001340.
264. Allefeld, C., Putz, P., Kastner, K., and Wackermann, J. (2011). Flicker-light induced visual phenomena: frequency dependence and specificity of whole percepts and percept features. *Consciousness and Cognition* *20*, 1344-1362. doi:10.1016/j.concog.2010.10.026.
265. Brown, C.R., and Gebhard, J.W. (1948). Visual field articulation in the absence of spatial stimulus gradients. *Journal of Experimental Psychology* *38*, 188-200. doi:10.1037/h0054433.
266. Young, R.S., Cole, R.E., Gamble, M., and Rayner, M.D. (1975). Subjective patterns elicited by light flicker. *Vision Research* *15*, 1291-1293. doi:10.1016/0042-6989(75)90177-7.
267. Smythies, J.R. (1957). A preliminary analysis of the stroboscopic patterns. *Nature* *179*, 523-524. doi:10.1038/179523a0.
268. Remole, A. (1971). Luminance thresholds for subjective patterns in a flickering field: effect of wavelength. *Journal of the Optical Society of America* *61*, 1164-1168.
269. von Helmholtz, H. (1867). *Handbuch der Physiologischen Optik*, (Leipzig: Leopold Voss).
270. Coppola, D., and Purves, D. (1996). The extraordinarily rapid disappearance of entoptic images. *Proceedings of the National Academy of Sciences of the United States of America* *93*, 8001-8004. doi:10.1073/pnas.93.15.8001.
271. Steinbuch, W. (1813). Beiträge zur Physiologie des Auges: 1. Das Sehen des im eigenen Auge fliessendes Blutes. *Jahrbücher der teutschen Medicin und Chirurgie* *3*, 270-285.

272. Rood, O.N. (1860). On a probable means of rendering visible the circulation in the eye. *American Journal of Science and Arts* 30, 264-265.
273. Vierordt, K. (1856). Die Wahrnehmung des Blutlaufes in der Netzhaut des eigenen Auges. *Archiv für physiologische Heilkunde* 15, 255-268.
274. Gudden, B. (1849). Ueber das Verhältniss der Centralgefäß des Auges zum Gesichtsfelde. *Archiv für Anatomie, Physiologie und wissenschaftliche Medicin*, 522-532.
275. Exner, S. (1884). Die mangelhafte Erregbarkeit der Netzhaut für Licht von abnormer Einfallssrichtung. *Sitzungsberichte der Kaiserlichen Akademie der Wissenschaften: Mathematisch-Naturwissenschaftliche Classe* 88, 103-108.
276. Deeley, R.M. (1913). Retinal shadows? *Nature* 90, 594-594. doi:10.1038/090594e0.
277. Aubert, H. (1865). *Physiologie der Netzhaut*, (Breslau: Morgenstern).
278. von Zehender, W. (1895). Ueber einige subjective Gesichtswahrnehmungen. II. Die Schattenbilder der Netzhautgefäße und der Eintrittsstelle des Sehnerven. *Klinische Monatsblätter für Augenheilkunde* 33, 112-125.
279. von Thomsen, E. (1919). Über Johannes Evangelista Purkinje und seine Werke. *Skandinavisches Archiv für Physiologie* 37, 1-116. doi:10.1111/j.1748-1716.1919.tb00120.x.
280. Kahn, R.H. (1908). Beiträge zur Physiologie des Gesichtssinnes. I. Farbige Schatten auf der Netzhaut. *Lotos* 56, 1-10.
281. Exner, S. (1868). Ueber einige neue subjective Gesichterscheinungen. *Archiv für die Gesammte Physiologie des Menschen und der Thiere* 1, 375-394. doi:10.1007/bf01640325.
282. Stigler, R. (1905). Eine neue subjektive Gesichterscheinung. *Zeitschrift für Psychologie und Physiologie der Sinnesorgane* 39, 332-340.
283. Sharpe, C.R. (1972). The visibility and fading of thin lines visualized by their controlled movement across the retina. *Journal of Physiology* 222, 113-134.
284. Drysdale, A.E. (1975). The visibility of retinal blood vessels. *Vision Research* 15, 813-818. doi:10.1016/0042-6989(75)90259-X.
285. Ditchburn, R.W. (1936). Shadows of the retinal blood-vessels seen by monochromatic light. *Nature* 137, 661-661. doi:10.1038/137661a0.
286. Bradley, A., Zhang, H., Applegate, R.A., Thibos, L.N., and Elsner, A.E. (1998). Entoptic image quality of the retinal vasculature. *Vision Research* 38, 2685-2696. doi:10.1016/S0042-6989(97)00345-3.
287. Wyatt, H.J. (1978). Purkinje's methods for visualizing the internal retinal circulation: A look at the source. *Vision Research* 18, 875-877. doi:10.1016/0042-6989(78)90133-5.
288. Cornsweet, T.N. (1966). Stabilized image techniques. In *Recent Developments in Vision Research*, Volume 1272, M.A. Whitcomb, ed. (Washington, DC: National Academy of Sciences).
289. Stockman, A., and Sharpe, L.T. (2000). Spectral sensitivities of the middle- and long-wavelength sensitive cones derived from measurements in observers of known genotype. *Vision Research* 40, 1711-1737. doi:10.1016/S0042-6989(00)00021-3.
290. Brainard, D.H., and Stockman, A. (2010). Colorimetry. In *The Optical Society of America Handbook of Optics*, 3rd edition, Volume III: Vision and Vision Optics, M. Bass, C. DeCusatis, J. Enoch, V. Lakshminarayanan, G. Li, C. Macdonald, V. Mahajan and E. van Stryland, eds. (New York: McGraw Hill), pp. 10.11-10.56.
291. Adams, D.L., and Horton, J.C. (2002). Shadows cast by retinal blood vessels mapped in primary visual cortex. *Science* 298, 572-576. doi:10.1126/science.1074887.
292. Adams, D.L., and Horton, J.C. (2003). A precise retinotopic map of primate striate cortex generated from the representation of angioscotomas. *Journal of Neuroscience* 23, 3771-3789.

293. Lucas, R.J., Hattar, S., Takao, M., Berson, D.M., Foster, R.G., and Yau, K.W. (2003). Diminished pupillary light reflex at high irradiances in melanopsin-knockout mice. *Science* *299*, 245-247. doi:10.1126/science.1077293.
294. Panda, S., Sato, T.K., Castrucci, A.M., Rollag, M.D., DeGrip, W.J., Hogenesch, J.B., Provencio, I., and Kay, S.A. (2002). Melanopsin (Opn4) requirement for normal light-induced circadian phase shifting. *Science* *298*, 2213-2216. doi:10.1126/science.1076848.
295. Brown, T.M., Gias, C., Hatori, M., Keding, S.R., Semo, M., Coffey, P.J., Gigg, J., Piggins, H.D., Panda, S., and Lucas, R.J. (2010). Melanopsin contributions to irradiance coding in the thalamo-cortical visual system. *PLoS Biology* *8*, e1000558. doi:10.1371/journal.pbio.1000558.
296. Noseda, R., and Burstein, R. (2011). Advances in understanding the mechanisms of migraine-type photophobia. *Current Opinion in Neurology* *24*, 197-202. doi:10.1097/WCO.0b013e3283466c8e.
297. Ecker, J.L., Dumitrescu, O.N., Wong, K.Y., Alam, N.M., Chen, S.-K., LeGates, T., Renna, J.M., Prusky, G.T., Berson, D.M., and Hattar, S. (2010). Melanopsin-expressing retinal ganglion-cell photoreceptors: cellular diversity and role in pattern vision. *Neuron* *67*, 49-60. doi:10.1016/j.neuron.2010.05.023.
298. Provencio, I., Rollag, M.D., and Castrucci, A.M. (2002). Photoreceptive net in the mammalian retina. *Nature* *415*, 493. doi:10.1038/415493a.
299. Smithson, H.E. (2014). S-cone psychophysics. *Visual Neuroscience* *31*, 211-225. doi:10.1017/S0952523814000030.
300. Martin, P.R., and Lee, B.B. (2014). Distribution and specificity of S-cone ("blue cone") signals in subcortical visual pathways. *Visual Neuroscience* *31*, 177-187. doi:10.1017/S0952523813000631.
301. ISO (2007). Ophthalmic instruments – Fundamental requirements and test methods. Part 2: Light hazard protection (ISO 15004-2), (Geneva: International Organization for Standardization).
302. Brainard, D.H. (1997). The Psychophysics Toolbox. *Spatial Vision* *10*, 433-436. doi:10.1163/156856897X00357.
303. Rushton, W.A., and Henry, G.H. (1968). Bleaching and regeneration of cone pigments in man. *Vision Research* *8*, 617-631. doi:10.1016/0042-6989(68)90040-0.
304. Kaiser, P.K., and Boynton, R.M. (1996). Human Color Vision, 2nd Edition, (Washington, D.C.: Optical Society of America).
305. Watson, A.B., and Yellott, J.I. (2012). A unified formula for light-adapted pupil size. *Journal of Vision* *12*, 12. doi:10.1167/12.10.12.
306. Hill, A.V. (1910). The possible effects of the aggregation of the molecules of haemoglobin on its dissociation curves. *Journal of Physiology* *40*, iv-vii.
307. Boynton, R.M. (1979). Human Color Vision, (New York: Holt, Rinehart and Winston).
308. Kelly, D.H. (1974). Spatio-temporal frequency characteristics of color-vision mechanisms. *Journal of the Optical Society of America* *64*, 983-990.
309. Kelly, D.H. (1983). Spatiotemporal variation of chromatic and achromatic contrast thresholds. *Journal of the Optical Society of America* *73*, 742. doi:10.1364/josa.73.000742.
310. Robson, J.G. (1966). Spatial and temporal contrast sensitivity functions of the visual system. *Journal of the Optical Society of America* *56*, 1141-1142.
311. De Lange, H. (1958). Research into the dynamic nature of the human fovea-cortex systems with intermittent and modulated light. I. Attenuation characteristics with white and colored light. *Journal of the Optical Society of America* *48*, 777-784.
312. Kelly, D.H. (1961). Visual Responses to Time-Dependent Stimuli I Amplitude Sensitivity Measurements. *Journal of the Optical Society of America* *51*, 422. doi:10.1364/josa.51.000422.

313. Kelly, D.H. (1984). Retinal inhomogeneity. I. Spatiotemporal contrast sensitivity. *Journal of the Optical Society of America A: Optics and Image Science* *1*, 107-113. doi:10.1364/JOSAA.1.000107.
314. Engel, S., Zhang, X., and Wandell, B. (1997). Colour tuning in human visual cortex measured with functional magnetic resonance imaging. *Nature* *388*, 68-71. doi:10.1038/40398.
315. Chaparro, A., Stromeier, C.F., 3rd, Huang, E.P., Kronauer, R.E., and Eskew, R.T., Jr. (1993). Colour is what the eye sees best. *Nature* *361*, 348-350. doi:10.1038/361348a0.
316. Benson, N.C., Butt, O.H., Brainard, D.H., and Aguirre, G.K. (2014). Correction of distortion in flattened representations of the cortical surface allows prediction of V1-V3 functional organization from anatomy. *PLoS Computational Biology* *10*, e1003538. doi:10.1371/journal.pcbi.1003538.
317. Liu, J., and Wandell, B.A. (2005). Specializations for chromatic and temporal signals in human visual cortex. *Journal of Neuroscience* *25*, 3459-3468. doi:10.1523/JNEUROSCI.4206-04.2005.
318. Lee, B.B., Sun, H., and Zucchini, W. (2007). The temporal properties of the response of macaque ganglion cells and central mechanisms of flicker detection. *J Vis* *7*, 1 1-16. doi:10.1167/7.14.1.
319. D'Souza, D.V., Auer, T., Strasburger, H., Frahm, J., and Lee, B.B. (2011). Temporal frequency and chromatic processing in humans: an fMRI study of the cortical visual areas. *J Vis* *11*. doi:10.1167/11.8.8.
320. Mullen, K.T., Thompson, B., and Hess, R.F. (2010). Responses of the human visual cortex and LGN to achromatic and chromatic temporal modulations: an fMRI study. *J Vis* *10*, 13. doi:10.1167/10.13.13.
321. Carandini, M., and Heeger, D.J. (2012). Normalization as a canonical neural computation. *Nature Reviews: Neuroscience* *13*, 51-62. doi:10.1038/nrn3136.
322. Busse, L., Wade, A.R., and Carandini, M. (2009). Representation of concurrent stimuli by population activity in visual cortex. *Neuron* *64*, 931-942. doi:10.1016/j.neuron.2009.11.004.
323. Gauthier, B., Eger, E., Hesselmann, G., Giraud, A.L., and Kleinschmidt, A. (2012). Temporal tuning properties along the human ventral visual stream. *Journal of Neuroscience* *32*, 14433-14441. doi:10.1523/JNEUROSCI.2467-12.2012.
324. Wandell, B.A., Poirson, A.B., Newsome, W.T., Baseler, H.A., Boynton, G.M., Huk, A., Gandhi, S., and Sharpe, L.T. (1999). Color signals in human motion-selective cortex. *Neuron* *24*, 901-909.
325. Seidemann, E., Poirson, A.B., Wandell, B.A., and Newsome, W.T. (1999). Color signals in area MT of the macaque monkey. *Neuron* *24*, 911-917.
326. Conway, B.R. (2014). Color signals through dorsal and ventral visual pathways. *Visual Neuroscience* *31*, 197-209. doi:10.1017/S0952523813000382.
327. Jayakumar, J., Roy, S., Dreher, B., Martin, P.R., and Vidyasagar, T.R. (2013). Multiple pathways carry signals from short-wavelength-sensitive ('blue') cones to the middle temporal area of the macaque. *Journal of Physiology* *591*, 339-352. doi:10.1113/jphysiol.2012.241117.
328. Mullen, K.T., Dumoulin, S.O., McMahon, K.L., de Zubicaray, G.I., and Hess, R.F. (2007). Selectivity of human retinotopic visual cortex to S-cone-opponent, L/M-cone-opponent and achromatic stimulation. *European Journal of Neuroscience* *25*, 491-502. doi:10.1111/j.1460-9568.2007.05302.x.
329. Hannibal, J., and Fahrenkrug, J. (2004). Target areas innervated by PACAP-immunoreactive retinal ganglion cells. *Cell and Tissue Research* *316*, 99-113. doi:10.1007/s00441-004-0858-x.

330. Davis, K.E., Eleftheriou, C.G., Allen, A.E., Procyk, C.A., and Lucas, R.J. (2015). Melanopsin-derived visual responses under light adapted conditions in the mouse dLGN. *PLoS One* *10*, e0123424. doi:10.1371/journal.pone.0123424.
331. Cole, G.R., Hine, T., and McIlhagga, W. (1993). Detection mechanisms in L-, M-, and S-cone contrast space. *Journal of the Optical Society of America A: Optics and Image Science* *10*, 38-51.